1977

Investigation into the effect of dissimilar metal coupling, potential, and processing on the mode and distribution of galvanic corrosion attack on 5086 aluminum alloy in synthetic seawater.

Locke, John Sinclair

Monterey, California. Naval Postgraduate School

INVESTIGATION INTO THE EFFECT OF DISSIMILAR METAL COUPLING, POTENTIAL, AND PROCESSING ON THE MODE AND DISTRIBUTION OF GALVANIC CORROSION ATTACK ON 5086 ALUMINUM ALLOY IN SYNTHETIC SEAWATER.

John Sinclair Locke

NAVAL POSTGRADUATE SCHOOL
Monterey, California

THESIS

INVESTIGATION INTO THE EFFECT OF
DISSIMILAR METAL COUPLING, POTENTIAL, AND PROCESSING
ON THE MODE AND DISTRIBUTION
OF GALVANIC CORROSION ATTACK ON 5086 ALUMINUM ALLOY
IN SYNTHETIC SEAWATER

by

John Sinclair Locke

September 1977

Thesis Advisor: J. Perkins

REPORT DOCUMENTATION PAGE

READ INSTRUCTIONS BEFORE COMPLETING FORM

1. REPORT NUMBER	2. GOVT ACCESSION NO. / 3. RECIPIENT'S CATALOG NUMBER
4. TITLE (and Subtitle): Investigation into the Effect of Dissimilar Metal Coupling, Potential, and Processing on the Mode and Distribution of Galvanic Corrosion Attack on 5086 Aluminum Alloy in Synthetic Seawater	5. TYPE OF REPORT & PERIOD COVERED: Master's Thesis; September 1977
	6. PERFORMING ORG. REPORT NUMBER
7. AUTHOR(s): John Sinclair Locke	8. CONTRACT OR GRANT NUMBER(s)
9. PERFORMING ORGANIZATION NAME AND ADDRESS: Naval Postgraduate School, Monterey, California 93940	10. PROGRAM ELEMENT, PROJECT, TASK AREA & WORK UNIT NUMBERS
11. CONTROLLING OFFICE NAME AND ADDRESS: Naval Postgraduate School, Monterey, California 93940	12. REPORT DATE: September 1977
	13. NUMBER OF PAGES: 126
14. MONITORING AGENCY NAME & ADDRESS (if different from Controlling Office)	15. SECURITY CLASS. (of this report): Unclassified
	15a. DECLASSIFICATION/DOWNGRADING SCHEDULE

16. DISTRIBUTION STATEMENT (of this Report)

Approved for public release; distribution unlimited.

17. DISTRIBUTION STATEMENT (of the abstract entered in Block 20, if different from Report)

18. SUPPLEMENTARY NOTES

19. KEY WORDS (Continue on reverse side if necessary and identify by block number)

Dissimilar Metal Coupling
Galvanic Corrosion
5086 Aluminum Alloy

20. ABSTRACT (Continue on reverse side if necessary and identify by block number)

The galvanic corrosion behavior of 5086 aluminum alloy in three tempers (H116, H117, H32) when coupled with three more noble metals (1040 steel, 60/40 naval brass, Ti-150A titanium) and immersed in aerated synthetic seawater has been characterized. In so doing, use was made of potentiodynamic polarization techniques, galvanic current density monitoring for twenty-four hours, and optical and scanning

(20. ABSTRACT Continued)

electron microscopic observations. The results obtained through the use of these techniques are presented and discussed. Galvanic corrosion of 5086 Al when coupled to the dissimilar metals was found to be independent of temper and to decrease in the order (of coupled metals) Ti-150A > 60/40 naval brass > 1040 steel. The effect of dissimilar metal coupling was found to be reduced by the formation on the anode and cathode of insulating corrosion product structures; this also caused an increased domination of the attack by localized corrosion modes. The effect of edges and crevices in concentrating attack and the correlation between distribution of corrosion product and metal dissolution is discussed.

Approved for public release; distribution unlimited.

Investigation into the Effect of Dissimilar Metal Coupling, Potential, and Processing on the Mode and Distribution of Galvanic Corrosion Attack on 5086 Aluminum Alloy in Synthetic Seawater

by

John Sinclair Locke
Lieutenant, United States Navy
B.S.E., University of Michigan, 1969

Submitted in partial fulfillment of the
requirements for the degree of

MASTER OF SCIENCE IN MECHANICAL ENGINEERING

from the

NAVAL POSTGRADUATE SCHOOL

September 1977

ABSTRACT

The galvanic corrosion behavior of 5086 aluminum alloy in three tempers (H116, H117, H32) when coupled with three more noble metals (1040 steel, 60/40 naval brass, Ti-150A titanium) and immersed in aerated synthetic seawater has been characterized. In so doing, use was made of potentiodynamic polarization techniques, galvanic current density monitoring for twenty-four hours, and optical and scanning electron microscopic observations. The results obtained through the use of these techniques are presented and discussed. Galvanic corrosion of 5086 Al when coupled to the dissimilar metals was found to be independent of temper and to decrease in the order (of coupled metals) Ti-150A > 60/40 naval brass > 1040 steel. The effect of dissimilar metal coupling was found to be reduced by the formation on the anode and cathode of insulating corrosion product structures; this also caused an increased domination of the attack by localized corrosion modes. The effect of edges and crevices in concentrating attack and the correlation between distribution of corrosion product and metal dissolution is discussed.

TABLE OF CONTENTS

I. INTRODUCTION ---------- 14

A. ALUMINUM IN MARINE APPLICATIONS ---------- 14

1. Background ---------- 14

2. Aluminum - Magnesium Alloys ---------- 14

3. Corrosion Problems ---------- 15

B. GALVANIC CORROSION ---------- 22

1. Background ---------- 22

2. Methods Used to Study Galvanic Corrosion ---------- 24

a. Potential Measurements ---------- 24

b. Current Measurements ---------- 24

c. Polarization Measurements ---------- 27

C. OBJECTIVES ---------- 28

II. EXPERIMENTAL ---------- 30

A. MATERIALS TESTED ---------- 30

1. 5086 Aluminum ---------- 30

2. 1040 Steel ---------- 30

3. 60/40 Naval Brass ---------- 31

4. Ti-150A Titanium ---------- 31

B. CORROSION TESTING OF PHYSICALLY COUPLED (PROXIMATE) DISSIMILAR METALS ---------- 31

1. Purpose ---------- 31

2. Apparatus and Test Conditions ---------- 32

3. Procedures ---------- 38

C. MEASUREMENT OF GALVANIC CURRENT DENSITY ------ 44

1. Purpose ---------- 44

2. Apparatus and Test Conditions ---------- 45

3. Procedure ---------- 48

D. MEASUREMENT OF POTENTIODYNAMIC ANODIC AND CATHODIC POLARIZATION CURVES ---------- 52

1. Purpose ---------- 52

2. Apparatus and Test Conditions ---------- 52

3. Procedure ---------- 55

III. RESULTS AND DISCUSSION ---------- 58

A. MICROSTRUCTURES OF ALUMINUM ALLOYS TESTED ---- 58

B. POTENTIODYNAMIC POLARIZATION TESTS ---------- 62

C. GALVANIC CURRENT DENSITY MEASUREMENTS -------- 69

D. CORROSION TESTING OF PHYSICALLY COUPLED (PROXIMATE) DISSIMILAR METALS ---------- 77

1. Morphology and Distribution of Precipitate Formations on the Cathodic Metal ---------- 77

2. Morphology of the Corrosion Product on the Aluminum Anode ---------- 88

3. Distribution of the Corrosion Product on the Aluminum Anode ---------- 105

4. Dissolution Damage to the Aluminum Anode Caused by Corrosive Attack --------- 110

IV. CONCLUSIONS ---------- 121

LIST OF REFERENCES ---------- 123

INITIAL DISTRIBUTION LIST ---------- 126

LIST OF TABLES

I. Comparison of Equilibrium Potentials (vs. SCE) for Various Metals ---------- 67

II. Average Galvanic Current Density ($\mu A/cm^2$) -------- 76

LIST OF FIGURES

1. Microstructure of exfoliation corrosion susceptible 5456-H321 hull plate [9] ---------- 18

2. Microstructure of exfoliation resistant 5456-H116 hull plate, 500X [9] ---------- 19

3. Microstructure of exfoliation resistant 5456-H117 hull plate, 500X [9] ---------- 20

4. Examples of zero resistance ammeter techniques [15]. (a) Electronic zero resistance ammeter with instantaneous null characteristics. (b) Use of potentiostat. (c) Use of an operational amplifier ---------- 26

5. Arrangement of equipment used for corrosion testing of physically coupled dissimilar metals -- 33

6. Conductivity bridge and electrode system used to measure electrolyte conductivity ---------- 35

7. Cambridge model S4-10 Steroscan Scanning Electron Microscope (SEM) with Princeton Gamma Tech (PGT) 1000 to left ---------- 37

8. Equipment used to form galvanic couple in plastic mount ---------- 40

9. 24X SEM photograph of joint formed between coupled dissimilar metals ---------- 42

10. 550X SEM photograph of joint between coupled dissimilar metals---------- 43

11. Arrangement of corrosion cell used to measure galvanic current density ---------- 46

12. Arrangement of potentiostat and strip chart recorder used to measure galvanic current density ---------- 47

13. Example of strip chart record obtained of galvanic current over a twenty-four hour period -- 51

14. Corrosion cell and working electrode used to obtain potentiodynamic polarization curves ------- 53

15. Arrangement of potentiostat, programmer and X-Y recorder used to obtain potentiodynamic polarization curves ---------- 54

16. 200X photographs of microstructure of 5086-H116 aluminum in two orientations (Kellers Etch) ----- 59

17. 200X photographs of microsctructure of 5086-H32 aluminum in two orientations (Kellers Etch) ----- 60

18. 200X photographs of microstructure of 5086-H117 aluminum in two orientations (Kellers Etch) ----- 61

19. Potentiodynamic polarization curves for:
1. Aluminum (anodic curve), and
2. 1040 Steel (cathodic curve) ---------- 63

20. Potentiodynamic polarization curves for:
1. Aluminum (anodic curve), and
2. TI-150A Titanium (cathodic curve) ---------- 64

21. Potentiodynamic polarization curve for:
1. Aluminum (anodic curve), and
2. TI-150A Titanium (cathodic curve) ---------- 65

22. Plot of galvanic current density versus time for 5086-H32 aluminum coupled electrically with: 1. TI-150A Titanium,
2. 60/40 Naval Brass, 3. 1040 Steel ---------- 70

23. Plot of galvanic current density versus time for 5086-H116 aluminum coupled electricity with: 1. TI-150A Titanium,
2. 60/40 Naval Brass, 3. 1040 Steel ---------- 71

24. Plot of galvanic current density versus time for 5086-H117 aluminum coupled electrically with: 1. TI-150A Titanium,
2. 60/40 Naval Brass, 3. 1040 Steel ---------- 72

25. Steel/H116 couple exposed for two weeks, 7X ----- 78

26. Brass/H32 couple exposed for two days.
(a) 6X. (b) 24X (SEM) ---------- 80

27. Corrosion product accumulation on titanium in TI/H116 couple exposed for three weeks.
(a) 23X (SEM). (b) 240X (SEM) ---------- 81

28. Corrosion product accumulation on titanium in TI/H32 couple exposed for two weeks.
(a) 22X (SEM). (b) 110X (SEM) ---------- 82

29. Corrosion product accumulations on cathodic metal. (a) Brass/H32 couple exposed for three weeks, 550X (SEM). (b) TI/H116 couple exposed for two weeks, 105X (SEM) ---------- 83

30. Corrosion product accumulation on steel in Steel/H32 couple exposed for one week, 540X (SEM) ---- 84

31. Corrosion product accumulation on steel in Steel/H32 couple exposed for three weeks. (a) 1150X (SEM). (b) 2300X (SEM) ---------- 86

32. Precipitate formation on steel in Steel/H32 couple exposed for three weeks. (a) 55X (SEM). (b) 105X (SEM) ---------- 87

33. Precipitate formations on brass in Brass/H32 couple exposed for two weeks, 230X (SEM) ---------- 89

34. Precipitate formations on brass in Brass/H32 couple exposed for eight weeks, 110X (SEM) ---------- 90

35. Precipitate formations on brass in Brass/H32 couple exposed for eight weeks. (a) 550X (SEM). (b) 550X PGT dot mapping of same area using characteristic calcium x-ray wavelength -------- 91

36. Precipitate formation remaining on cleaned brass in Brass/H32 couple exposed for eight weeks, 550X (SEM) ---------- 92

37. Brass/H32 couple exposed for one week, 7X ---------- 94

38. Corrosion product accumulation on H116 in TI/H116 couple exposed for three weeks. (a) 23X (SEM) (b) 1150X(SEM) 95

39. Typical corrosion product accumulation on H116 in Steel/H116 couple exposed for one week. (a) 150X (SEM) (b) 1150X (SEM) ---------- 96

40. Typical corrosion product accumulation on H116 in TI/H116 couple exposed for two weeks, 55X (SEM) ------ 97

41. Two types of corrosion product accumulations. (a) 570X (SEM) (b) 1100X (SEM) ---------- 98

42. Corrosion products on H32 in Steel/H32 couple exposed for one week, 2200X (SEM) ---------- 100

43. Corrosion product on H116 in Steel/H116 couple exposed for three weeks, 1100X (SEM) ---------- 101

44. Corrosion product on H32 in Steel/H32 couple exposed for three weeks, 540X (SEM) ---------- 102

45. Corrosion product on H32 in Brass/H32 couple exposed for one week, 575X (SEM) ---------- 103

46. Corrosion product on H32 in Steel/H32 coupled exposed for two days, 110X, (SEM)---------- 104

47. (a) Steel/H32 couple exposed for one week, 7X.
(b) Brass/H32 couple exposed for one week, 7X ------ 107

48. Cathode/anode joint area on TI/H32 couple exposed for three weeks. (a) 22X (SEM). (b) 52X (SEM) ---- 109

49. TI/H32 couple exposed for two days, 6X ---------- 112

50. TI/H32 couple exposed for two days. (a) 100X (SEM). (b) 500X (SEM) ---------- 113

51. Corrosive attack on (a) H32 in Steel/H32 couple exposed for three weeks, 55X (SEM). (b) H32 in Brass/H32 couple exposed for eight weeks, 55X (SEM) ---------- 114

52. 240X SEM photograph of plastic and metal (dark) interface on coupled specimen ---------- 116

53. (a) Brass/H32 couple exposed for two days, 550X (SEM).
(b) TI/H116 couple exposed for two days, 600X (SEM) ---------- 117

54. Steel/H32 couple exposed for two days, 1050X (SEM) - 118

55. (a) TI/H32 couple exposed for two weeks, 22X (SEM)
(b) Brass/H32 couple exposed for eight weeks, 550X (SEM) ---------- 119

TABLE OF SYMBOLS AND ABBREVIATIONS

E_{CORR}	Potential of individual metals
E_{COUPLE}	Potential of coupled metals
EMF	Electromotive force
H116	5086-H116 Al alloy
H117	5086-H117 Al alloy
H32	5086-H32 Al alloy
i_{couple}	Galvanic current density
mA	Milliampere
mV	Millivolt
N·cm	Newton-centimeter
SCE	Standard calomel electrode
SEM	Scanning electron microscope
V	volt
vs	versus
μA	Microampere
$\mu A/cm^2$	Microampere per centimeter squared
μm	Micrometer
>	Greater than

ACKNOWLEDGMENT

The author wishes to express his appreciation to Professor A.J. Perkins for the guidance provided during the conduct of the research and his special assistance given during the editing of the manuscript. Also, the support of Roy Edwards, Material Science Laboratory Technician, was instrumental in completion of this work as was the timely assistance of Ken Graham, Research Chemist.

I. INTRODUCTION

A. ALUMINUM IN MARINE APPLICATIONS

1. Background

The use of aluminum for marine applications dates back to 1890 when the 5.2 m vessel "Zepher" was launched [1]. By 1960 more than 1000 merchant ships were using substantial amounts of aluminum for structural applications [1]. In U.S. Navy ships, most of the superstructure above the main deck is made of aluminum. Additionally, many other uses for aluminum are found throughout the ship. For example, the USS DEWEY was built containing about 167 tons of aluminum, mostly 5456-H321 plate and 5086-H32 sheet [1]. Aircraft carriers such as the USS INDEPENDENCE carry about 900 tons of aluminum while a GEORGE WASHINGTON class submarine has about 20 tons of aluminum [1]. Additionally many all-aluminum craft such as submersibles and patrol boats, have been and are still being built. Since the use of aluminum saves weight, we can expect use in ever-increasing quantities, especially on the forthcoming generation of high speed surface effect ships and craft.

2. Aluminum-Magnesium Alloys

Aluminum has good corrosion resistance to the atmosphere and to many aqueous media [2]. It is a reactive metal, being very active in the EMF series, but develops an oxide coating or film that protects it in many environments. As

was shown by Pourbaix [2] in his work with potential versus pH diagrams, the corrosion behavior of aluminum is determined essentially by the formation and behavior of the passivating layer of oxide film, Al_2O_3. This oxide film is generally complex and can consist of $Al_2O_3 \cdot H_2O$ bohmite, $Al_2O_3 \cdot 3H_2O$ bayerite or $Al_2O_3 \cdot 3H_2O$ hydragillite [2]. Hart [3] showed the film formed on pure aluminum immersed in water (at temperatures less than 60°C) develops in three stages: first amorphous hydroxide is formed, then orthorhombic γ-AlO·OH and then bayerite. The final film according to Hart is then made up of three layers. This film of Al_2O_3 is estimated to be 20Å to 100Å thick when formed in air [4].

Aluminum alloy with Mg content up to three percent has a corrosion resistance about the same as pure aluminum and low mechanical strength [5]. Increasing the amount of Mg increases the strength of the alloy but lowers its corrosion resistance somewhat. This is due to the magnesium being more anodic than the aluminum. The aluminum alloys designated 5086, 5456 and 5083, containing four to five percent magnesium, are used extensively in marine vehicle applications. In addition to corrosion resistance, they have good weldability and high strength to weight ratio [6]. Typically, the strain hardened tempers designated as 5086-H32, 5083-H321 and 5456-H321 were selected.

3. Corrosion Problems

It was known by naval architects and marine engineers that galvanic corrosion would occur when (5XXX series)

aluminum was coupled with other structural metals, which are typically more noble than aluminum. Therefore, features for prevention of this type of corrosion were incorporated into the designs of marine vehicles using aluminum. This was normally accomplished through the use of insulating materials to prevent electrical contact and paint coatings to prevent electrolyte contact with a dissimilar metal. For a variety of reasons corrosion problems did develop [7]. Strasburg [8], reported the considerable expenditure of maintenance effort required to repair damage at the aluminum superstructure to steel deck interface on destroyer type ships. He also found extensive corrosion damage on aluminum plate adjacent to pipe penetrations.

Additionally, corrosion problems were encountered in the bilge areas of aluminum-hulled (5456-H321) patrol boats used in Vietnam [9]. These boats experienced extensive exfoliation corrosion. The conditions that existed in the bilge areas of the boats were extremely favorable to the initiation of pitting corrosion. Pitting would start and then give way to exfoliation or intergranular corrosion once the interior metallurgical structure of the alloy was opened up. The exfoliation susceptibility of 5456-H321 was related primarily to an elongated grain structure with relatively continuous precipitation of a Al_3Mg_2 phase along the grain boundaries [9].

The H32 and H321 tempers apply to products which are strain hardened and then stabilized by a low-temperature heat treatment to slightly lower the strength and to increase ductility and stress-corrosion resistance. This process results in a microstructure in which the precipitate is present in a continuous line. Doig and Edington [10] in their work with a Al-7.2 percent Mg alloy, explained that the microstructure may be divided into three regions; the grain boundary precipitate of Al_3Mg_2, its associated solute depleted zone, and the matrix with bulk composition. The corrosion is then determined by the respective electrochemical properties of these three regions. The Al_3Mg_2 is more anodic than the matrix or the adjacent solute-depleted zone [10,11]. This anodic precipitate is attacked and eaten away. The corrosion products which form occupy more space than the metallic compound and therefore exert a force on the metal which causes delamination. This is called exfoliation. To prevent exfoliation, the continuous network of the Al-Mg precipitate must be broken up. To do this Reynolds developed the H116 temper and Alcoa developed the H117 temper for both 5456 and 5086 alloys [11].

The H116 and H117 tempers apply to products which are strain hardened less than quarter-hard and do not undergo a stabilizing heat treatment [11]. These alloys both have a grain structure predominately free of continuous grain boundary network as opposed to the continuous grain boundary network found in the H32, and H321 tempers. Figures 1, 2 and 3

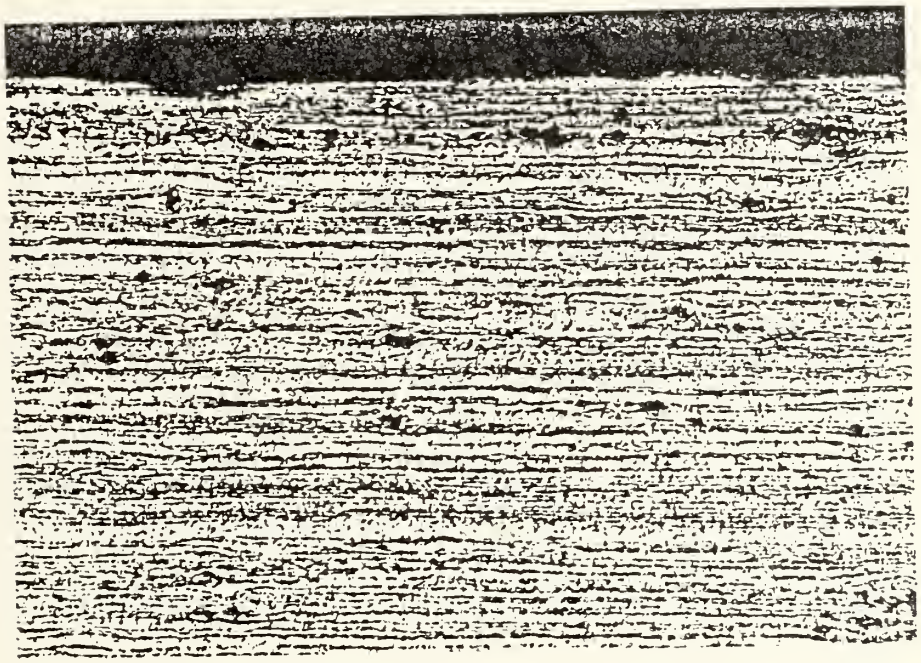

Figure 1. Microstructure of exfoliation corrosion susceptible 5456-H321 hull plate [9]

Figure 2. Microstructure of exfoliation resistant 5456-H116 hull plate, 500X [9]

Figure 3. Microstructure of exfoliation resistant 5456-H117 hull plate, 500X [9]

show examples of the typical grain structures of 5456 aluminum alloy in the three different tempers.

However, even with these tempers, a sample which contains continuous precipitate can be formed by natural aging. Since 5456 contains five percent Mg while 5086 contains only four percent Mg, this problem occurs more readily in 5456 [12]. Work by Czyryca and Hack [11], suggests that the H116 temper produces material less susceptible to natural aging.

The use of the H116 and H117 tempers should give improved performance, with respect to exfoliation and intergranular corrosion. However, corrosion will still occur whenever galvanic couples are allowed to exist.

To combat the severe corrosion that was occurring at the aluminum superstructure-steel deck interface, the Navy is now using an explosively bonded joint for repair of old corroded joints and for installation on new construction [7]. The use of explosive bonded material eliminates the mechanical crevice normally present at the joint. However, when exposed to a corrosive marine environment, corrosion does occur preferentially at the bond interface as was shown by Keelean [7]. The extent to which this detracts from the mechanical properties of the bond is unknown.

Even with the above advances in corrosion control, galvanically induced corrosion occurring between Al alloys and other metals is still a problem in marine applications.

In many cases the most efficient design requires the use of dissimilar metals. Criteria such as strength, fabricability, cost, availability and appearance are, many times, weighed more heavily than corrosion control in the design process [13]. Numerous examples can be cited. As previously mentioned, pipe penetrations through an aluminum bulkhead usually brings steel and aluminum together. Watertight doors which penetrate the aluminum superstructure also provide a place for galvanic corrosion to take place. For strength reasons, brackets on aluminum bulkheads usually involve steel nuts and bolts. Heavy equipment mounted above the main deck usually requires steel for support and provides another opportunity for galvanic corrosion.

B. GALVANIC CORROSION

1. Background

Galvanic corrosion occurs when two or more metals in electrical contact are also in contact through an electrolyte. To predict the behavior of a metal in a galvanic couple, a galvanic series is often used. This series is constructed by listing the different metals according to their equilibrium potentials in a specific environment. Metals with more active potentials become the anode, and metals with more noble potential become the cathode when the two metals are electrically coupled. A galvanic series of some metals in flowing sea water is given by LaQue [14]. The damage incurred by coupling the two metals is dependent

on many factors, one of which is separation on the galvanic series (open circuit potential difference). The further apart, (greater the potential difference) the more damage. However, the area ratio of the two metals, the polarization behavior of the metals, and the conductivity of the electrolyte are also important factors. The simple approach of selecting metals based on the galvanic series can be a poor indicator of galvanic corrosion rates, as pointed out recently by Mansfeld and Kenkel [15]. When the two metals in a electrolyte are coupled, both metals are polarized so that each corrodes at a new rate. The corrosion rates are changed to the extent that the more active metal corrodes more and the more noble metal corrodes less. This change, called polarization, is defined as the extent to which the potential of the metal is changed due to the induced galvanic current. The more active metal is polarized along its anodic polarization curve in the direction of increasing potential (becoming more noble in potential), the more noble metal is polarized along its anodic polarization curve in the direction of decreasing potential (becoming more active in potential). The behavior of the metal as it is polarized is extremely important in determining the final equilibrium potential between the two metals, the galvanic corrosion current and the ensuing metal dissolution of the anode.

Techniques for predicting galvanic corrosion include potential measurements, current measurements, and polarization

measurements. As pointed out by Baboian [16], only by using these methods can an overall characterization of the behavior of the metal in a galvanic couple be completed.

2. Methods Used to Study Galvanic Corrosion

a. Potential Measurements

Potential measurements are used to construct a galvanic series which can be quite useful when the polarization characteristics for the metals are straightforward [17]. However there are other factors which can significantly decrease the usefulness of this method. For example, if a surface film forms so that the metal remains passive, then that film will influence the corrosion rate over a wide range of potentials. Also, the potential of a metal may vary with time thus changing its position on the galvanic series. Additionally, the polarizability of the metal could change according to the environment and time. From the above, it can be seen that the simple measurement of the corrosion potential, while useful, does not yield enough information on which to base a prediction of galvanic corrosion behavior.

b. Current Measurements

There are various ways to measure the current flowing between two electrically coupled dissimilar metals which are immersed in an electrolyte. The first and most obvious way is to measure the voltage drop across a known resistance. This method is considered unsatisfactory because the two metals are not at the same potential but are separated

by the resistor voltage drop. This causes the measured value of the current to be smaller than the actual galvanic current [15]. Additionally the effect of the reduced polarization caused by this voltage difference could give misleading conclusions when comparing results obtained for different dissimilar metal couples. This would be dependent upon the polarization characteristics of each metal. Early attempts to remove the effect of the resistor were described originally by Brown and Mears in 1938 and referenced recently by Mansfeld and Kenkel [15]. These involved using a set of switches and balancing circuitry. This introduced transients when the system was not in balance which required a recovery period, and could not be used for continuous observations.

Numerous investigators, including Cummings [18] in this laboratory, have had success using a clip-on milli-ammeter to measure the current through an extremely low resistance wire connecting the two metals. However, this system is limited to currents greater than 300 μA.

The systems currently in greatest use take advantage of operational amplifiers to maintain a zero potential difference between the two dissimilar metals while measuring by some means the current required to do this. The balancing current then equals the galvanic current.

An "electronic zero resistance ammeter with instantaneous null characteristics" was developed by Henry and Wilde and is shown in Figure 4(a). The principle of

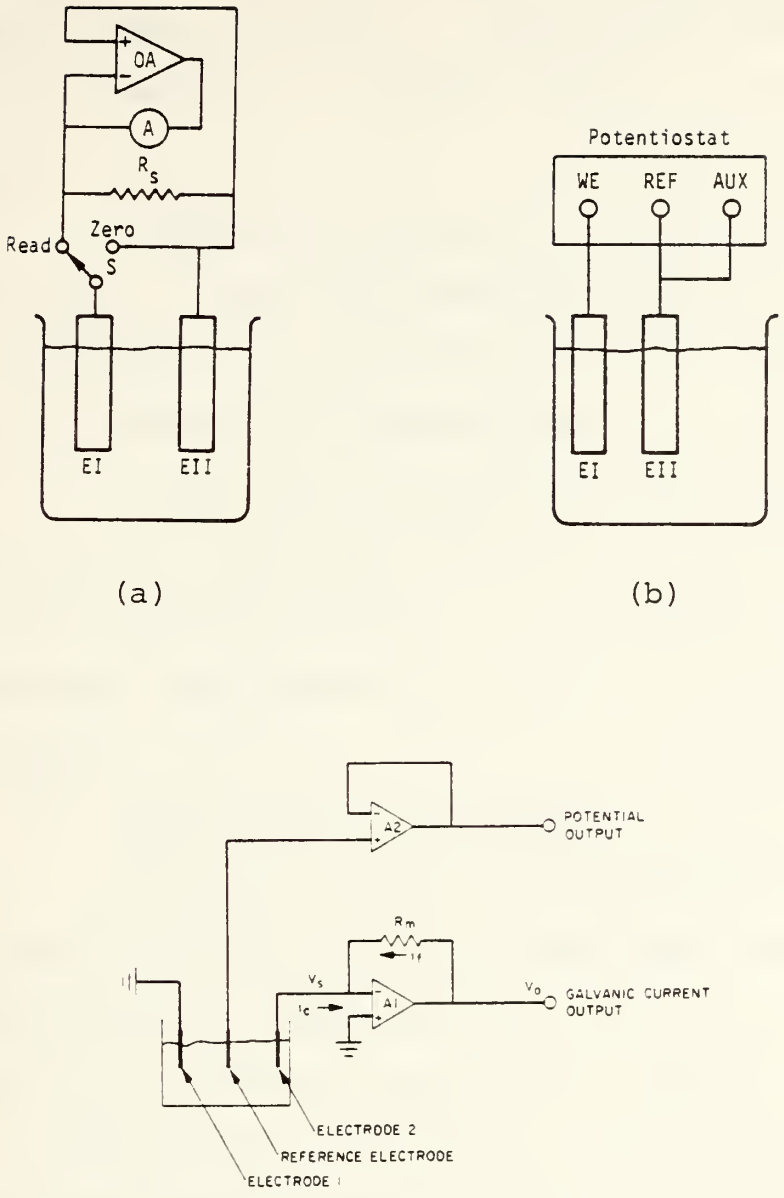

Figure 4. Examples of zero resistance ammeter techniques [15], (a) Electronic zero assistance ammeter with instantaneous null characteristics, (b) Use of potentiostat, (c) Use of an operational amplifier

operation is based on the use of an operational amplifier to replace manual balancing. The galvanic current is read on the microammeter, A, when the switch is in the "read" position.

A method for the use of a potentiostat is shown in Figure 4(b). With the potentiostat set at zero millivolts applied potential, the galvanic current is read directly on the current meter of the potentiostat.

A simple use of an operational amplifier is shown in Figure 4(c). The output voltage, V_o, is directly proportional to cell current. In this system the potential of the couple with respect to a reference electrode can also be measured.

c. Polarization Measurements

Polarization behavior is important since metals that corrode uniformly as an isolated metal may undergo severe localized corrosion when polarized [16] or may become passive. Therefore it is important to know the shape of the potential versus current curve to be able to predict the equilibrium potential and current density of the coupled metals. This may be done by adding the currents of the cathodic curves to get a total cathodic curve then adding the currents of the anodic curves to get a total anodic curve. The intersection of the total anodic and total cathodic curves will give a equilibrium potential and current density. Or, if the potential of the couple has already been measured, then the

current density may be predicted by finding the intersection of the horizontal line equal to the potential and the anodic curve for the particular metal.

C. OBJECTIVES

The objectives of the present research were to investigate and characterize the behavior of the aluminum alloy designated 5086 when coupled with other, more noble, metals and immersed in seawater. In so doing, it was intended to add to the understanding of the basic mechanisms involved in galvanic corrosion situations.

5086 aluminum was selected because of its widespread use in marine applications. Since recent work had been carried out in the development of two new tempers to reduce exfoliation susceptibility of that alloy, it would also be convenient to use it in its three temper conditions to investigate the effect the microstructural differences would have on the processes involved in galvanic corrosion.

The general plan of attack was to corrode bimetallic couples in synthetic seawater for various lengths of time after which the corrosion product formation and distribution would be studied macroscopically and microscopically. Corrosion product formation and distribution along with the resulting damage to the anodic metal would be correlated with the macroscopic and microscopic features of the base metal.

Also of interest was the effect of coupling with metals at a variety of more noble potentials in the galvanic series

and changes with increasing time of exposure. Polarization curves and galvanic current density data would be used to gain an understanding of the dynamics associated with the different couples and to correlate macroscopic and microscopic data with the processes that had taken place thereby rounding out the characterization.

Three metals noble in potential to aluminum were selected based on their position in the galvanic series for flowing seawater. The three were selected so that one (steel) was near aluminum in potential, one (titanium) was near the noble end of the galvanic series and the third (brass) was roughly half-way in between. By using these three, the effect of coupling at different open circuit potential differences could be studied. Experimental procedures were then developed to meet the above objectives.

II. EXPERIMENTAL

A. MATERIALS TESTED

1. 5086 Aluminum

5086 aluminum alloy was obtained in H32, H116, H117 tempers. Unless otherwise stated, materials already on hand in the NPS Mechanical Engineering Department were used. The 5086-H32 alloy was in the form of a piece 8 cm by 13 cm cut from a sheet of 0.483 cm thickness; the sheet was marked as being manufactured by Alcan Aluminum Corp. The H116 was in the form of various sized sheets of thickness 0.483 cm, marked as being manufactured by Kaiser Aluminum. The H117 was obtained on request from Mare Island Naval Shipyard in the form of two 10 cm by 27 cm plates of 1.427 cm thickness and was not marked as to the manufactuer. 5086 aluminum alloy has a specified nominal percentage chemical composition of 0.45 manganese, 4.0 magnesium, 0.15 chromium, and the balance aluminum [19]. Percentage compositional limits are specified as 3.5 - 4.5 magnesium, 0.5 iron, 0.2 - 0.7 manganese, 0.4 silicon, 0.25 zinc, 0.05 - 0.25 chromium, 0.1 copper, and 0.15 titanium.

2. 1040 Steel

Pieces of 1040 steel in the form of charpy V-notch samples, 1 cm by 1 cm by 5 cm, were obtained. Nominal percentage composition of 1040 steel is specified, as 0.37 - 0.44 carbon, 0.50 - 0.90 manganese, maximum of 0.040 phosphorus, maximum of 0.050 sulfur, and the balance iron [20].

3. 60/40 Naval Brass

A round bar of 60/40 naval brass was obtained. It was approximately 2.5 cm in diameter and 30 cm long. The nominal percentage composition for naval brass is 60 copper, 0.75 tin, and the balance zinc [20].

4. Ti-150A Titanium

A square bar of titanium, 1.25 cm by 1.25 cm by 35 cm, labeled Ti-150A, was obtained. Nominal percentage composition for this metal is specified as 2.7 chromium, 1.3 iron, 0.02 nitrogen, maximum of 0.04 tungsten, 0.02 carbon and the balance titanium [20].

B. CORROSION TESTING OF PHYSICALLY COUPLED (PROXIMATE) DISSIMILAR METALS

1. Purpose

The purpose of this test was to expose various bimetallic couples in synthetic seawater in order to study the corrosion product morphology and distribution on the anodic member. The anodic member was in all cases one of the three temper types of 5086 Al, while the cathodic member was one of the three other metals (steel, brass, or titanium). Testing was accomplished by mechanically mating the two different metals in such a way that a relatively crevice-free joint was produced. The samples were so designed that they could subsequently be examined in a scanning electron microscope (SEM) without disturbing their corrosion product formations. In design of all test procedures, the guidelines

set down in National Association of Corrosion Engineers Standard TM-01-69 were carefully followed [21].

2. Apparatus and Test Conditions

The apparatus used to contain the synthetic seawater and sample is shown in Figure 5. An eight cell system was used, thus allowing eight different samples to be exposed at the same time. Each cell consisted of a 1000 ml beaker filled with 1000 ml of synthetic seawater prepared according to Kester et al. [22]. The following amounts of gravimetric and volumetric salts, combined with enough distilled water for a total weight of 1 kilogram, were used per kilogram of synthetic seawater solution:

Gravimetric Salts

salt	g/kg of solution
NaCl	23.926
Na_2SO_4	4.008
KCI	0.677
NaHCO	0.196
KBr	0.098
H_3BO_3	0.026
NaF	0.003

Volumetric Salts

salt	Conc (Moles/Liter)	ml/kg of solution
$MgCl_2 \cdot 6H_2O$	1.000	53.27
$CaCl_2 \cdot 2H_2O$	1.000	10.33
$SrCl_2 \cdot 6H_2O$	0.100	0.90

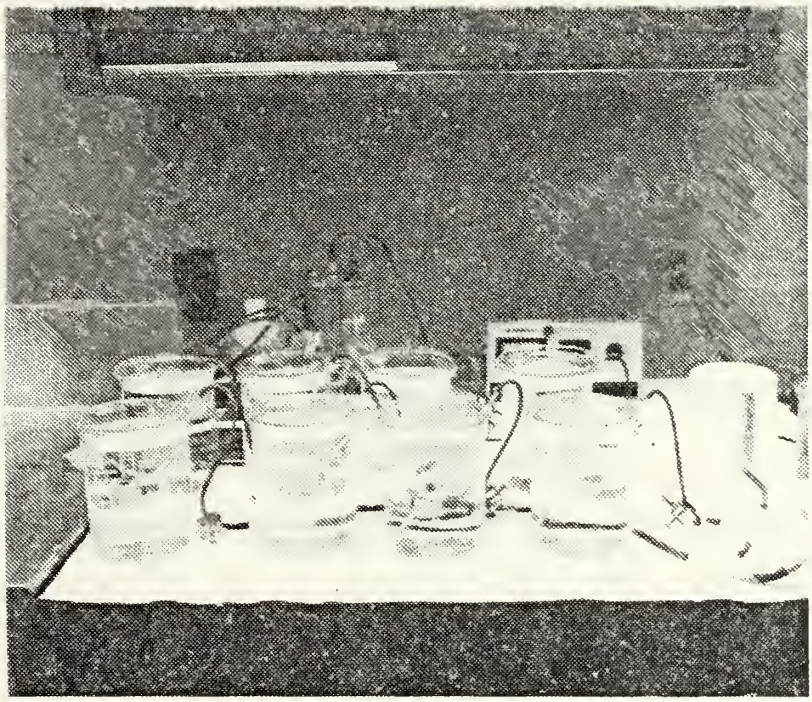

Figure 5. Arrangement of equipment used for corrosion testing of physically coupled dissimilar metals

Oxygen concentration was maintained at a constant saturated level through the use of an air sparging system. Physically, this was accomplished by pumping air from an aquarium type pump through a system of rubber hoses into each beaker via a small glass tube. Volume control of the air was accomplished by adjusting the screw type clamps located one on each hose and one on a pump hose. The pump hose, which was vented to the atmosphere, was used to reduce back pressure. The beakers were covered with watch glasses to prevent contamination and reduce evaporation.

Hydrogen ion concentration was measured with a Photovolt Corporation Model 115 Electronic pH meter. A Beckman pH 9.18 Buffer was used to standardize the instrument prior to use. pH measurements averaged 8.22 and varied from 8.1 to 8.5 with a standard deviation of 0.07 units.

Conductivity was measured with a Barnstead Conductivity Bridge Model PM-70CM and a sensing electrode set as shown in Figure 6. The bridge and electrode set combination were calibrated using a 0.020 normal KCl solution. A correction factor of $404. cm^{-1}$ was computed. This factor was divided by the bridge reading in ohms to get conductivity in millimhos per cm. Conductivity measurements averaged 48.6 millimhos per cm and varied from 47.0 millimhos per cm to 49.9 millimhos per cm. One standard deviation was found to be 0.7 millimhos per cm.

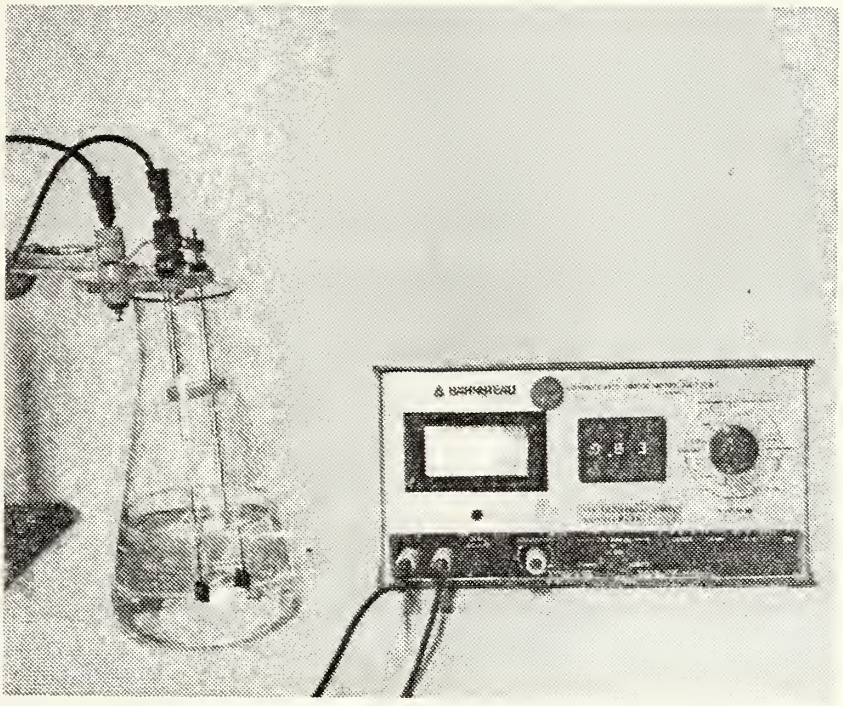

Figure 6. Conductivity bridge and electrode system used to measure electrolyte conductivity

The temperature of the corrosive medium was allowed to change to stay in equilibrium with the room temperature. Room temperature averaged about 21.5°C and varied from a low of 18°C at night during the month of May to a high of 24°C during the day in August. Normal day/night variations were about ± 1.5°C.

A Cambridge Model S4-10 Stereoscan Scanning Electron Microscope (SEM) (Figure 7) was utilized to study the corrosion product morphology and distribution and the damage resulting from the corrosive attack. Also shown to the left in Figure 7 is a Princeton Gamma Tech (PGT) 1000 energy-dispersive X-ray analyzer. This system enables the operator to identify elements present in the SEM field of view through processing of X-rays emitted by the specimen atoms. Additionally, the operator may choose to present on the SEM a mapping of the locations of material emitting X-rays characteristic of a certain element. This provides a map of elemental distribution which can be photographed and compared with the SEM photograph to correlate physical features with the presence or absence of a certain element. This capability is a valuable aid for identification of corrosion products.

Various light microscopes were also used to observe and photograph the samples to provide a record of the distribution of corrosion products after exposure. A 35mm camera with close-up lenses was also used to obtain 35mm color slides of corrosion product distribution.

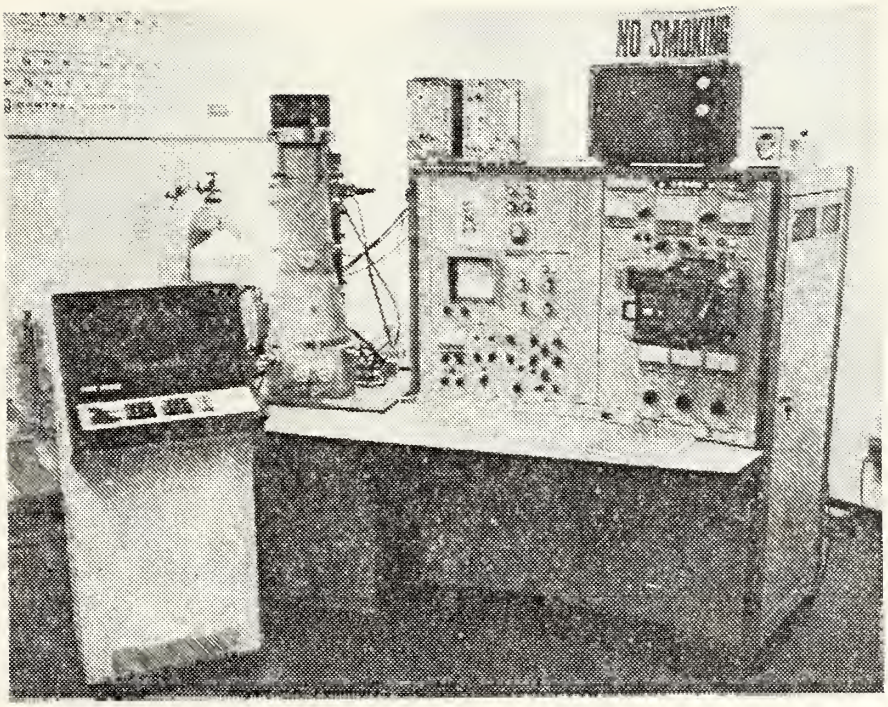

Figure 7. Cambridge model S4-10 Steroscan Scanning Electron Microscope (SEM) with Princeton Gamma Tech (PGT) 1000 to left

3. Procedures

The nine couples tested were as follows:

	ANODE	CATHODE
1.	5086-H32 Al	1040 Steel
2.	5086-H32 Al	60/40 Naval Brass
3.	5086-H32 Al	Ti-150A Titanium
4.	5086-H116 Al	1040 Steel
5.	5086-H116 Al	60/40 Naval Brass
6.	5086-H116 Al	Ti-150A Titanium
7.	5086-H117 Al	1040 Steel
8.	5086-H117 Al	60/40 Naval Brass
9.	5086-H117 Al	Ti-150A Titanium

The six different metals to be tested were milled into square test coupons 1 cm by 1 cm of thickness about 0.48 cm. In the case of the Al, at least one face was left untouched so that it could later be mounted exposed to the synthetic seawater with the direction of rolling horizontally oriented.

The individual coupons were first mounted in a cylindrical plastic mount, using a quick setting plastic, with one of the 1 cm by 0.48 cm sides exposed. The exposed side was lightly sanded flat on a 180 grit belt sander. The coupon was then broken out of the plastic sanding mount. Next, a bimetallic couple with a flat tight electrically conductive joint was formed by joining the sanded surfaces. The device used to form the bimetallic couple is shown

in Figure 8. It consists of a ring into which has been drilled and tapped two diametrically opposed holes. Through these holes are threaded two 4-40 thread screws which were then torqued, using the torque wrench shown in the figure, to 0.7N·cm to hold the two metals together, with a constant and reproducible stress. Then, a quick setting plastic was mixed and poured into the ring to harden. After hardening, the screws were removed and the plastic with the couple encased was removed. The finished couple in plastic is shown to the right in Figure 8.

After the plastic had hardened the sample was sanded with a 50 grit belt sander on both the front and back to remove excess plastic. This was done on the front only to the point that metal was exposed. On the back however a large portion of the plastic was removed to thin the sample so it would fit in the SEM. After this initial sanding, the sample back was ground on a grinding wheel to remove additional plastic to expose the two metals. This area would later be painted with silver conducting paint for SEM mounting.

The grinding was followed by sanding the face of the sample first on the 180 grit belt sander until all plastic was removed from the metal faces and the surfaces were flat This was followed by fifty strokes of hand sanding on 0 grit paper. Additionally, a hole was drilled in the plastic portion of the sample to allow it to hang so that the joint was vertical when immersed.

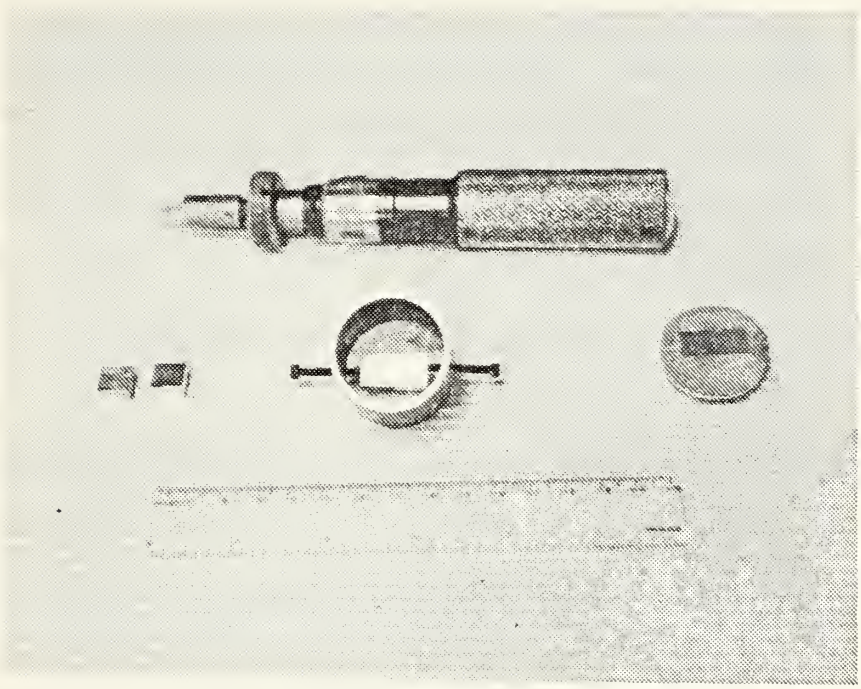

Figure 8. Equipment used to form galvanic couple in plastic mount

The above steps illustrate the initial sample preparation. For about one day prior to immersion 1000 ml of synthetic seawater were aerated in the beaker to be used. When the sample was to be immersed, the following sequence of steps would take place. First the face was sanded with fifty strokes by hand on 000 grit paper this was followed by cleaning in an ultrasonic bath with tap water, then rinsing in alcohol, then blow drying under warm air. The samples were then placed in a vacuum desicator for about fifteen minutes to remove any traces of water. The exposed backs of the samples and the holes left by the bolts were then filled with hot liquid paraffin which was then allowed to cool and solidify. The above procedure was able to produce a high quality crevice free joint as shown in Figures 9 and 10.

After the paraffin hardened, a piece of nylon thread was cut for use in hanging the sample in thewater. Conductivity and pH were measured and recorded. Then the sample was immersed using the nylon thread and masking tape to hold it in midwater in the beaker.

The different samples were immersed for one day, one week, two weeks, and three week exposure periods. One additional sample was exposed for eight weeks for comparison purposes. After the specified exposure period was over the individual sample was removed from the synthetic seawater and dipped in distilled water for about three seconds. After dipping, photographs were taken of the condition of the

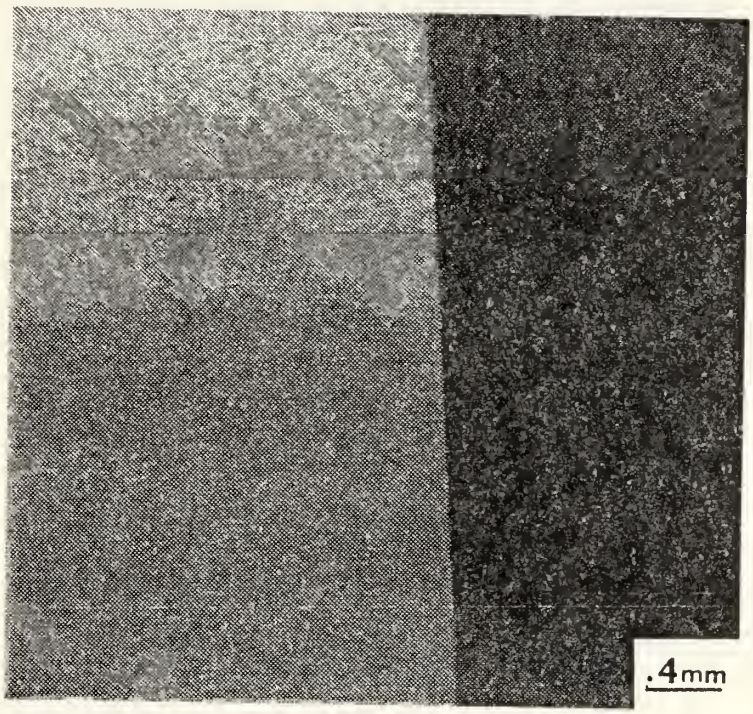

Figure 9. 24X SEM photograph of joint formed between coupled dissimilar metals

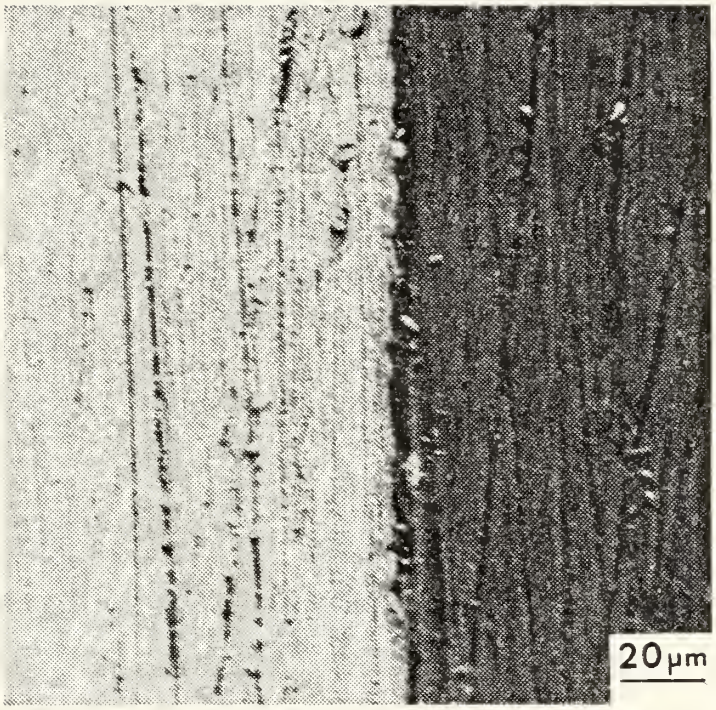

Figure 10. 550X SEM photograph of joint between coupled dissimilar metals

sample while still wet and also after drying, using both a low power light microscope and a 35 mm camera. At the same time observations were logged as appropriate.

Next the wax was removed from the back of the sample thus exposing the metal. Silver conducting paint was painted on the bottom of the sample and used to "glue" the sample to the SEM mounting stub. The sample was then examined in the SEM using the energy dispersive X-ray analyzer when required. Observations were logged and recorded on Polaroid film when deemed necessary.

After SEM observations, the samples were cleaned using distilled water and a commercial cleaning product called Micro mixed to the manufactures recommendations. This solution was used in an ultrasonic cleaner to clean the samples for ten minutes. After cleaning, they were rinsed in distilled water, then rinsed in alcohol, and then air dried. Observations of corrosion damage were then made using the SEM. Whenever the samples were not being examined in some way they were stored in a vacuum desicator.

C. MEASUREMENT OF GALVANIC CURRENT DENSITY

1. Purpose

The purpose of this test was to expose the same bimettalic couples to the same environment of the physically coupled samples and to record the galvanic current between the two. These measurements would, as explained in the introduction, give an indication of the corrosion rates of

the various couples to be correlated with the observations made on the physically coupled samples and with the potentiodynamic polarization curves obtained.

2. Apparatus and Test Conditions

The corrosion cell used for these measurements is shown in Figure 11. The cell consisted of a 1000 ml beaker which was filled with 1000 ml of synthetic seawater prepared as previously described. Oxygen concentration was maintained at a constant saturated level through the use of an air sparging system arranged as previously shown for the physically coupled cells. The beaker was covered with a watch glass as before. The same equipment was used to measure pH, which averaged 8.2 and varied from 8.1 to 8.3. Conductivity was also measured in the same way as the physically couled samples and averaged 48.0 millimhos per cm and varied from 45.9 to 49.9 millimhos per cm. The temperature of the liquid was allowed to equilibrate with the room air temperature which varied from 21°C to 24°C.

A Princeton Applied Research Model 173 Potentiostat/Galvanostat shown in Figure 12 was used as a zero impedance ammeter to maintain zero potential between the two dissimilar metals while at the same time measuring galvanic current. The measured current output of the potentiostat was monitored as a function of time using a Hewlett Packard 7100B Strip Chart Recorder shown to the left in Figure 12.

Figure 11. Arrangement of corrosion cell used to measure galvanic current density

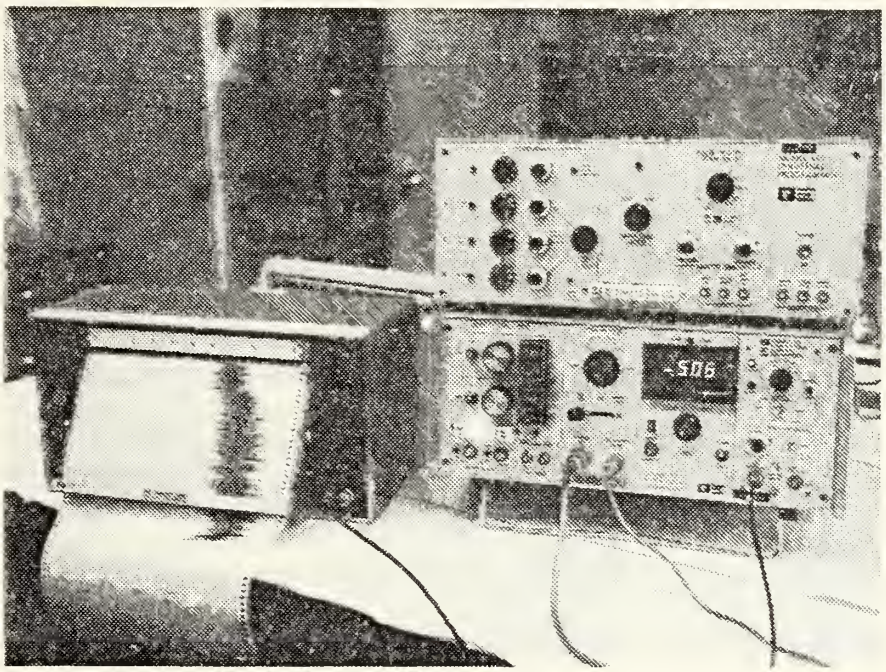

Figure 12. Arrangement of postentiostat and strip chart recorder used to measure galvanic current density

3. Procedure

Nine runs were made using this procedure. In each run, a different anode/cathode combination of an Al alloy and one of the three other metals was used.

For this test, one cm square test coupons milled as before were drilled and tapped for 3-48 threads on one of the 1 cm by .483 cm sides. In the case of the Al the tapping was done so the hole was perpendicular to the rolling direction.

The same rings that were used to form the bimetallic couple were used as molds to form the plastic around the single coupon. Through one of the holes in the ring was threaded a 3-48 thread screw which was also threaded onto the test coupon. The screw was lightly greased with silicon grease for ease of removal. The other hole was plugged. Quick drying plastic was then mixed and poured into the mold. Upon drying, the screw was removed and the plastic with the test coupon encased was removed from the ring mold. The rest of the specimen preparation was identical to that previously described for the physically coupled samples.

Additionally, a 12 gauge copper wire was cut into two 20 cm lengths. Both ends of each wire were stripped of insulation for about 1.5 cm. One end of each were immersed in hot wax then threaded into the plastic encased coupon. Additional wax was swabbed onto the joint between the wire insulation and the plastic to seal it. Continuity was then

checked between the wire and the exposed face of the sample using an ohmmeter. The two finished anode and cathode are shown in Figure 11 as they would sit in a beaker. To ensure the distance between the two was always equal, the two plastic pieces were always touching on the plastic edge between them.

Prior to immersion, the potentiostat and strip chart recorder were turned on and various initial settings were made. The potentiostat was set up as follows:

Channel A +0.000 Volts,
Channel B +0.000 Volts,
Push button A,
External signal off,
Operating mode switch in control E,
Cell selector off,
Meter in Current and in position 1,
1 mA full scale,
Input filter 10ms.
IR compensation off,
Meter Mode in I output.

The Strip Chart recorder which had been previously calibrated to the potentiostat's 0 to 1 volt output was set to 2 in. per hour and 1 volt range. A BNC jack connected the I output connection of the potentiostat with the input to the recorder. Upon immersion, the working lead of the potentiostat was connected to the wire from the Al and the auxiliary electrode lead was connected to the wire from cathodic member. Additionally another lead normally used for the reference electrode was connected to the wire from the cathodic metal and terminated at the electrometer probe. Three minutes after immersion the cell selector switch on

the potentiostat was switched to "external cell" thus enabling the circuitry. At the same time, the full scale current was changed as required to keep the indicator within range on the strip chart recorder. Normally, an initial 1 mA full scale was used for a few minutes and then changed to 100 μA full scale as the current changed.

For each run, pH, conductivity, start time, and full scale setting was recorded. After the 24 hour run was complete, the chart data was used to plot galvanic current density versus time on graph paper. To do this, the strip chart records were converted to tabular data by recording the value of current at intervals of one hour and at other selected times to retain the shape of the curve. Since there was considerable variation of the trace on the recorder paper, as shown in the sample trace on Figure 13, the value selected was the mean at that particular point (time). The tabulated valves of current were then used to plot the curves of current density versus time. The direct conversion from current to current density was made possible through the use of the one-square-cm test area.

Upon completion of the run the samples were removed, dipped in distilled water, air dried, and stored in a vacuum desiccator.

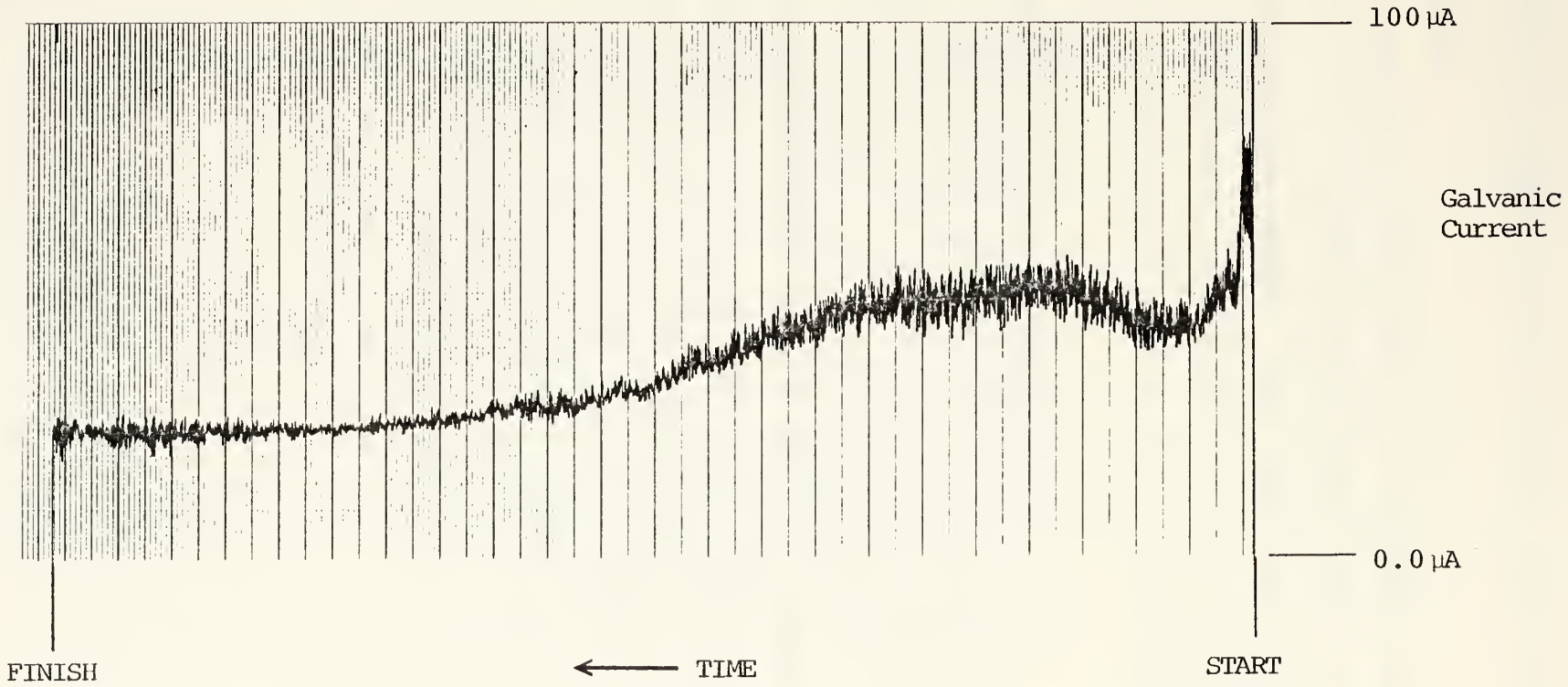

Figure 13. Example of strip chart record obtained for galvanic current over a twenty-four hour period

D. MEASUREMENT OF POTENTIODYNAMIC ANODIC AND CATHODIC POLARIZATION CURVES

1. Purpose

The purpose of this test was to obtain the characteristic anodic and cathodic polarization curves for the different metals being tested. This data was to be correlated with the galvanic current density measurements and the observation of the corrosive attack on the physically coupled samples.

2. Apparatus and Test Conditions

The corrosion cell used for these measurements is shown in Figure 14. The working electrode is shown to the left in the figure with a prepared sampled attached. The reference electrode shown inserted is a standard calomel reference electrode. The auxiliary electrodes are graphite rods. Oxygen concentration was maintained at a constant saturated level through the use of an air sparging system. This system consisted of an air pump pumping air through a rubber hose to an assembly containing an air stone which was immersed in the corrosion cell. The previously described equipment was used to measure pH and conductivity. pH averaged 8.14 and varied from 8.0 to 8.2. Conductivity averaged 47.9 millimhos per cm and varied from 47.0 to 48.7 millimhos per cm. The temperature of the liquid was allowed to equilibrate with the room air temperature which varied from 21°C to 24°C. Figure 15 shows the Princeton Applied Research Model 173 Potentiostat/Galvanostat, the Princeton

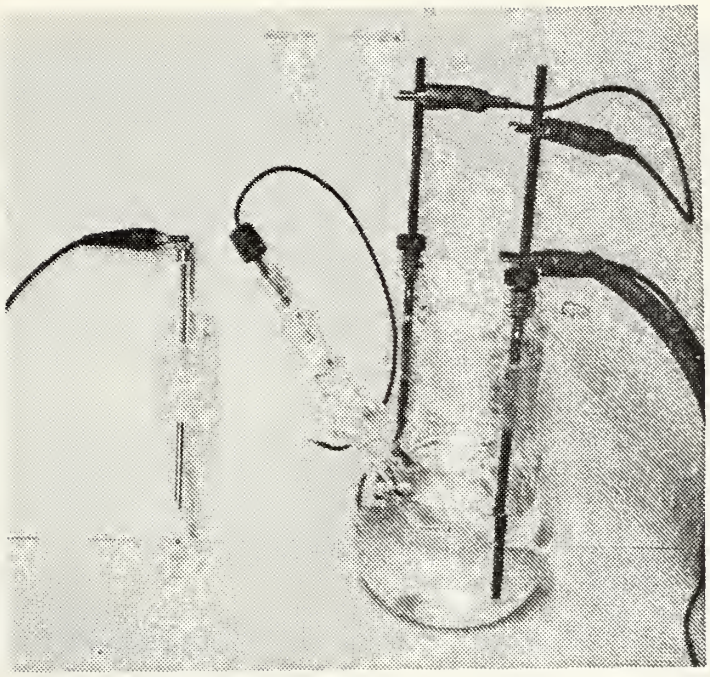

Figure 14. Corrosion cell and working electrode used to obtain potentiodynamic polarization curves

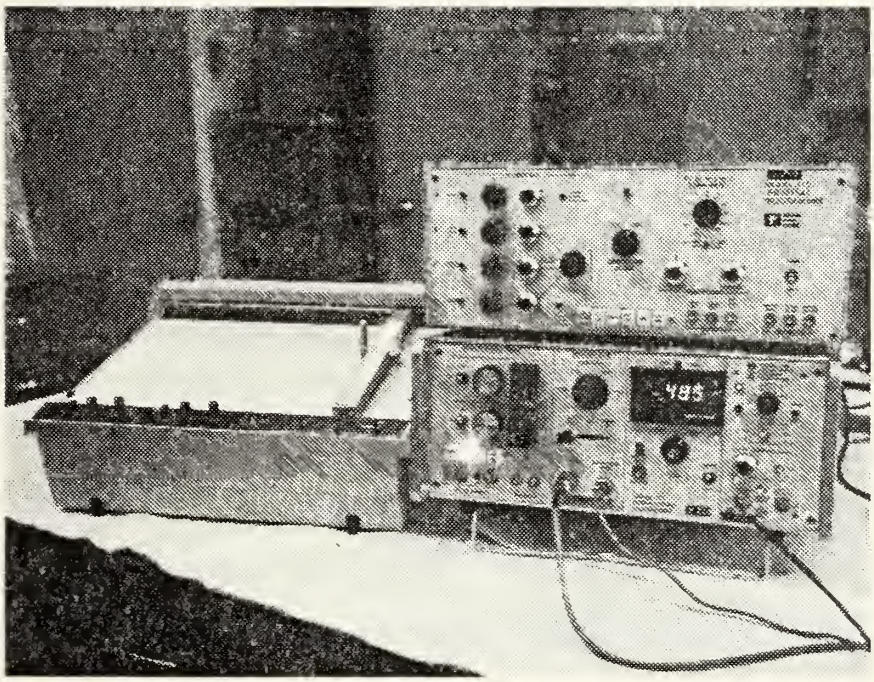

Figure 15. Arrangement of Potentiostat, programmer and X-Y recorder used to obtain potentiodynamic polarization curves

Applied Research Model 175 Universal Programmer and the Hewlett Packard 7040A X-Y Recorder which were used in conjunction with the corrosion cell to obtain the polarization curves.

3. Procedure

Preparation of the test coupon encased in plastic was identical to that used for the measurement of galvanic current. Additionally the top edge of the plastic portion of the sample was ground flat leaving about 3 mm of plastic. This was required so that the specimen holder would screw in far enough to make contact with and hold the sample. Once the sample was screwed into the holder continuity was checked. The corrosion cell was filled about two thirds full with synthetic seawater that had been aerated for about one day in another beaker. It was then stirred and aerated. The stirring was stopped after about five minutes. While the stirring was being done, the recorder was zeroed and calibrated as required for the run. After calibration, cables were connected from the recorder X-axis input to the potentiostat log I output, from the recorder Y-axis input to the potentiostat electrometer monitor output, and from the programmer signal output to the potentiostat external signal input. (For the benefit of follow-on researchers in this project, the following operational details are listed.)

Initial settings were then made on the potentiostat, programmer and recorder as follows.

Potentiostat:

Channel A at corrosion potential,
Channel B + 0.000V,
Push button B,
External signal input on,
Meter on current and 5,
Operating mode in Control E,
External cell off,
Full scale deflection 100 ma,
Input filter 10 ms,
IR compensation off,
Meter switch on log I output,

Programmer:

A potential set to starting potential,
B potential set to ending potential,
End of cycle switch in B,
Initial scan direction set as desired,
Sweep/Pulse to sweep,
Scan Rate/mV/sec,
Initial push button depressed,
Single cycle switch depressed.

X-Y Recorder:

Servo. in standby.

Upon immersion the various leads were attached as required and the tip of the reference electrode was adjusted to be centered 1 mm away from the sample face.

Four minutes after immersion, the cell selector was switched to external cell and the recorder servo was turned on. After an additional twenty seconds the pen was put down on the recorder and the activate push button on the programmer was depressed. Runs were made to determine the anodic portion of the curve by starting slightly cathodic and increasing potential during the run. The cathodic portion of the curves were done in the opposite way. For each run a different but identically prepared sample was used with

fresh electrolyte. At the end of the run the sample was rinsed in distilled water, air dried and stored in the vacuum desiccator.

III. RESULTS AND DISCUSSION

A. MICROSTRUCTURES OF ALUMINUM ALLOYS TESTED

The microstructures of the 5086 Al alloy in H32 and H116 tempers, shown in Figures 16 and 17, respectively, were in agreement with micrographs published by other researchers [6,9,11,12]. The 5086-H116 microstructure consists of a discontinuous network of precipitate, while the 5086-H32 has a more continuous network.

The microstructure of the 5086-H117 (Figure 18), however, contained an even more continuous network than the 5086-H32, which is not normally expected but could be caused by prior sensitization. A greater tendency for material in the H117 temper to become sensitized (than material in the H116 temper) was pointed out by Czyryca and Hack [11]. Sensitization is of course dependent on the time/temperature profile which the particular piece of metal has experienced after manufacturing. Experiments by Czyryca and Hack [11] showed sensitization could occur after one week at 100°C.

These results even though unexpected in the one case, form three of the variables involved in this research and contribute to the objective of investigating the effect microstructural differences would have on the processes involved in galvanic corrosion. In this regard, the photographs of the microstructures presented in this section for the three temper conditions of the 5086 Al alloy provide a

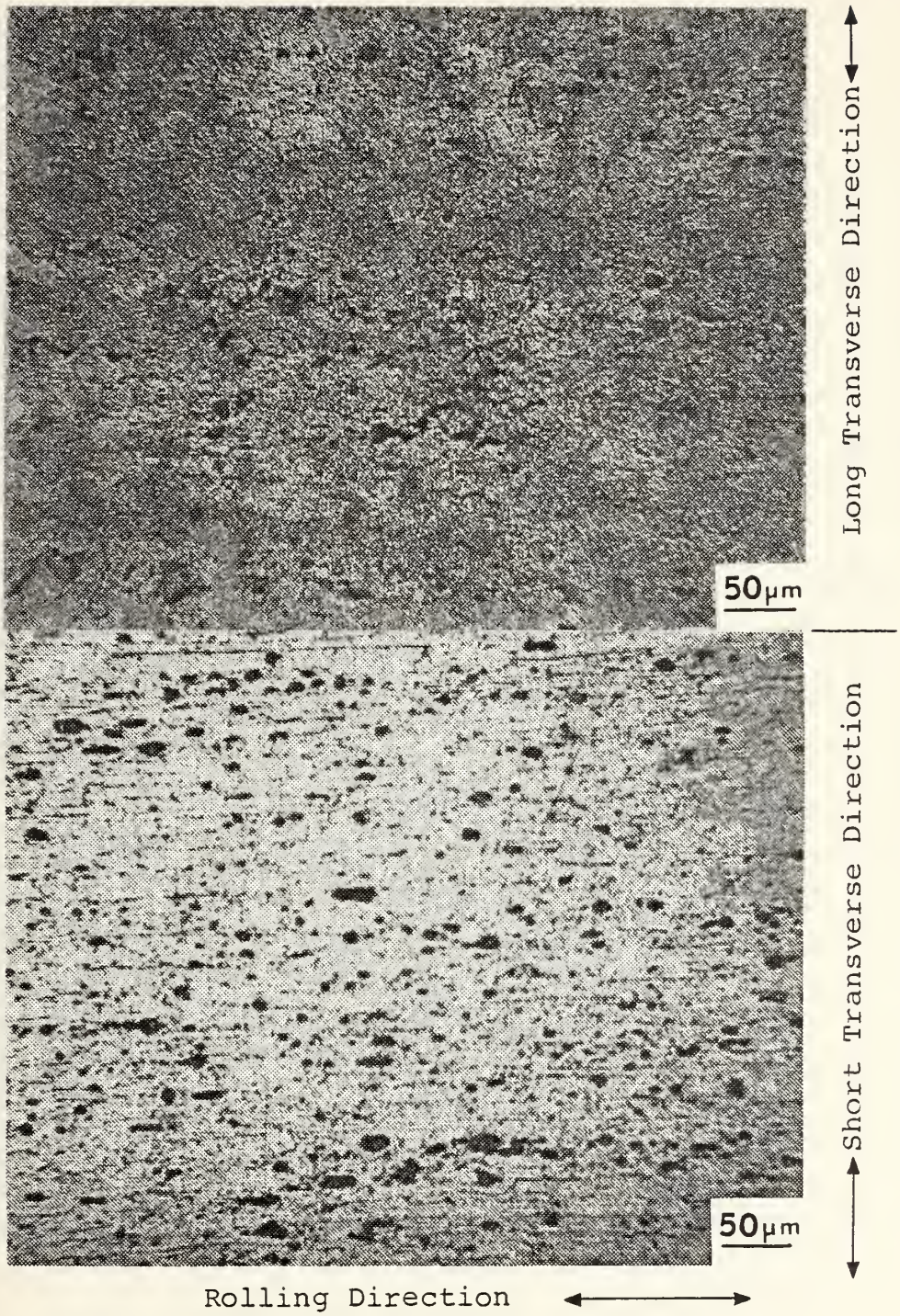

Figure 16. 200X photographs of microstructure of 5086-H116 aluminum in two orientations (Kellers etch)

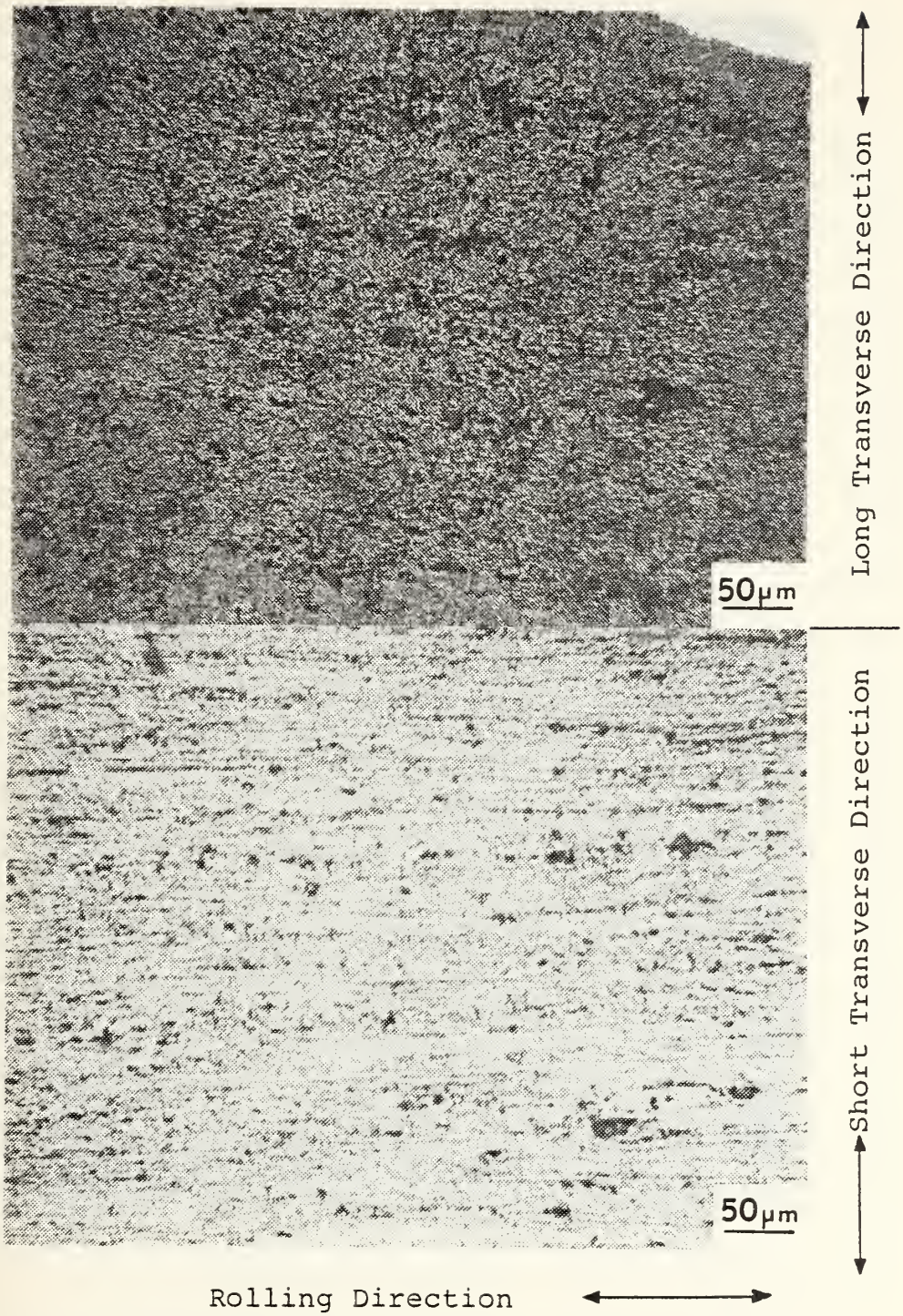

Figure 17. 200X photographs of microstructure of 5086-H32 aluminum in two orientations (Kellers etch)

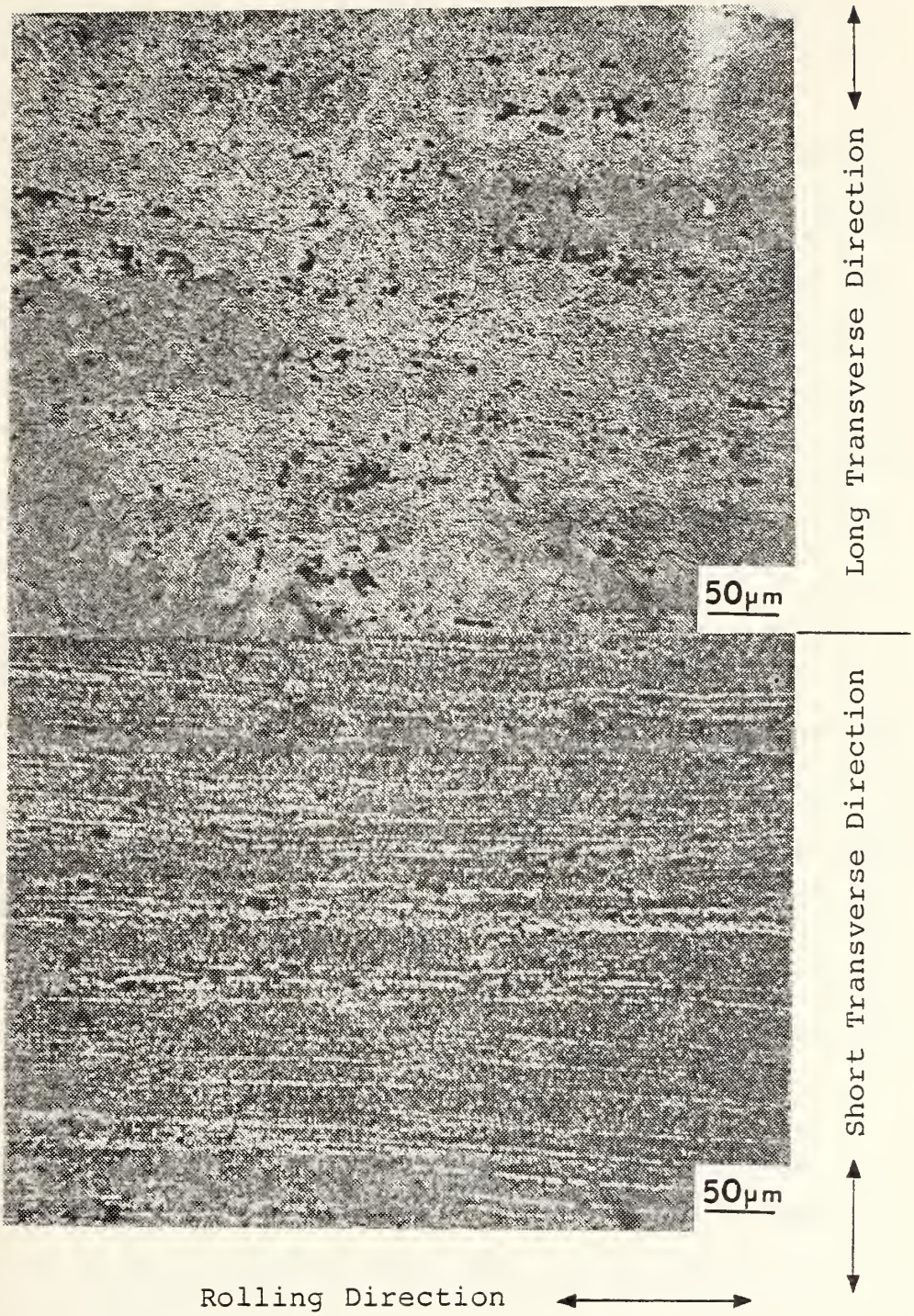

Figure 18. 200X photographs of microstructure of 5086-H117 aluminum in two orientations (Kellers etch)

basis for correlating corrosive attack with the microstructural (temper) condition of the alloy.

Other characterizations, of course, of the corrosive behavior are also needed to reinforce visual observations. One of the most important of these is the polarization behavior of the metal. This macroscopic electrochemical technique can be used to help determine microscopic processes which are taking place on the metal surface. The results of the polarization testing are shown and discussed in the following section.

B. POTENTIODYNAMIC POLARIZATION TESTS

Potentiodynamic polarization curves for the six test metals are shown in Figures 19-21. In these figures, the curve labeled "1" is the anodic polarization curve, which was essentially identical for all three tempers of the 5086 Al alloy. This result indicates that the tendency of this Al alloy to corrode in a galvanic couple is not dependent, at least macroscopically, on its temper condition.

The curves labeled "2" in Figures 19-21 are the respective cathodic polarization curves for the three more noble metals to be deployed in the galvanic couples. The purpose of jointly plotting the graphs as in Figures 19-21 is to use the intersection points to predict the value of galvanic current density, i_{couple}, and thus the corrosion rate for the anodic metals. The predicted galvanic current density i_{couple} for the three types of couples, taken from Figures 19-21 are:

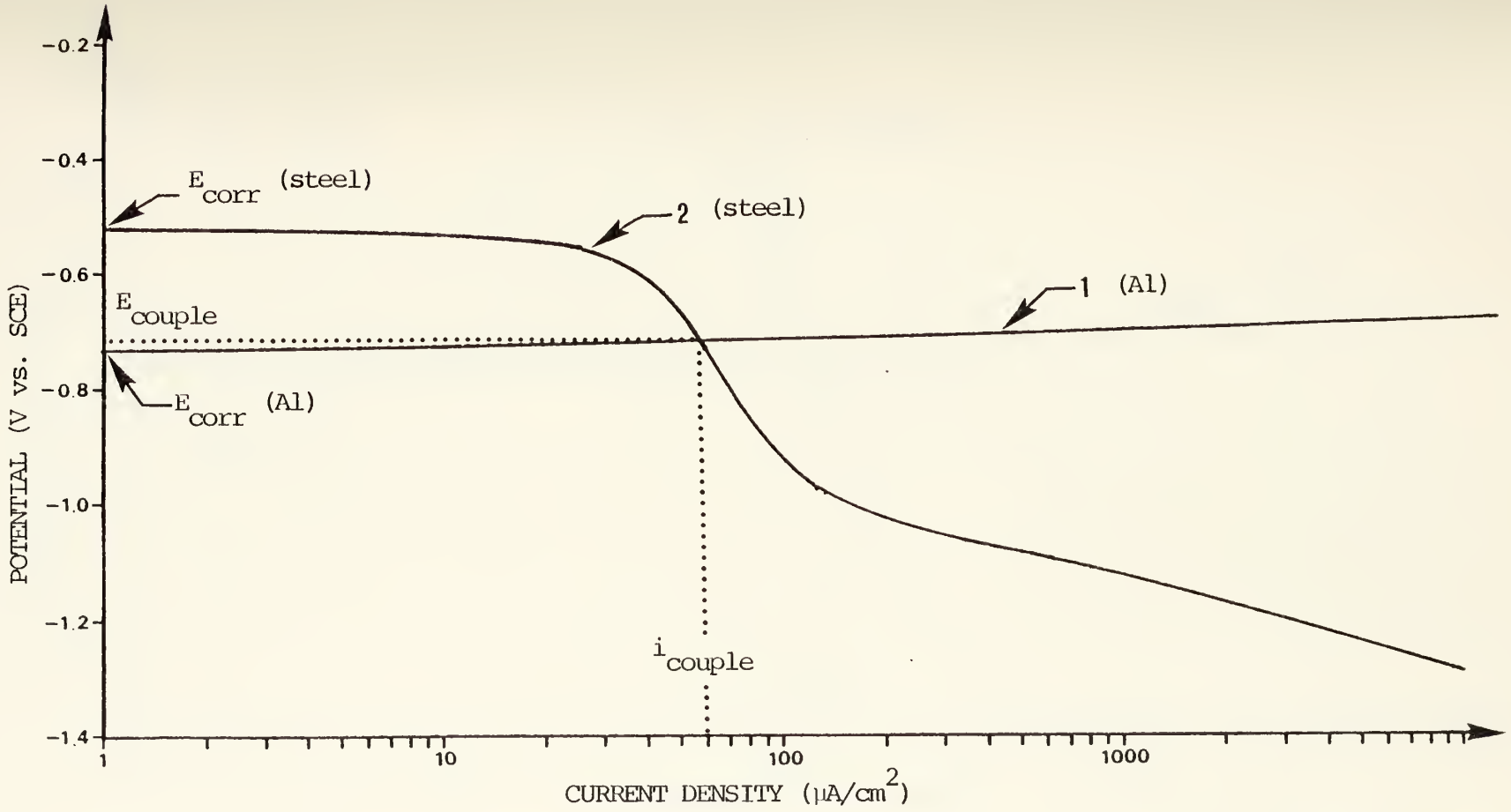

Figure 19. Potentiodynamic polarization curves for: 1. Aluminum (anodic curve), and 2. 1040 steel (cathodic curve)

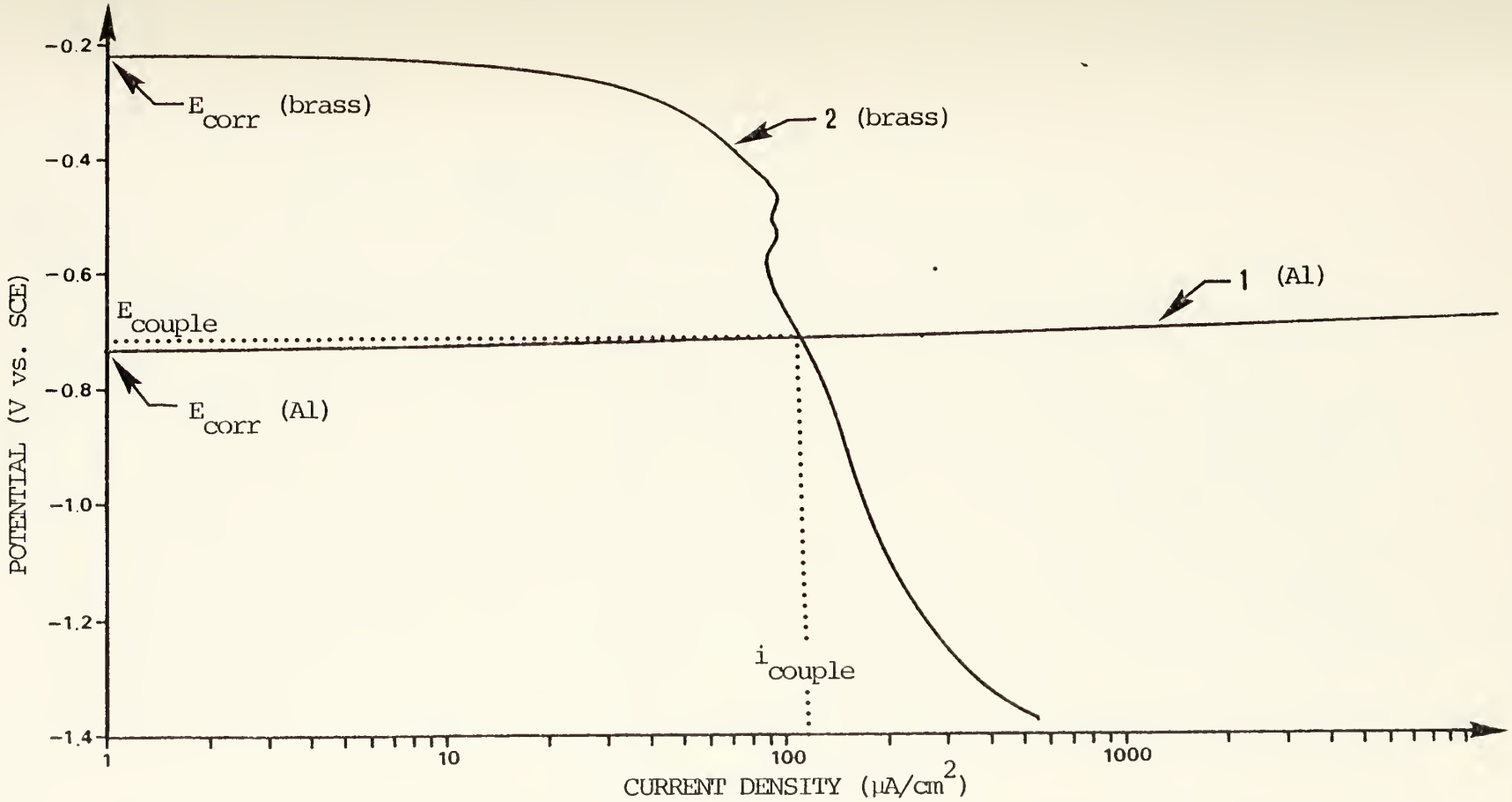

Figure 20. Potentiodynamic polarization curves for: 1. Aluminum (anodic curve), and 2. 60/40 naval brass (cathodic curve)

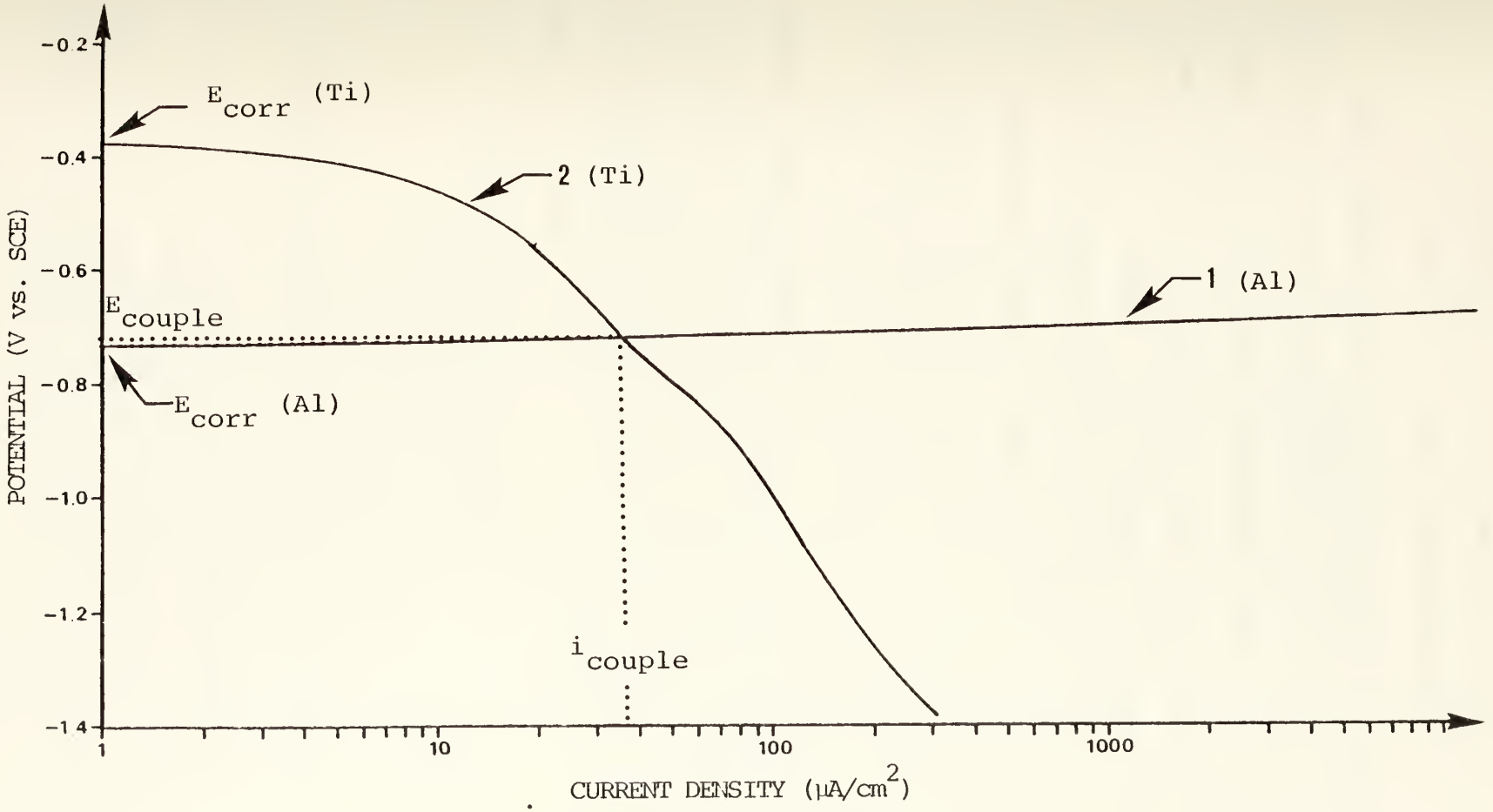

Figure 21. Potentiodynamic polarization curve for: 1. Aluminum (anodic curve), and 2. Ti-150A Titanium (cathodic curve)

112 $\mu A/cm^2$ for the brass/Al couple,

60 $\mu A/cm^2$ for the steel/Al couple,

37 $\mu A/cm^2$ for the Ti/Al couple.

This ordering of i_{couple} (brass/Al > steel/Al > Ti/Al) would not be obvious from the relative position of these materials in galvanic series for seawater, where the potentials of the three cathodic materials are ordered Ti > brass > steel. This demonstrates that the galvanic series potential differences cannot be taken as an indicator of dissolution rates. This point has also been made recently by Mansfeld and Kenkel [23], who recommended that galvanic series be considered as only "very qualitative guidelines."

Also, using the curves shown in Figures 19-21 the equilibrium potentials, E_{corr}, of the independent metals is determined, and E_{couple} for each couple type can be predicted. E_{couple} is the value of the potential at the intersection of the two curves. The values for E_{couple} were found to be (all vs. SCE):

-.725 V for Ti/Al,

-.715 V for brass/Al,

-.720 V for steel/Al.

The E_{corr} values were found to be (all vs. SCE):

-0.22 V for 60/40 Naval Brass

-0.36 V for Ti-150A,

-0.52 V for 1040 Steel, and

-0.76 V for 5086 Al.

According to the galvanic series in flowing seawater developed by LaQue, the potentials of these materials are in the order: Ti > brass > steel > Al. The measurements made in this work show that there is a reversal in the order of the brass and Ti in the present experiments. Again a difficulty in gaining insight from the various galvanic series is exemplified. Mansfeld and Kenkel [23, 24], for conditions similar to the present experiments, recently reported similar potential results, for similar alloys immersed in aerated 3.5 percent NaCl. A comparison of the measured potentials is shown in Table I.

TABLE I

Comparison of Equilibrium Potentials (vs. SCE) for Various Metals

Present Work (synthetic seawater)		Mansfeld and Kenkel [23,24] (3.5 percent NaCl)	
Material	Potential	Material	Potential
60/40 Naval Brass	- 0.22V	Cu	- 0.237V
Ti-150A	- 0.36V	Ti-6Al-4V	- 0.352V
1040 Steel	- 0.52V	4130 Steel	- 0.591V
5086 Al	- 0.76V	6061-T651 Al	- 0.756V

The measured values of E_{corr} and predicted values of E_{couple} and i_{couple} are data which reflect the importance of the polarization behavior of the respective metals.

The cathodic polarization curve for the steel shows a value for E_{corr} which is lower than the E_{corr} determined for the brass or Ti. However, the current density (i_{couple}) predicted for steel/Al is midway between those values predicted for Ti/Al and brass/Al couples. As illustrated by the Figures 19-21, the reason for this lies primarily in the polarization behavior (curve) of the respective cathodic metals. As the potential of the cathodic metal is decreased, each particular metal behaves differently. Ti polarizes to a greater extent than steel (current density for Ti does not increase as fast with decreasing potential), thus crossing the Al anodic polarization curve at a lower value of current density. Brass, with the highest single metal value of E_{corr}, does obtain an i_{couple} intersection which is the highest of the three couple types tested. The relatively low current obtained by the character of the Ti cathodic polarization behavior has been noted by other researchers such as LaQue [25] and Petitibone and Kane [26].

Polarization behavior helps characterize a metal at a specific condition at a specific time. For example, in these experiments, immersion for polarization determinations was only a few minutes. (At a potential scan rate of one mV per second the entire curve was finished in about ten minutes with a total immersion time of about 15 minutes.) The next investigation to be performed then should examine the changes which occur with increasing time of immersion. To investigate the time variable, the actual i_{couple} of the

three pairs of metals was measured over a time period of 24 hours. In addition to these galvanic current measurements, physically coupled (proximate) samples were immersed for longer periods, and subsequently examined in terms of their physical appearance.

C. GALVANIC CURRENT DENSITY MEASUREMENTS

The galvanic current density versus time data can be correlated with predictions from the potentiodynamic polarization measurements. The current density in the galvanic couples which would be predicted on the basis of the polarization curves (Figures 19-21) was low for the Ti/Al, higher for the steel/Al and highest for the brass/Al. These predictions are confirmed by the initial i_{couple} values recorded for the actual couples, as presented in Figures 22-24. These correlations then give a starting point from which to begin to analyze the dynamics involved in the galvanic current density vs. time curves (Figures 22-24) and thus the corrosion characteristics of the metal couple/electrolyte systems. Figures 22-24 each show three curves representing the results of three separate runs in which the temper of the Al alloy was common. For example, the three curves in Figure 22 show the galvanic current densities (as they varied with time) for 5086-H32 coupled to the three different cathodic metals.

The curves shown in these figures have certain characteristics in common. The curves in which the Ti is the

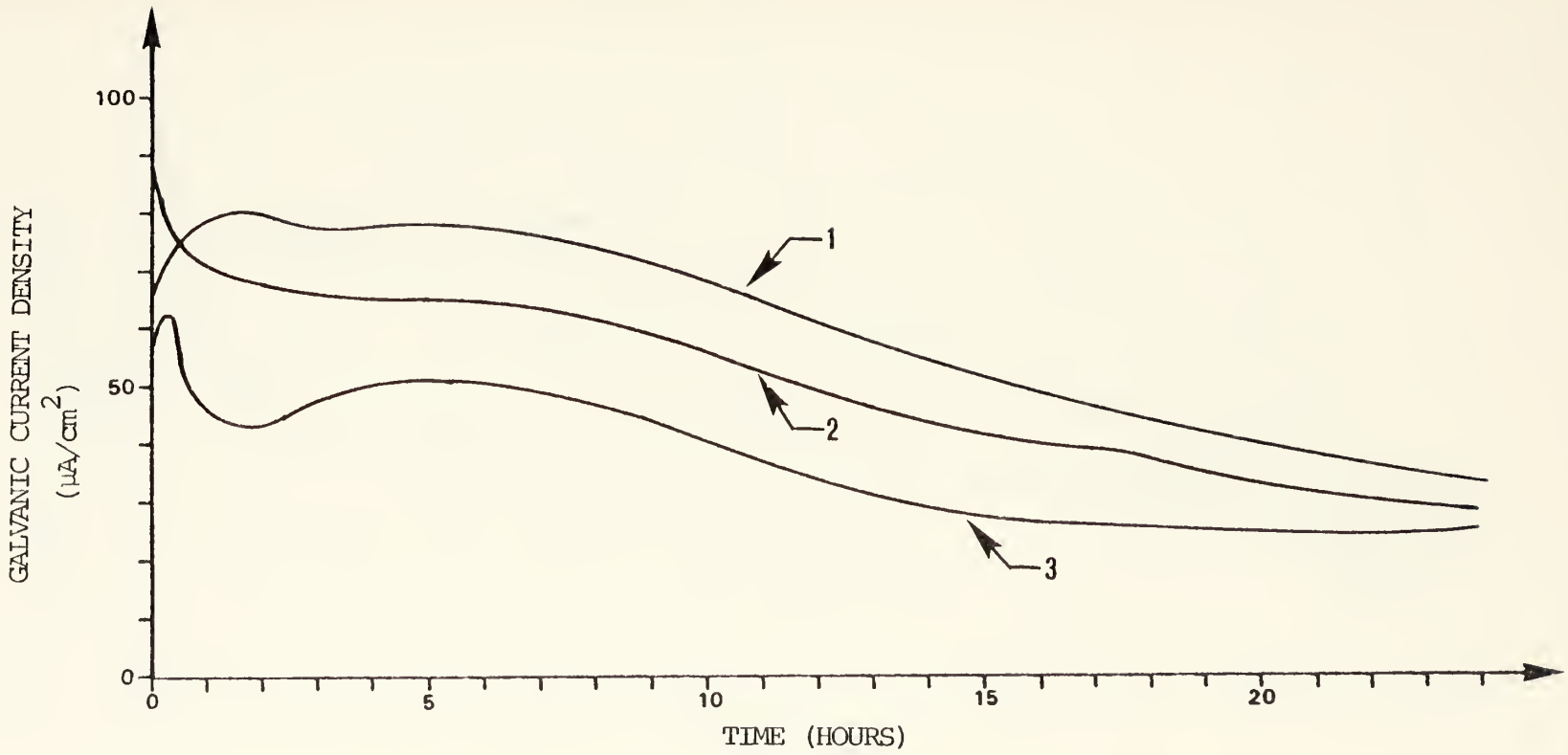

Figure 22. Plot of galvanic current density versus time for 5086-H32 aluminum coupled electrically with: 1. Ti-150A Titanium, 2. 60/40 Naval Brass, 3. 1040 Steel

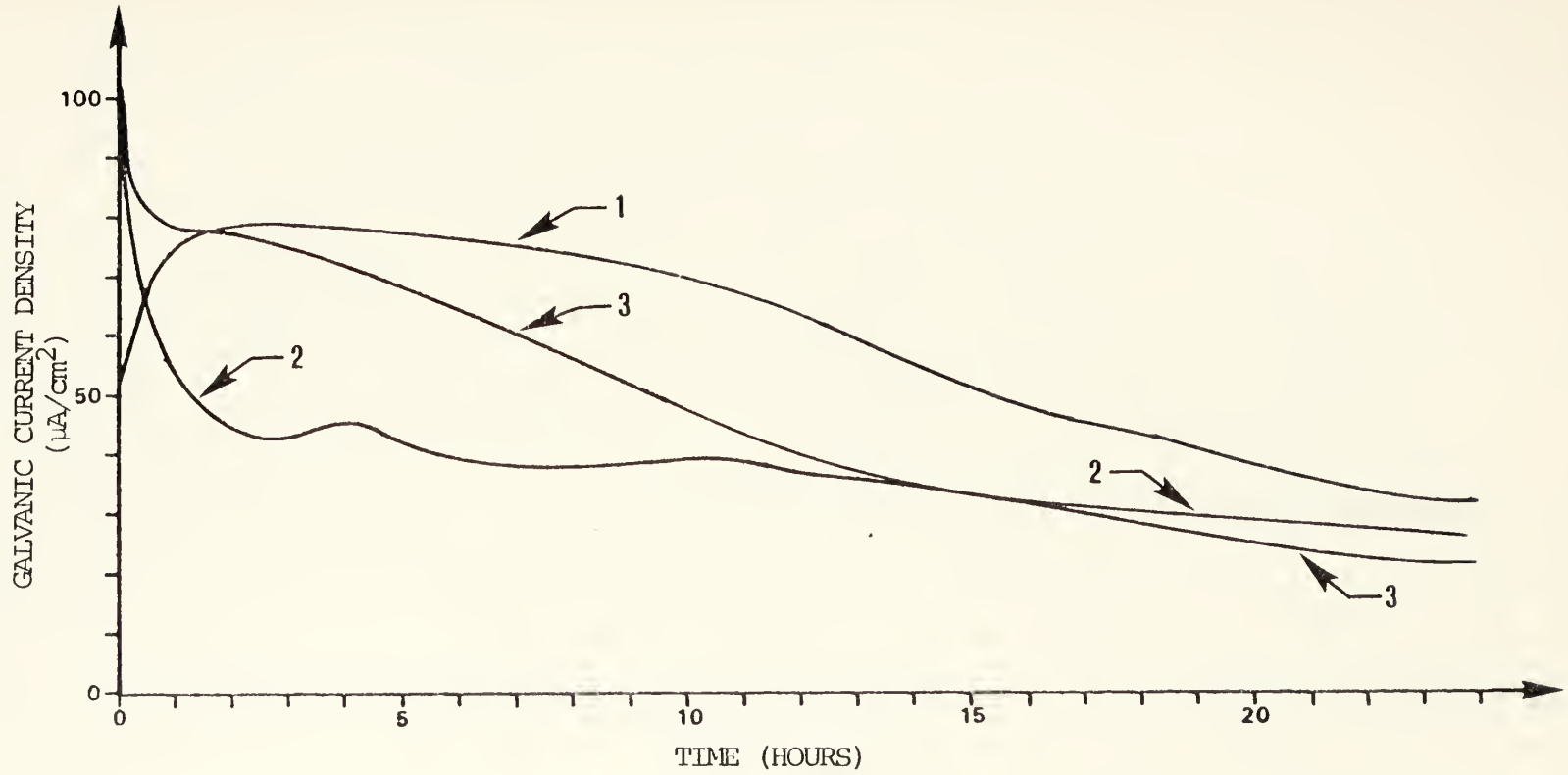

Figure 23. Plot of galvanic current density versus time for 5086-H116 aluminum coupled electrically with: 1. Ti-150A Titanium, 2. 60/40 Naval Brass, 3. 1040 Steel

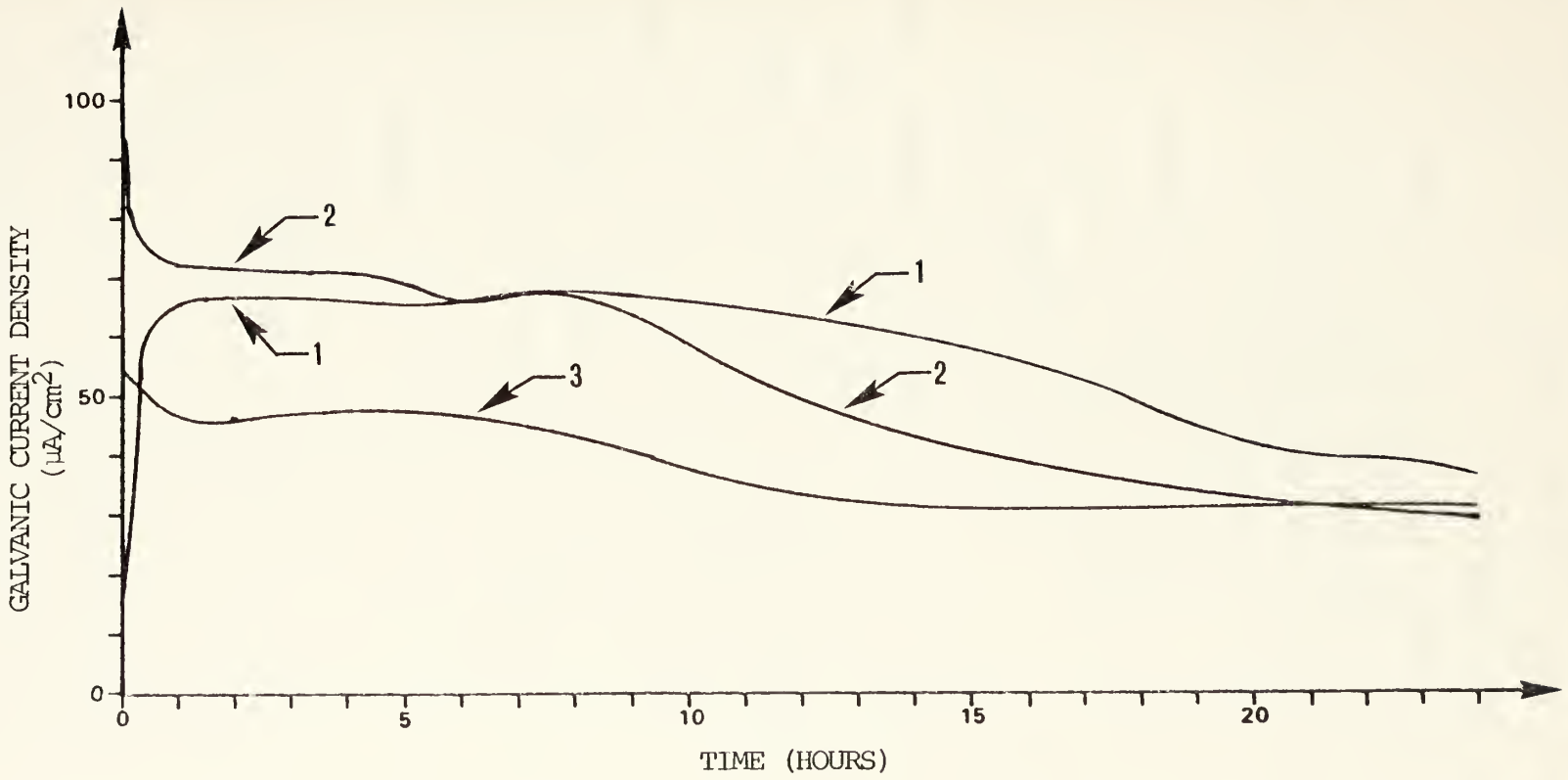

Figure 24. Plot of galvanic current density versus time for 5086-H117 aluminum coupled electrically with: 1. Ti-150A Titanium, 2. 60/40 Naval Brass, 3. 1040 Steel

cathodic metal. all start low (about 45μA/cm^2), rapidly increase to a plateau (about 75μA/cm^2), then gradually decrease to about 33μA/cm^2. As discussed, the initial value is well predicted by i_{couple} as determined from the intersection of the Al and Ti polarization curves (Figure 21). The increase in current with time from this initial value is considered to be caused by the build up of an oxide film on the initially "clean" Ti surface. Since titanium is a reactive metal, it normally depends on a protective film of TiO_2 for corrosion resistance [23]. The sanding involved in the sample preparation procedure in these experiments removed the oxide layer, thus making the metal potential more active (closer to that of Al). The initial rise of current is believed to be associated with passivation of the Ti surface by oxide layer growth after immersion. This causes the potential to increase obtaining a noble value and a greater potential difference with the aluminum. Such behavior has been reported by Pettibone and Kane [26] who commented that the potential of Ti changes from -0.8V when first immersed to -0.1V "after a matter of minutes" due to the development of a protective oxide coating.

The sharp initial rise in current density shown by couples involving Ti was in contrast to the behavior of couples with brass or steel. The curves for brass-coupled samples typically started high (about 100μA/cm^2), as predicted by the polarization curves, decreased rapidly to about 70μA/cm^2, and then showed a gradual decrease to about

30μA/cm^2 after twenty-four hours. The steel couples did not start as high (about 60μA/cm^2), and after an initial decrease dropped gradually to about 28μA/cm^2 after twenty-four hours. The initial drop in current exhibited by couples with steel or brass can probably be attributed to the initial formation of corrosion product on the Al anode. Fontana and Greene [27] explained that as corrosion progresses reaction products or corrosion products may accumulate at either the anode or cathode or both, reducing the speed at which corrosion procedes.

Once the currents pass this initial transient period, other characteristics become evident. In the case of the 5086-H32 (Figure 22) for example, the respective current curves maintain (except for the first half hour), the same relative position for the entire twenty-four hour period, with the current densities being ordered from high to low as: Ti/Al, brass/Al, steel Al. This ordering is consistent with that which would be predicted using the traditional criteria of position on the galvanic series.

Figures 23 and 24 show some fluctuations in the curves and do not clearly show the same relative positions. Upon examination, the curves for steel/H116 and brass/H116 are not characteristic of the other curves for which the cathode is common. For example the curves for steel/H32 and steel/H117 are closely matched while the curve for steel/H116 is higher than the others.

These apparent discrepancies are believed to be associated with variations in the aeration system flow rate during the runs involving H116/brass and H116/steel (Figure 23). In these tests, it was found that the magnitude of the measured galvanic current was strongly dependent on the rate at which air was bubbled into the exposure beaker. Increasing the air flow increased the value of current measured and decreasing the air flow decreased the current, probably associated with a cathodic depolarizing effect of more solution agitation for higher air flow rates. Therefore, while a concerted effort was made to adjust the air flow each time a run was initiated so that all exposures were subject to the same air flow, some variations inevitably occurred in practice. It is presumed that the curves for steel/H116 and brass/H116 represent a deviation in behavior caused by fluctuations in air flow from that which was normal for the other runs. When the data are processed to obtain average galvanic current density values for each run, the suggestion that the H116/brass and H116/steel runs are out of line is confirmed.

To calculate the average values of galvanic current density for each curve a simple numerical integration scheme was used. The area under each curve was found by multiplying each of the tabulated values of current by an appropriate time interval to get incremental areas all of which were then added to get the total area. The average current density was then found by dividing the area by

twenty-four. The calculated average i_{couple} values are shown in Table II.

TABLE II

Average Galvanic Current Density ($\mu A/cm^2$)

	Temper of Al Anode		
Cathode	H32	H116	H117
Ti-150A	60	60	57
60/40 Naval Brass	51	36	52
1040 Steel	37	48	38

The trend shown in Table II is quite consistent if one ignores the data points for brass/H116 and steel/H116. The average galvanic current density decreases as the cathodic metal becomes more active (in terms of a galvanic series). This also reinforces the observation that the corrosion rate of the Al alloy when coupled to the other metals tested can be ordered from high to lowest as: Ti/Al, brass/Al, steel Al. Also, for the short (twenty-four hour) time period examined in these experiments, the galvanic corrosion rate of the 5086 aluminum alloy is not affected by the temper condition. It is also observed that at the end of the twenty-four hour time period the values of current density have decreased so that they all appear to be converging to a level of about $30 \mu A/cm^2$. The gradual decrease to this value is probably caused by a stabilization of the corrosion

product accumulation process on the Al anode [25,27]. It is postulated that after twenty-four hours anodic film accumulation is sufficient in all cases to cause the galvanic current density (and therefore the anodic corrosion rate) to be nearly the same for all couples. In terms of the polarization curves, one can speculate therefore that the slope of the anodic Al corrosion curve is increasing, and is the major determinant of the observed decay of i_{couple} with time.

These ideas regarding anodic corrosion product formation were explored further through macroscopic and microscopic examination of physically coupled samples which were immersed for longer periods.

D. CORROSION TESTING OF PHYSICALLY COUPLED (PROXIMATE) DISSIMILAR METALS

1. Morphology and Distribution of Precipitate Formations on the Cathodic Metals

Macroscopically, most of the cathodic members of the coupled samples appeared to have little precipitate formation on their surfaces. Figure 25 is a macro photograph taken with a polaroid camera attached to a low power light microscope and is typical of the photographic records made of the physically coupled samples after drying. These photographs and the SEM photographs included in this work are all oriented on the pages in the same way that they were hung in the water. That is the top of the photo represent the top of the samples as they were exposed. Also in all photographs presented for the vertical couple interface, the Al is on the right side in the photo.

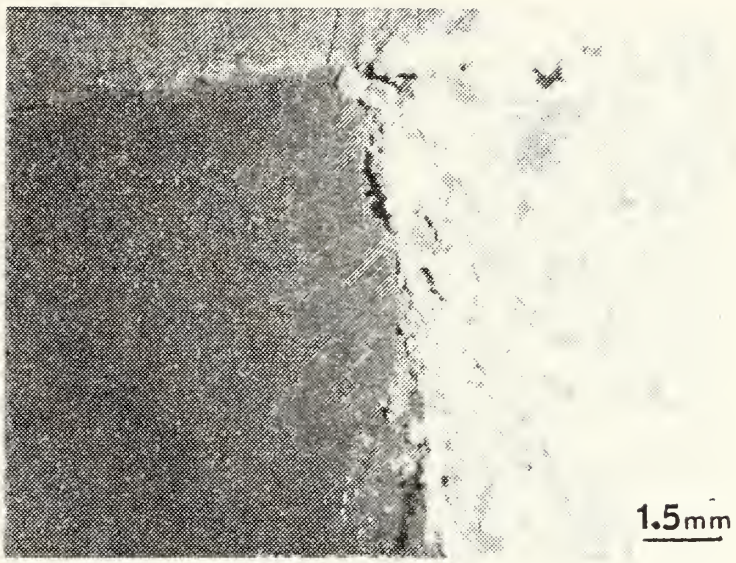

Figure 25. Steel/H116 couple exposed for two weeks, 7X

Figure 25 shows a couple exposed for two weeks; the cathodic member shows only small amounts of precipitate deposit. This sample showed the least accumulation of any of the samples. Another typical sample is shown in Figure 26. Even though this sample was exposed for only two days, there is an accumulation of precipitate on the cathode that seems to have been strewing from the vicinity of the anode/cathode joint. Figure 26(b) is a higher magnification SEM view of the center of the joint area shown in Figure 26(a). Note in both views the precipitate accumulation seems to be pointed toward the anode and upward. This is quite possibly caused by corrosion product coming loose from the Al anode and flowing down over the cathode with the flow of water in the beaker and then being deposited and accumulating on the cathode. This correlates with the circulation of water actually observed in the beaker during the testing; the flow was in a sort of circle, starting at the end of the glass tube used for aeration. From that point the water would rise with the air bubbles flowing across the top then sink and angle back towards the air outlet. The flow across the sample was therefore in approximately the same direction as the orientation of the precipitate accumulation seen in Figure 26.

Microscopic examination of the cathodic accumulation of precipitate on other samples showed some variation in details but similarities in gross geometry, as can be seen by comparing Figures 27-30.

(a)

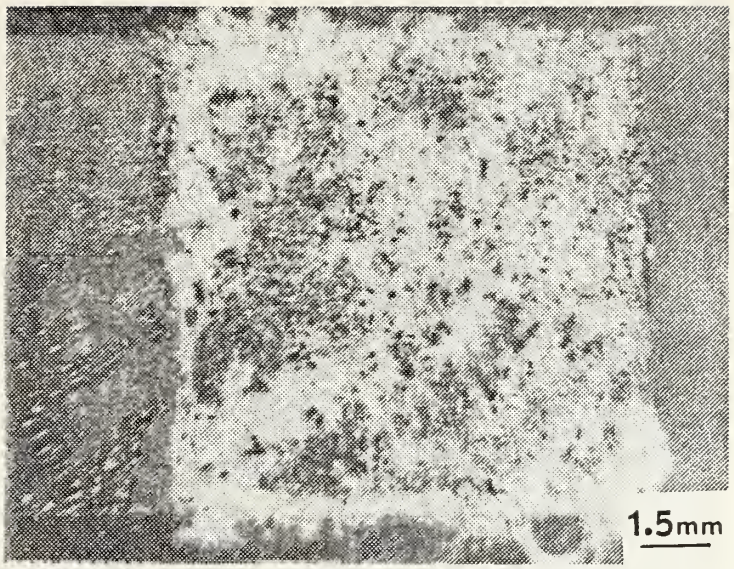

(b)

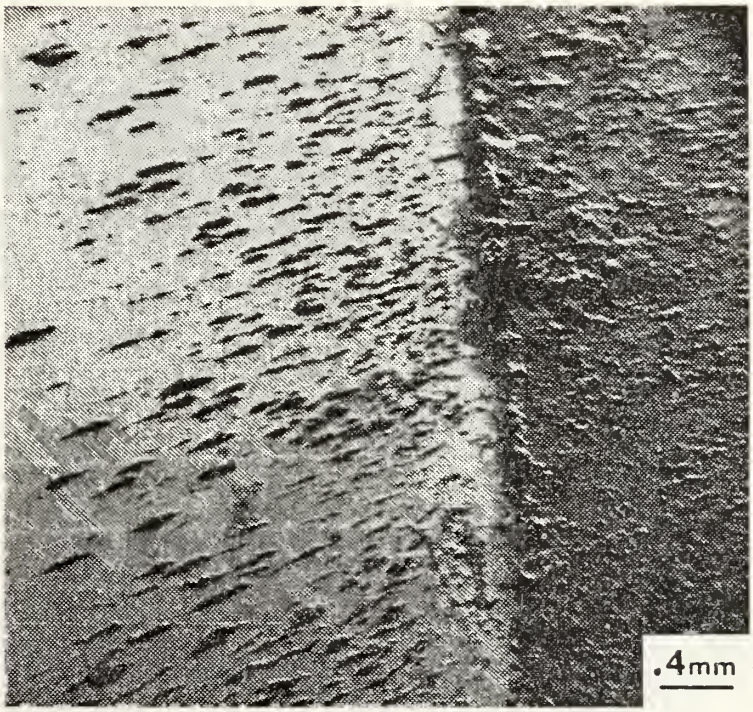

Figure 26. Brass/H32 couple exposed for two days, (a) 6X, (b) 24X (SEM).

(a)

(b)

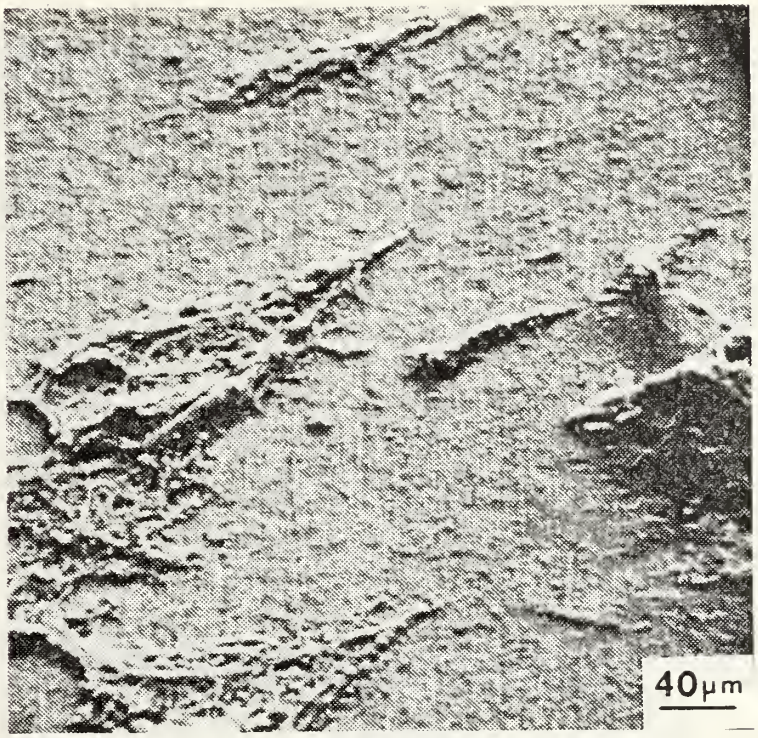

Figure 27. Corrosion product accumulation on titanium in TI/H116 couple exposed for three weeks, (a) 23X (SEM), (b) 240X (SEM).

(a)

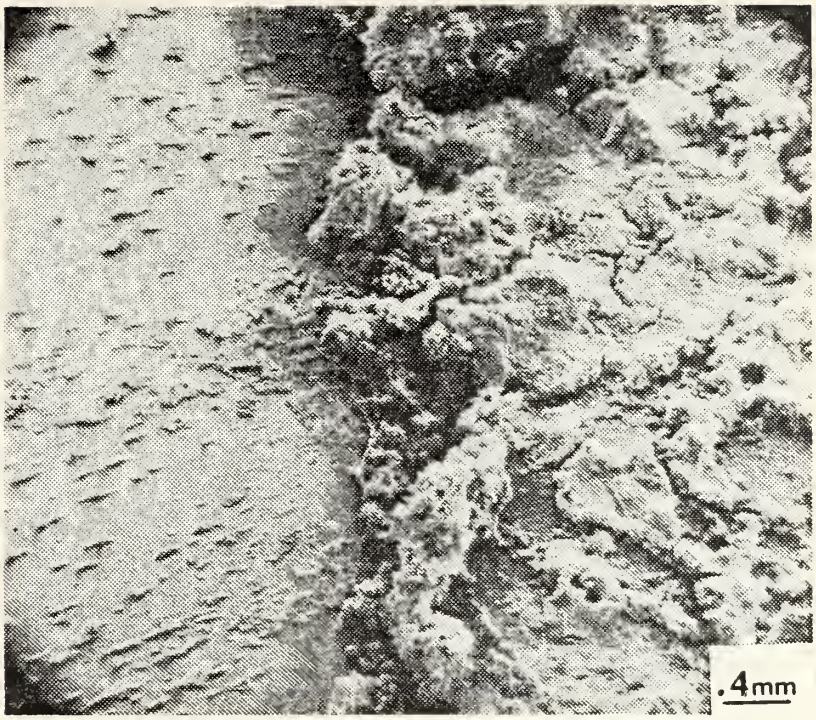

(b)

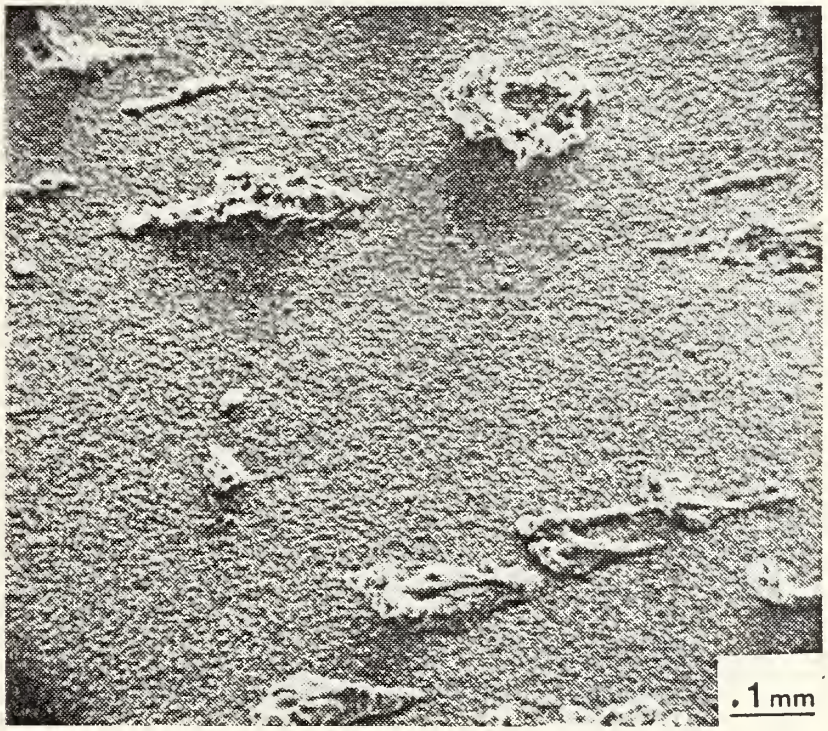

Figure 28. Corrosion product accumulation on titanium in TI/H32 couple exposed for two weeks, (a) 22X (SEM), (b) 110X (SEM).

(a)

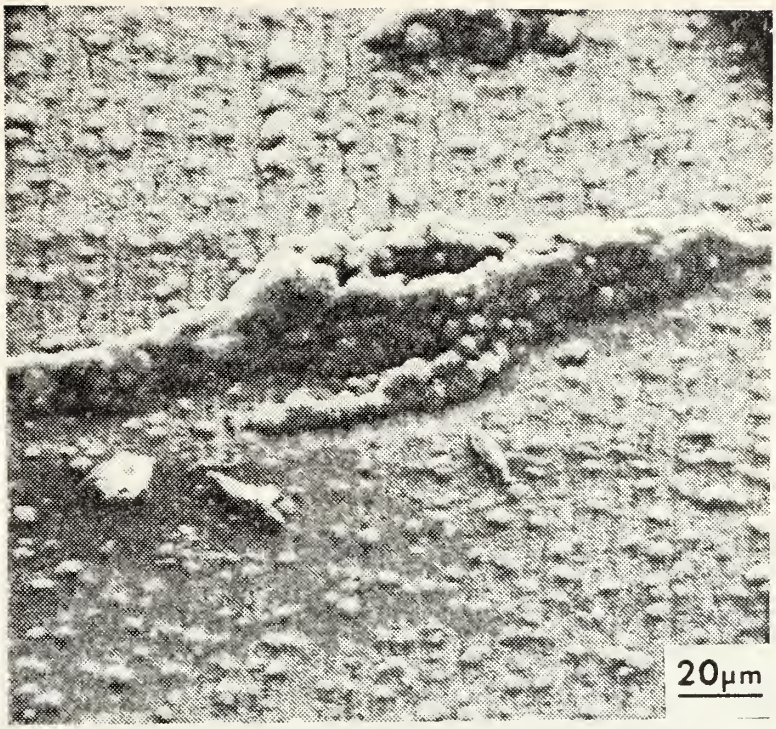

(b)

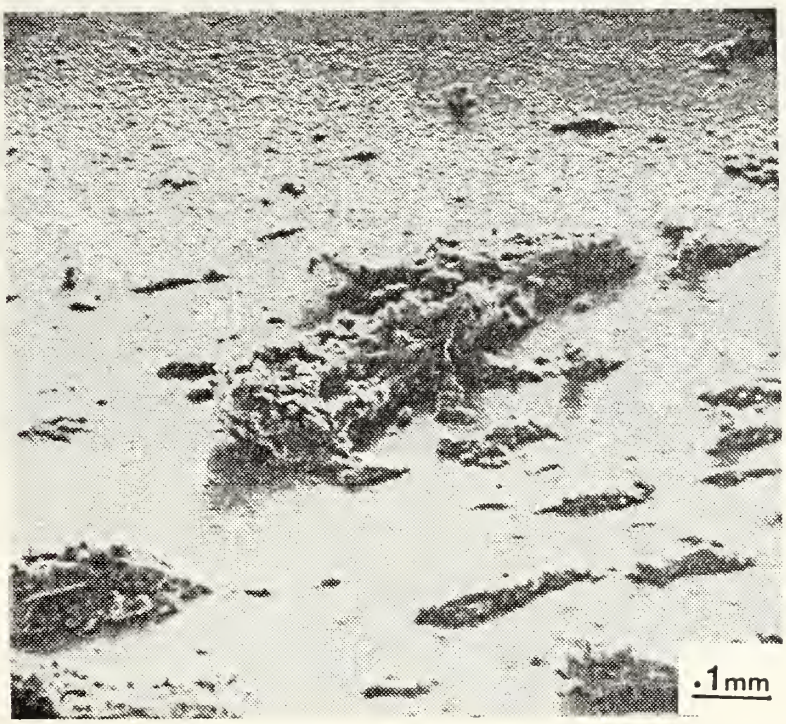

Figure 29. Corrosion product accumulations on cathodic metal. (a) Brass/H32 couple exposed for three weeks, 550X (SEM), (b) TI/H116 couple exposed for two weeks, 105X (SEM).

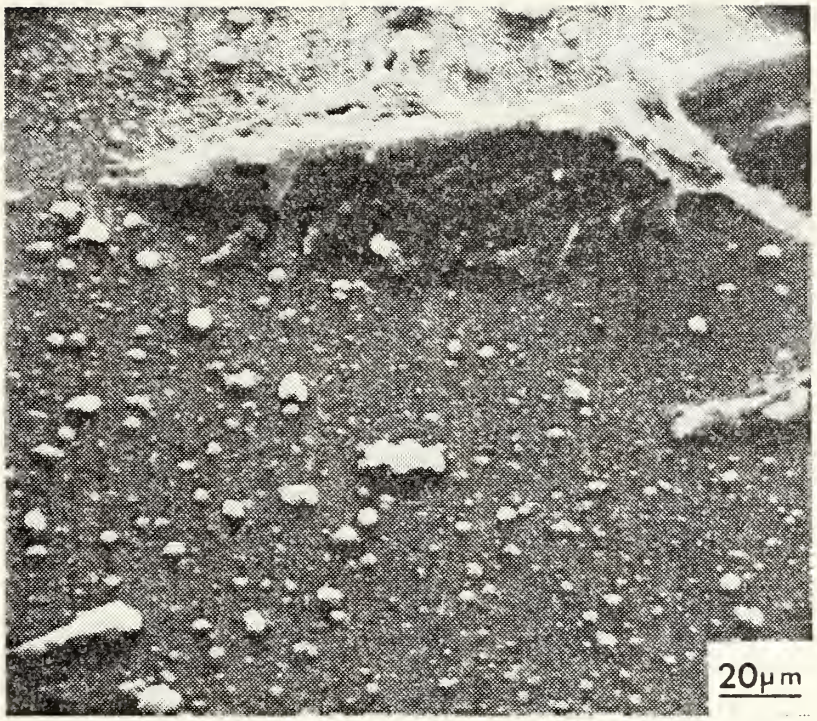

Figure 30. Corrosion product accumulation on steel in Steel/H32 couple exposed for one week, 540X (SEM).

In addition to the longer, more obvious formations on the cathodic members of the couples, there existed a more complete base layer covering the cathodic metal; the details of this layer were observable only at higher magnification. Figures 27(b), 28(b), 29 (a and b) and 30 show this formation, which was present on all samples. At very high magnification, the structure of this formation appeared to be made up of very fine crystallites. Figure 31 shows high magnification SEM photographs of the structure observed on the steel cathode in one of the couples, and is considered to exemplify the typical layer formation present.

Analysis (by energy-dispersive X-ray spectroscopy) of the cathode-located precipitates and the base film layers showed that these are both Al compounds. It is therefore obvious that these products originate in anodic dissolution processes then migrate to and accumulate on cathodic regions as well.

The observation of an Al based compound on the cathode metal was also reported by Keelean [7] in his work with explosively bonded steel/Al couples in seawater.

Figure 32 shows another type of precipitate formation which was observed on one of the steel/Al samples. This structure was observed only on one sample, and is reported only because of its unusual and interesting appearance.

(a)

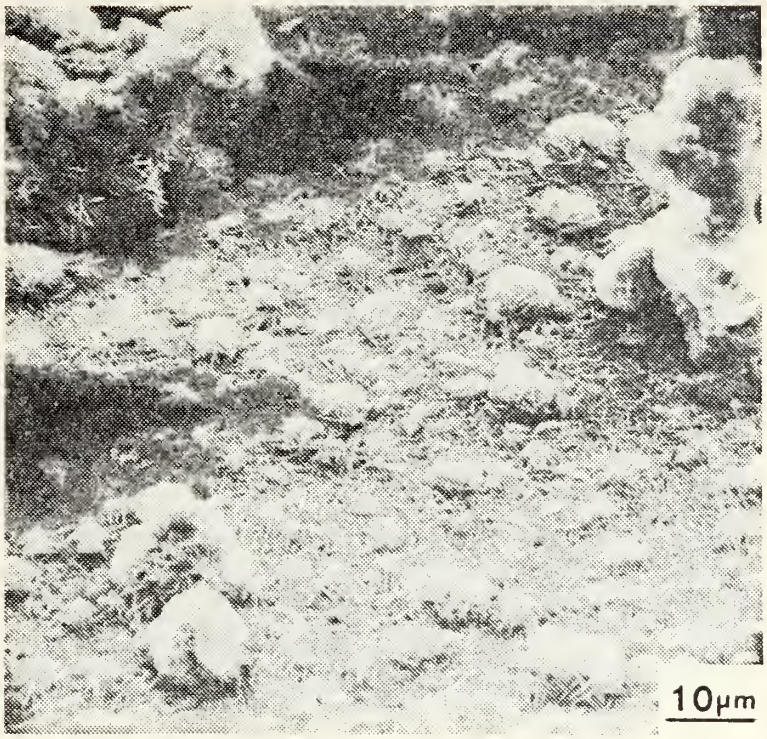

(b)

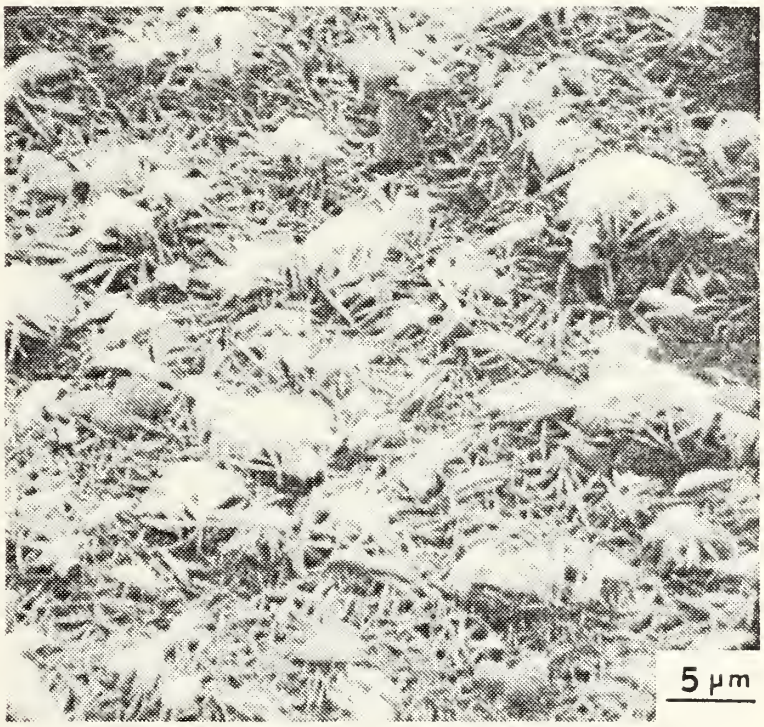

Figure 31. Corrosion product accumulation on steel in Steel/H32 couple exposed for three weeks, (a) 1150X (SEM), (b) 2300X (SEM).

(a)

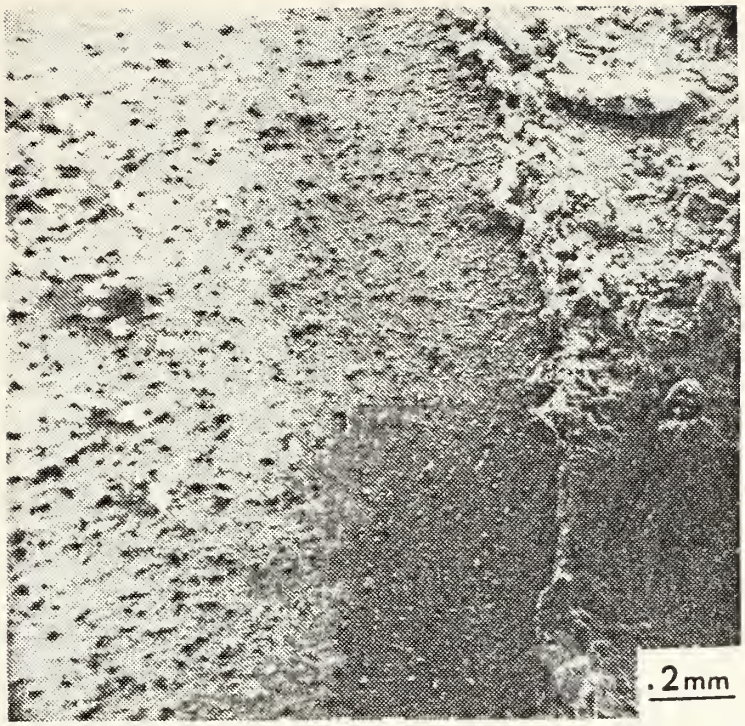

(b)

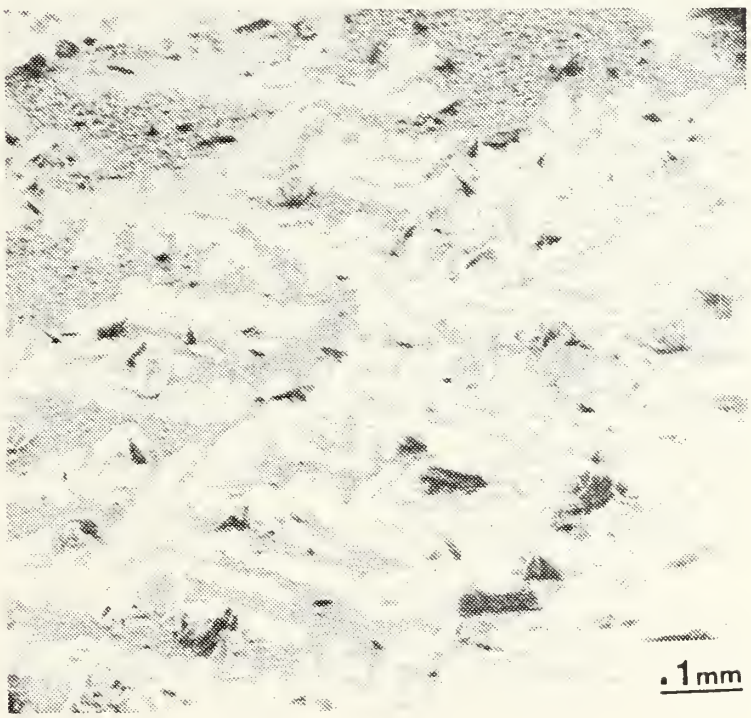

Figure 32. Precipitate formation on steel in Steel/H32 couple exposed for three weeks, (a) 55X (SEM), (b) 105X (SEM).

Another interesting structure observed is described as "corn husk" formations on the cathodic metal as shown in Figures 33 and 34. These features were found on only a few of the samples. Analysis of the features using the energy-dispersive X-ray analyzer (Figure 35) revealed that they were a calcium compound, devoid of Al. However, the surface of the metal upon which they stood is covered with an Al compound. Figure 36 shows several of these "corn husk" features, and what remains of a base cathodic film coating after cleaning.

These observations of the cathodic metal confirm the existence of extensive films and precipitate formations on the cathodic members of galvanic couples after seawater exposures. These structures can insulate the cathode and thereby reduce the net galvanic effect as pointed out by LaQue [25]. The effect of this on the anode would be to lower the galvanically induced corrosion rate as was indicated by the galvanic current density measurements presented earlier. In order to investigate the further effects of corrosion-related product structures, the corrosion products and associated damage to the anodic member of the couples (the Al) was also investigated.

2. Morphology of the Corrosion Product on the Al Anodes

In order to further investigate the effects of corrosion-induced product structures, the corrosion products and associated dissolution damage to the anodic (Al)

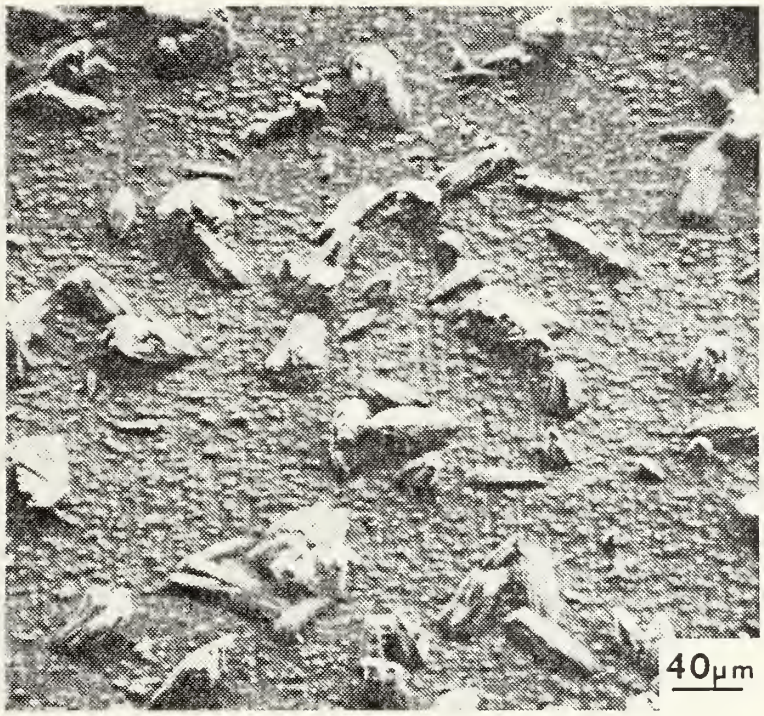

Figure 33. Precipitate formations on brass in Brass/H32 couple exposed for two weeks, 230X (SEM).

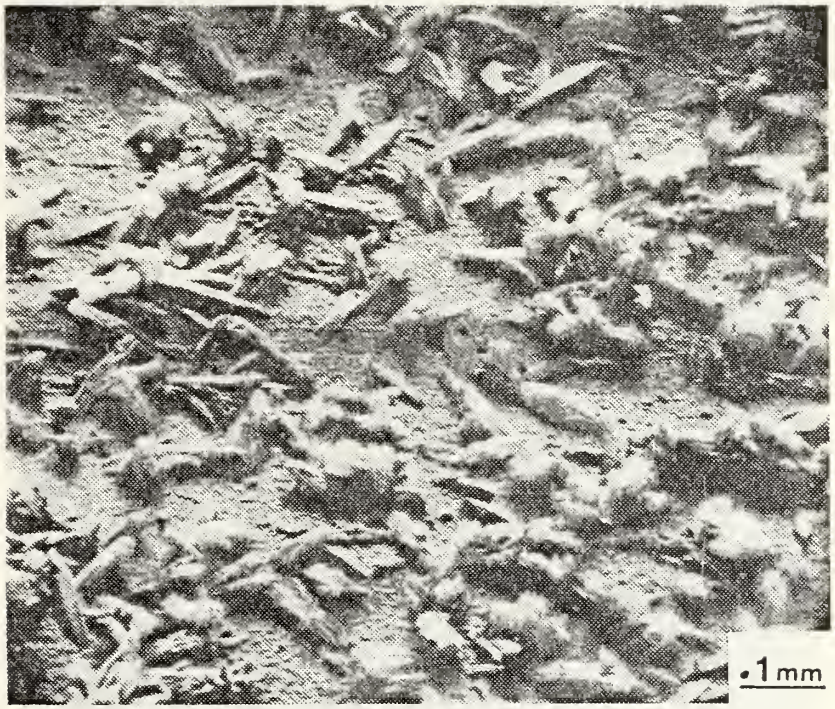

Figure 34. Precipitate formations on brass in Brass/H32 couple exposed for eight weeks, 110X (SEM).

(a)

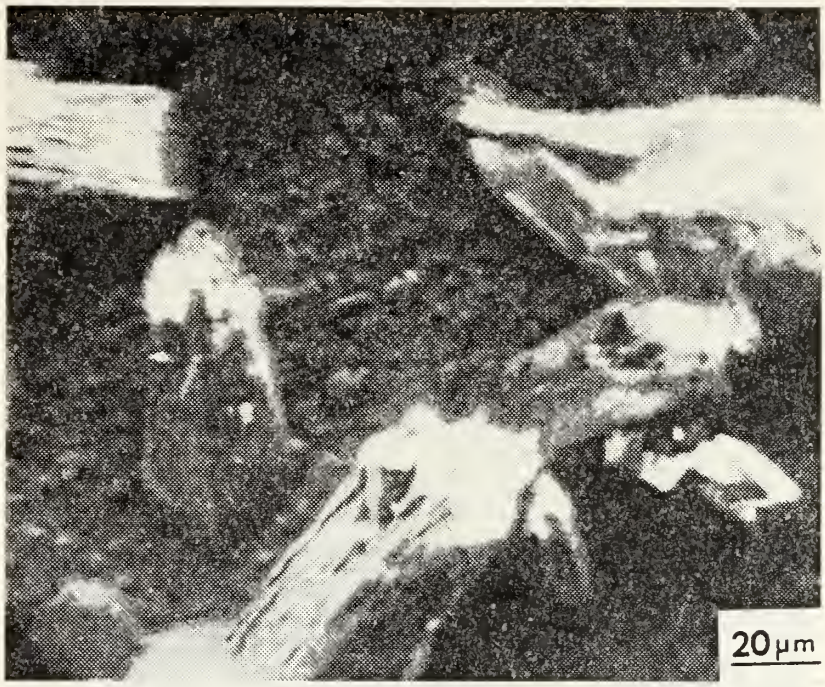

(b)

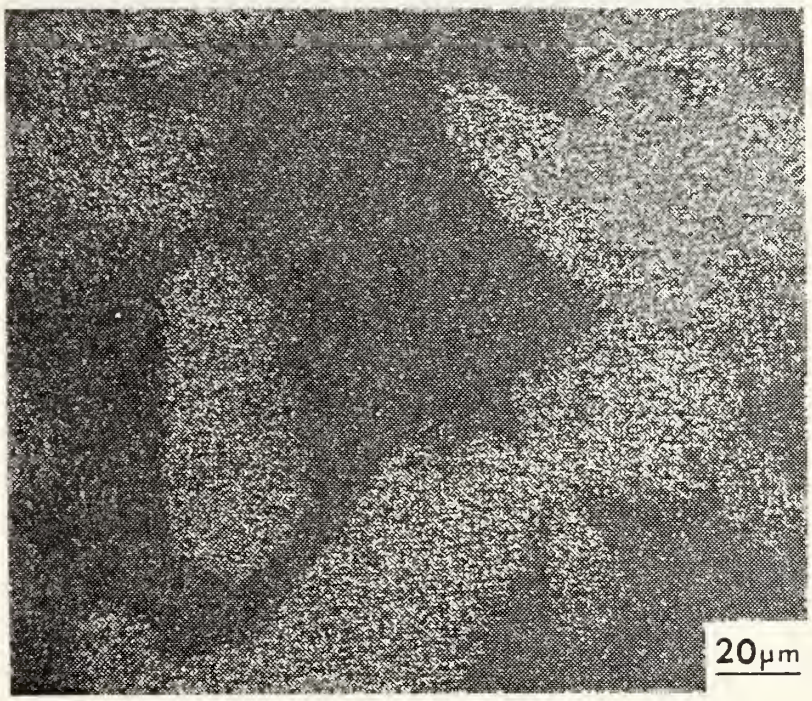

Figure 35. Precipitate formations on brass in Brass/H32 couple exposed for eight weeks, (a) 550X (SEM), (b) 550X PGT dot mapping of same area using characteristic calcium X-ray wavelength.

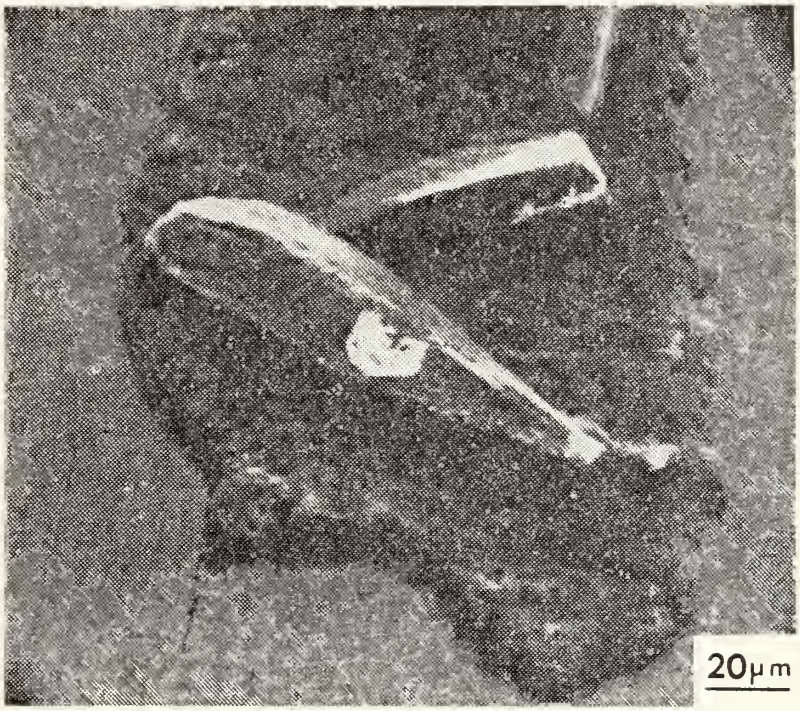

Figure 36. Precipitate formation remaining on cleaned brass in Brass/H32 couple exposed for eight weeks, 550X (SEM).

member of the couples was also studied. The morphology of the corrosion product on the Al anode typically consisted of a white amorphous product as seen in Figure 37. As pointed out by various references [28,29] this is the commonly observed corrosion product found on Al alloys and consists principally of various forms of hydrous Al_2O_3 [28,29].

Examination of the corrosion products using the SEM showed the corrosion products in more detail. Observations of the structure of the corrosion product formed on the Al varied at low magnification from a somewhat loose structure as shown in Figures 38(a) and 39(a) to what appears to be a closely packed structure as shown in Figure 40.

At higher magnification the product whether loose or closely packed appears in a white "snow"-like structure as shown in Figures 38(b), and 39(b). At higher magnifications, morphological differences between individual deposits are evident. For example, in Figure 41(a) the deposits appear to be light and resemble the appearance of dry cold snow while the deposits shown in Figure 41(b) exhibit a more "globule"-like appearance much like wet snow. This is probably due to slight differences in the environment encountered during the drying process and is probably not related to any particular variable of the corrosion exposure.

These observations of the Al corrosion product morphology are similar to those reported by previous researchers. Wright [30] for example observed the same "snow"-like corrosion product in SEM-level microscopic observation

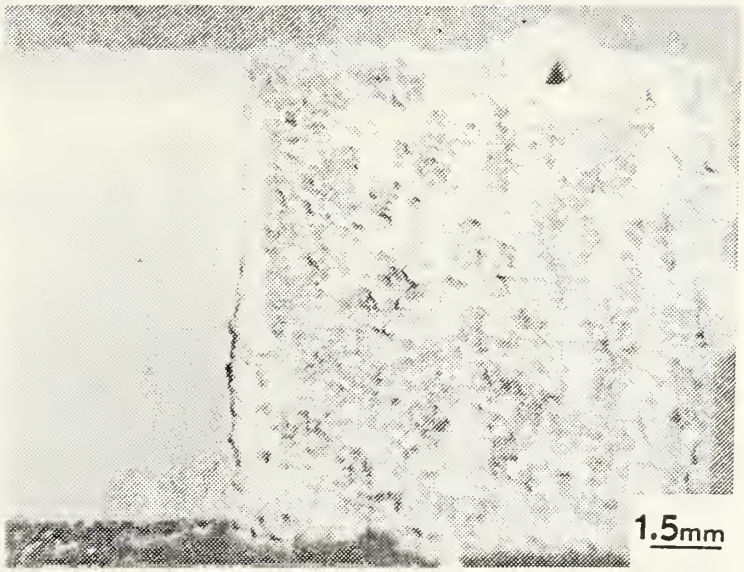

Figure 37. Brass/H32 couple exposed for one week, 7X.

(a)

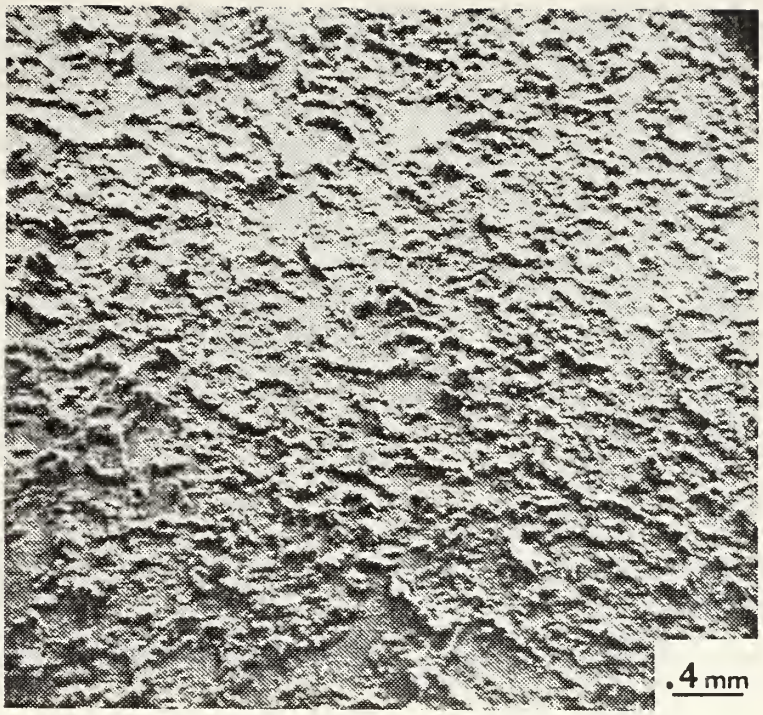

(b)

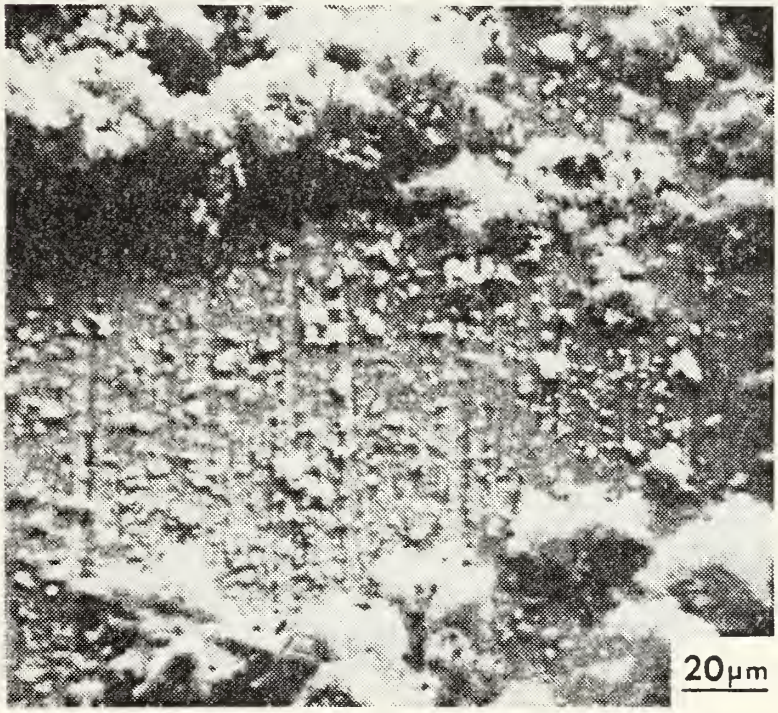

Figure 38. Corrosion product accumulation on H116 in TI/H116 couple exposed for three weeks, (a) 23X (SEM), (b) 550X (SEM).

(a)

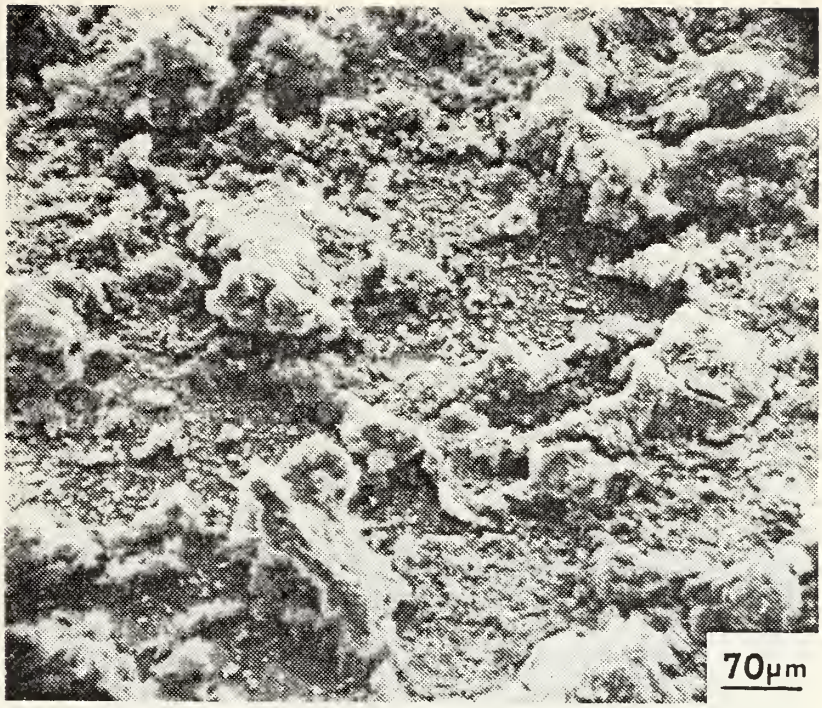

(b)

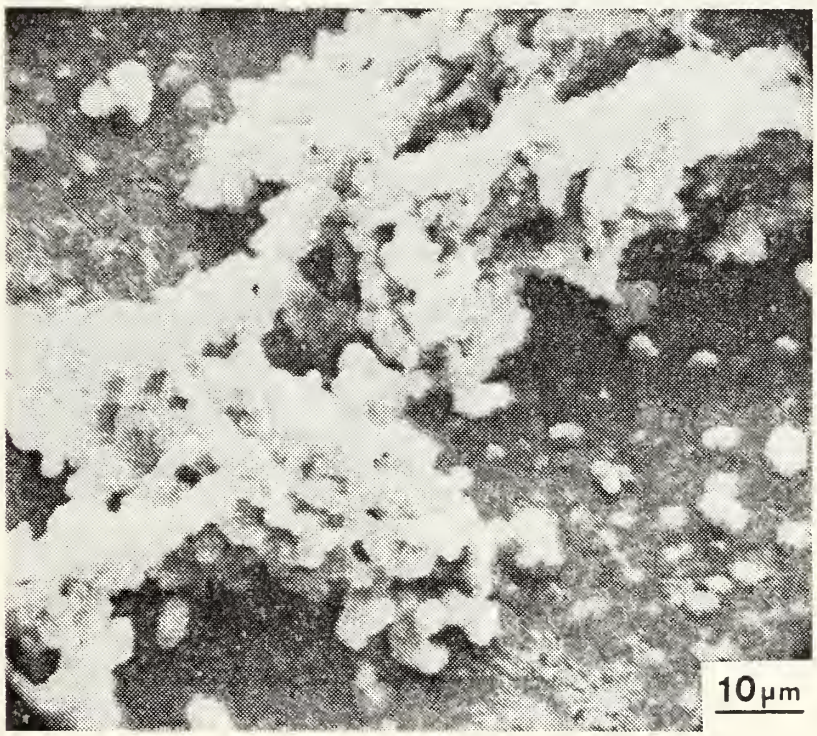

Figure 39. Typical corrosion product accumulation on H11 6 in Steel/H11 6 couple exposed for one week, (a) 150X (SEM), (b) 1150X (SEM).

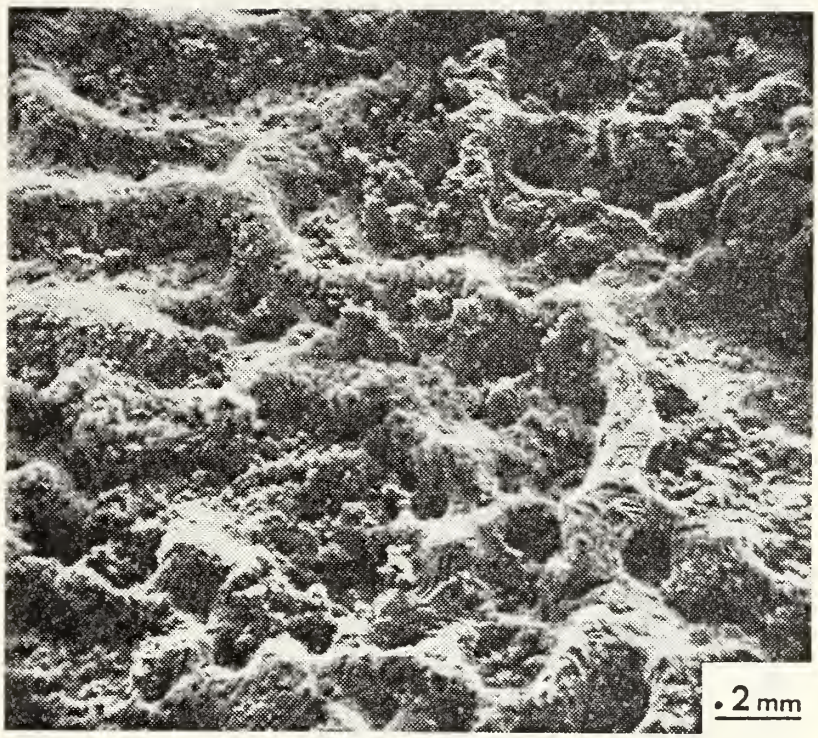

Figure 40. Typical corrosion product accumulation on H116 in TI/H116 couple exposed for two weeks, 55X (SEM).

(a)

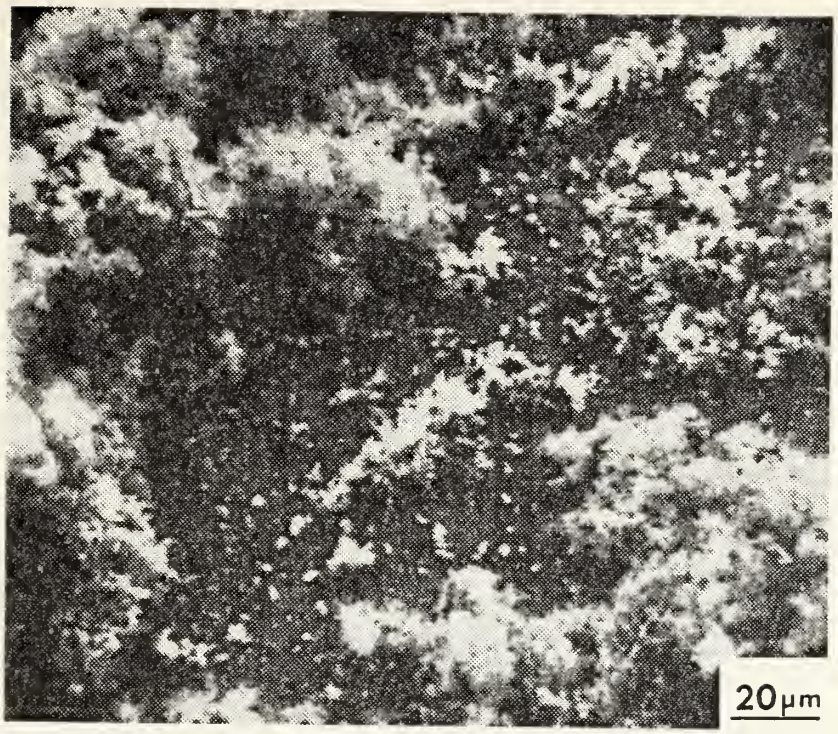

(b)

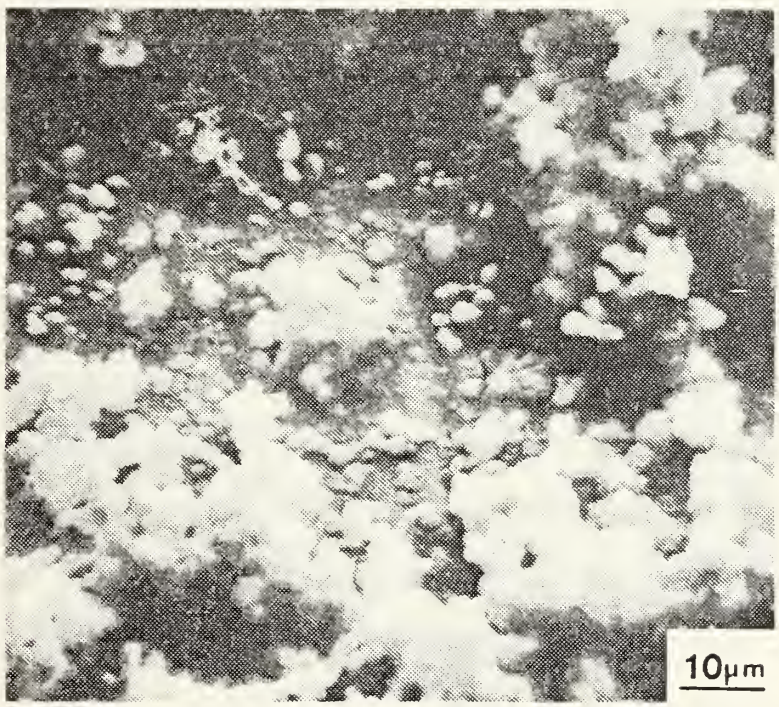

Figure 41. Two types of corrosion product accumulations, (a) 570X (SEM), (b) 1100X (SEM).

on Al sacrificial anodes. Some other examples of the corrosion product morphologies observed in this study are shown in Figures 42-45.

Also shown in these figures is a thin fibrous base film which seem to almost completely cover the anodic Al. This structure can particularly be seen in Figure 43 in the upper right. The structure seems to be extremely thin, since one can still observe the original sanding marks on the base metal, to which the film conforms. Figures 39(b) and 41(b) also show this base coating quite well. Keelean [7] observed the presence of a similar coating in his work.

An additional type of structure was observed on the Al although infrequently: Figure 46 shows this structure, on H32 in a steel/H32 couple. Notice the "mud crack" pattern especially prevalent in the lower right of the picture.

These observations of corrosion product formations and coatings of the Al anode, together with the previously observed coatings on the cathodic metals, help to explain the previously-presented variations in galvanic current density with time. From these combined results certain conclusions regarding the galvanic corrosion processes of these bimetallic couples in seawater can be deduced. As previously noted, the plots of current density versus time indicate that as the immersion time approached twenty-four hours the current density curves converged to a level of about $30\mu A/cm^2$, and it was postulated that this must be due

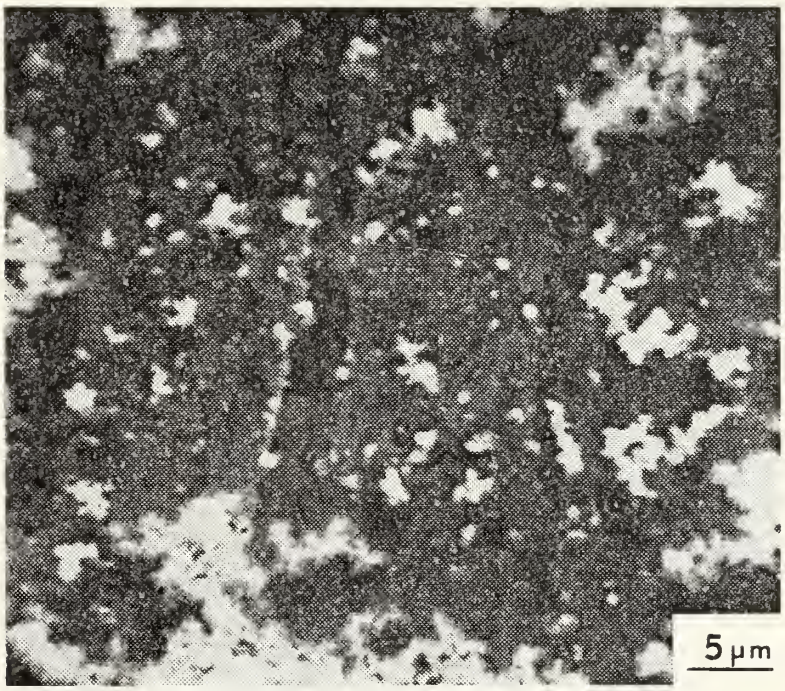

Figure 42. Corrosion products on H32 in Steel/H32 couple exposed for one week, 2200X (SEM).

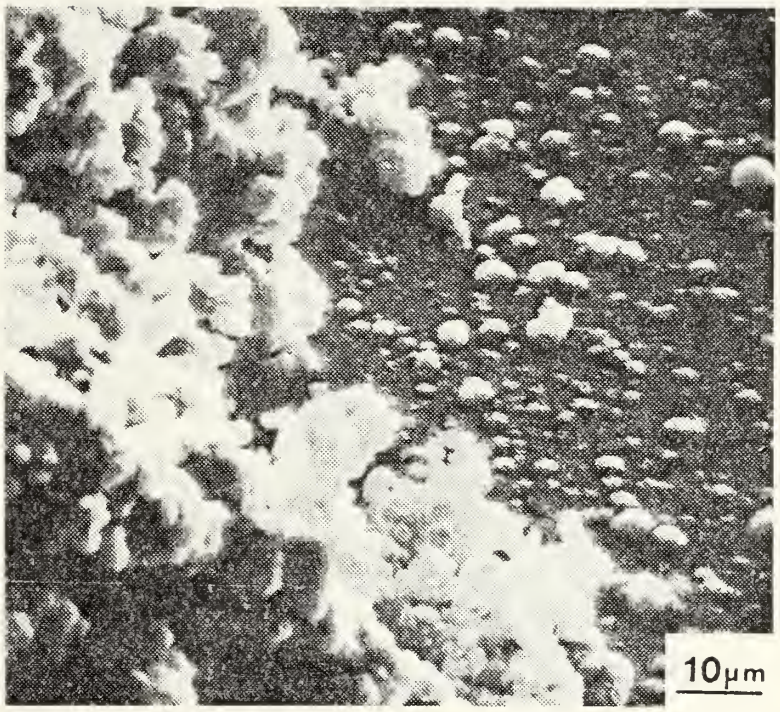

Figure 43. Corrosion product on H116 in Steel/H116 couple exposed for three weeks, 1100X (SEM).

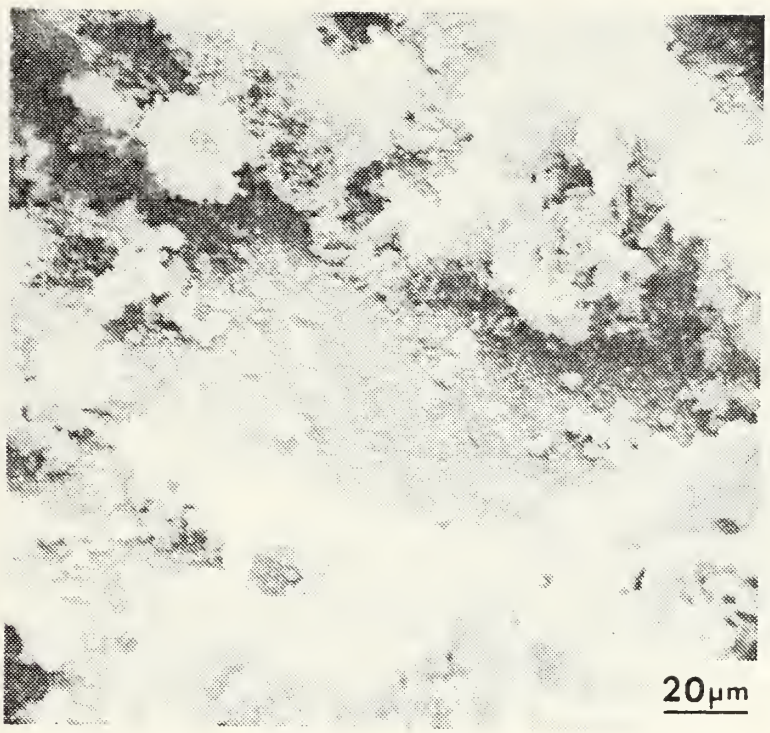

Figure 44. Corrosion product on H32 in Steel/H32 couple exposed for three weeks, 540X (SEM).

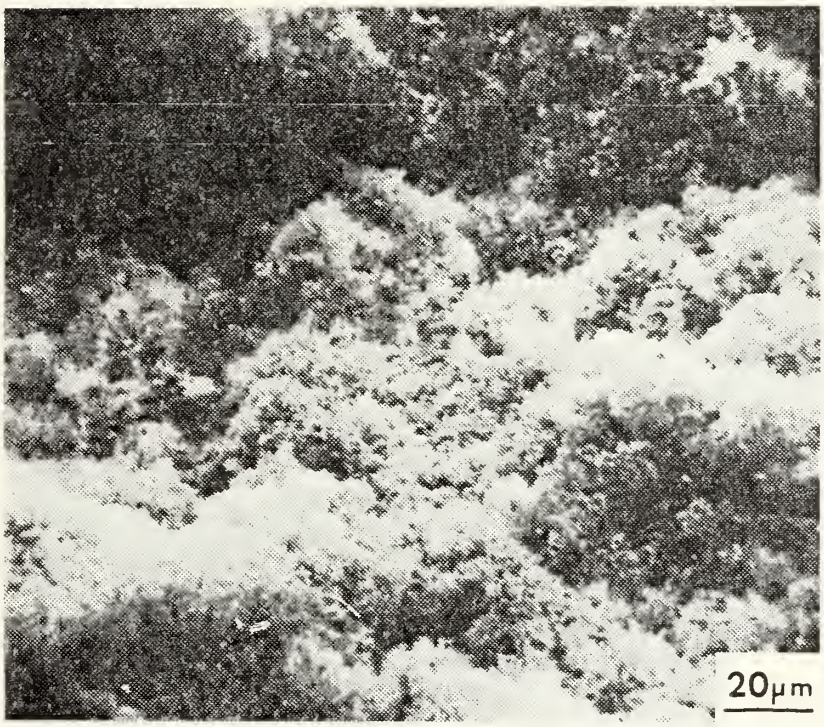

Figure 45. Corrosion product on H32 in Brass/H32 couple exposed for one week, 575X (SEM).

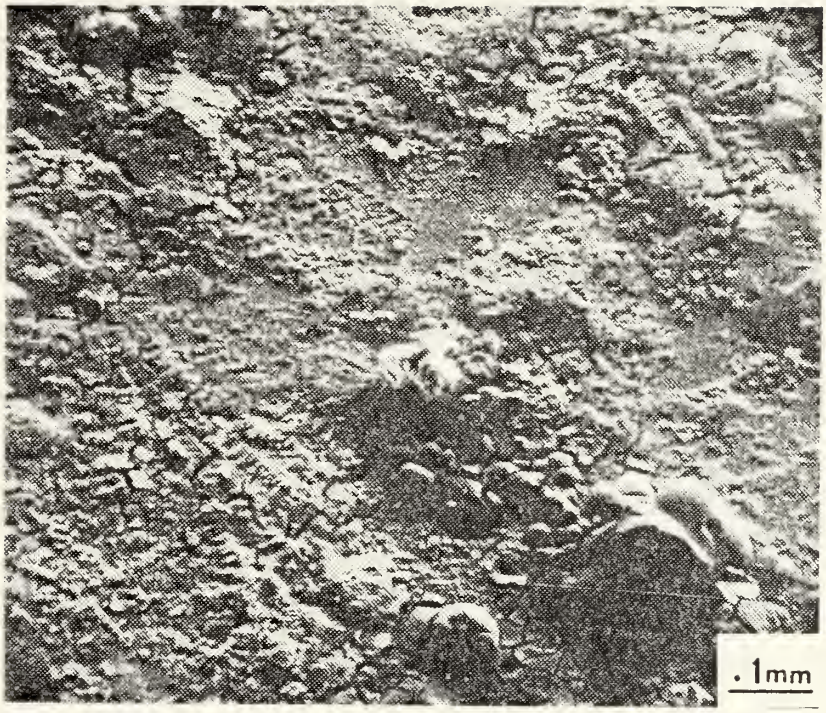

Figure 46. Corrosion product on H32 in Steel/H32 coupled exposed for two days, 110X (SEM).

to the formation of insulating layers on the electrode surfaces. It is now confirmed that layers form and cover both the anodic and cathodic surfaces, at least in proximate couples. A further question regarding these observations is whether, due to the extent of these coatings, the galvanic effect becomes small in comparison to local corrosion modes such as crevice corrosion and pitting. In order to determine whether or not this is true we next turned to a study of corrosion product distribution and especially the distribution of dissolution damage over the anodic surfaces, as might be observed on samples cleaned of corrosion products.

3. Distribution of Corrosion Products on the Aluminum Anode

Visual examination of all samples taken as a group produced some general observations of corrosion product distribution. Corrosion product accumulations on the Al member of the couple tended to be greater with longer exposure times, as expected. Some exceptions to this were noted; such as the Ti/H32 (three week exposure), Ti/H116 (three week exposure) and Ti/H117 (two week exposure) all of which had significantly less accumulations. Since duplicate specimens were not examined, the explanation for these exceptions is not certain but the variations in coverage by products could be due to corrosion product removal by circulation patterns in the cells, or more likely, by the washing procedure of dipping the samples in distilled water after exposure.

Another observation of a general nature was that for samples exposed for two days or one week, the couples containing H32 showed greater corrosion product accumulation than the couples containing either H116 or H117. This difference was not obvious when the exposure duration became two weeks or greater. Since, as noted earlier the microstructure of the H117 seemed to be more like the H32 than the H116, microstructural differences between the alloys do not seem to be obviously correlated with this observation.

Observations on representative individual samples will illustrate some of the common characteristics of corrosion product distribution. For example the couples shown in Figure 47 contain features which were present on many of the samples. As can be seen, the edges of the exposed area of the Al were covered by a heavier accumulation of corrosion product, in contrast to the relatively uniform distribution over the central surface area of the sample.

The joint between the steel and Al in Figure 47(a) was particularly covered with corrosion product over its entire length. This feature was observed on about twenty five percent of the samples exposed. Other samples showed corrosion product coverage over the anode/cathode joint which varied considerably and could not be correlated with any particular variable such as immersion time, cathodic metal or temper of the Al. Figure 47(b) shows an example of less coverage at the anode/cathode joint.

(a)

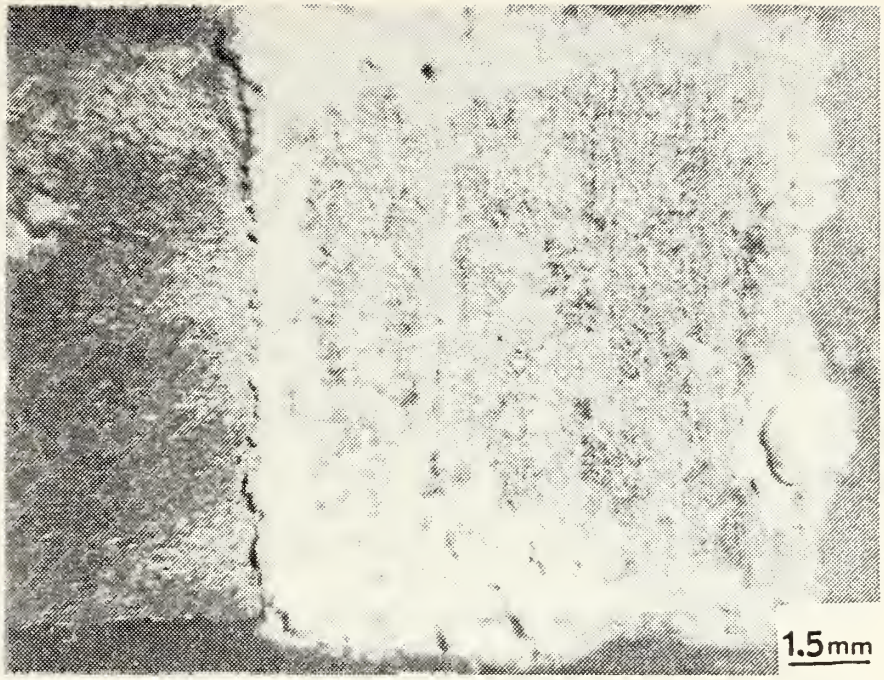

(b)

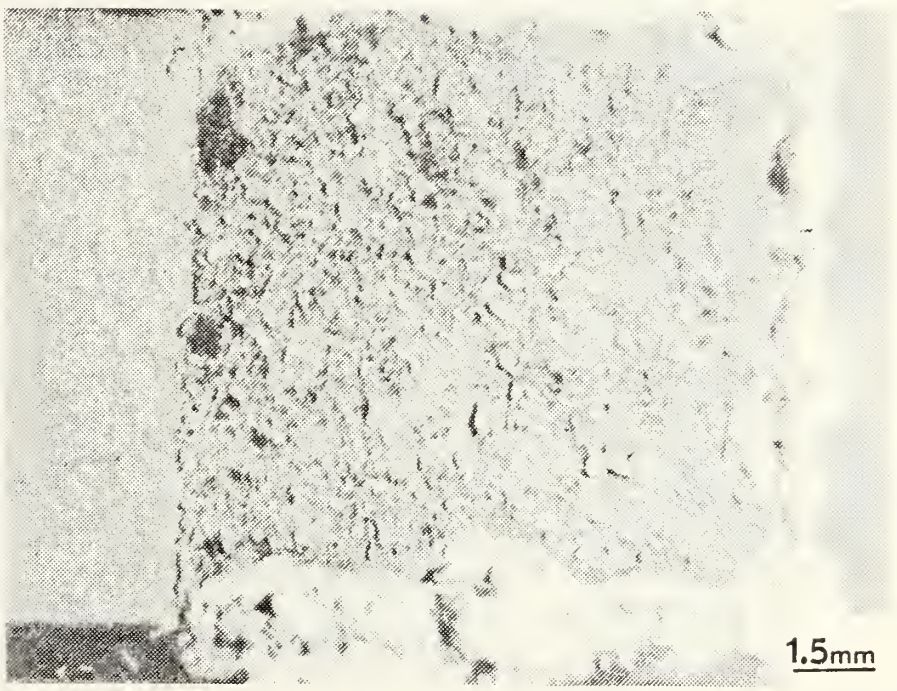

Figure 47. (a) Steel/H32 couple exposed for one week, 7X
(b) Brass/H32 couple exposed for one week, 7X.

The joint areas of the couples showed a variety of physical features. Of particular interest was what could be called a "corridor" on the Al, immediately adjacent to the build up of corrosion products at the joint, as shown in Figure 48. This "corridor", seen in the top middle of Figure 48(a) shows much less corrosion product on the Al immediately to the right of the joint. Figure 48(b) shows a higher magnification view of the areas under discussion. Areas such as this were prevalent on almost all samples. They varied as to location on the sample but were always adjacent to a build up of corrosion product. The cathode/anode joint interface, however, experienced less accumulation of corrosion products built up than that at the other three (Al plastic) edges. An attempt to quantify this observation was made. The (one) galvanic joint and (three) Al plastic edges of each sample were rated as to light moderate or heavy accumulations of corrosion product. These ratings were then weighted, added, and averaged. This was done several times. The results always showed that the accumulation for the galvanic joints was slightly less than a moderate build up and the average for the Al plastic edges was slightly less than half way between a moderate and a heavy build up.

The results seem at first to be contrary to expectations based on traditional treatment of what interactions occur in a galvanic couple. It was expected that the quantity of corrosion product build up and dissolution damage

(a)

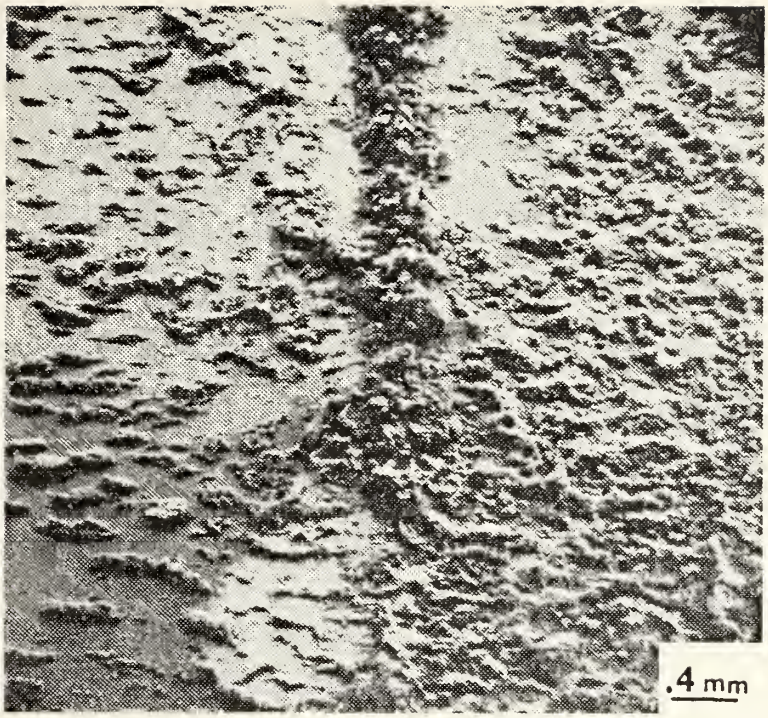

(b)

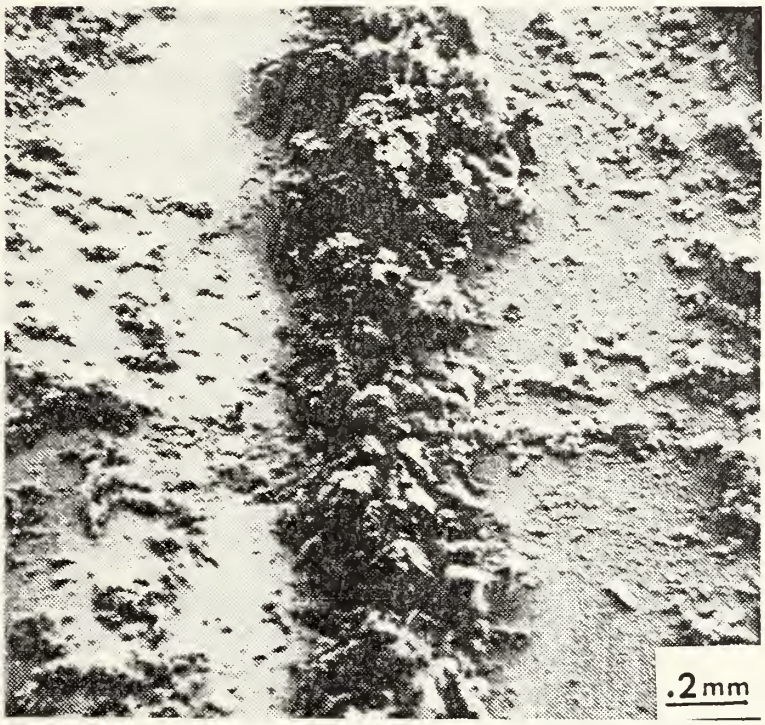

Figure 48. Cathode/anode joint area on TI/H32 couple exposed for three weeks, (a) 22X (SEM), (b) 52X (SEM).

would be concentrated particularly at the anode/cathode joint and decrease smoothly as some function of distance away from that interface. This did not occur. Instead, corrosion product accumulations were highest at the Al to plastic interface, next highest at the anode to cathode joint and next highest but generally uniform over the rest of the anode. In fact out of 36 samples examined only six contained accumulations on the joint that were equivalent to the quantity observed on the interfaces of the Al/plastic and none were greater than the accumulations the Al/plastic interface.

This unexpected effect, of increased attack at the Al/plastic edges, was easily rationalized when it was realized that the specimen design tended to produce an edge concentration of electrode current (at slight elevation steps betwen the Al and plastic mount) and that a crevice situation was promoted between the Al and plastic as well. Some of the results reported in the next section, for samples cleaned of corrosion products, will support these explanations of sample mount edge effects. It should be noted that these edge effects are not so great as to confuse the general observations of corrosion product form and distribution over the members of the galvanic couples.

4. Dissolution Damage to the Aluminum Anode Caused by Corrosive Attack

After cleaning the corrosion product off the samples, correlations between the corrosive attack and the distribution

of corrosion product were obvious. If an area showed a large accumulation of corrosion product then, after cleaning, a cavity or other form of concentrated corrosive attack, almost without exception would be observed at that position. A good example of this is shown in Figures 49 and 50. Figure 49 shows the macrophotograph taken of a particular sample after exposure and drying. Notice the large accumulation of corrosion product at the top of the Al near the cathode/anode joint and the relative lack of corrosion product on the lower middle of the joint. Figure 50 (a and b) shows the damage incurred in those two areas, respectively.

The area near the anode/cathode joint where there was extensive corrosion product accumulation had been severely attacked (Figure 50(b)), whereas the region along the joint where there was less product accumulation had been only lightly attacked. This correspondence between accumulation and damage was also evident at the Al/plastic interfaces, and on the central areas of the exposed faces of the anode samples. Figure 51 shows severe attack on two different samples which corresponded (not shown) with corrosion product accumulation.

In Figure 51(b), the existence of a raised edge of Al (on the left side along the Al/plastic interface) is illustrated, the probable cause of the concentrated attack at the Al/plastic interface was noted earlier. As previously noted, considerable effort had gone into designing and

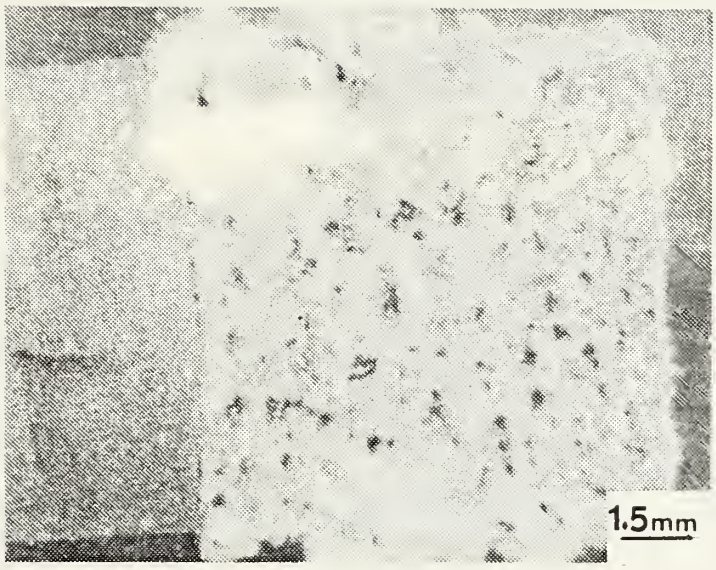

Figure 49. TI/H32 couple exposed for two days, 6X.

(a)

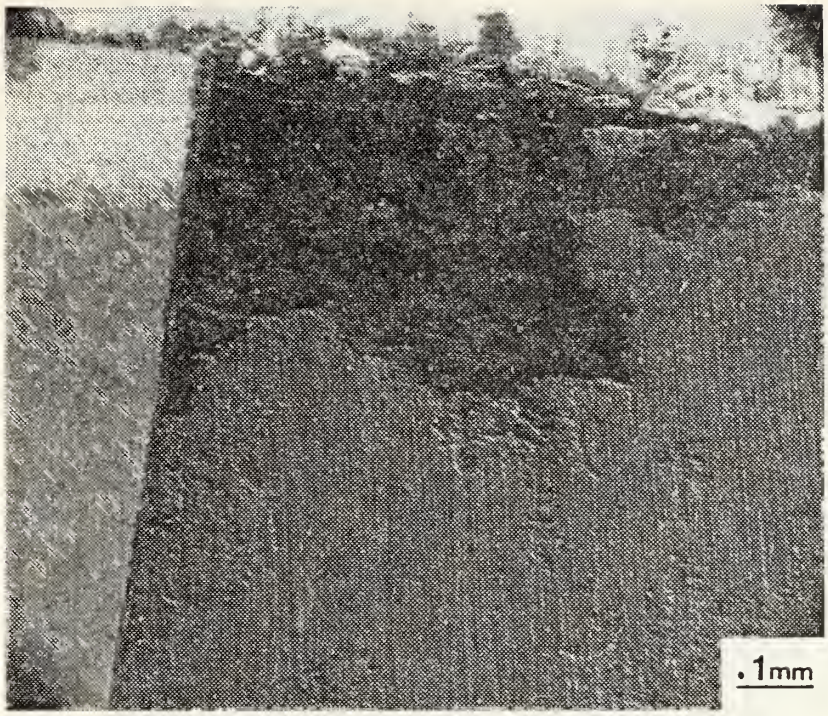

(b)

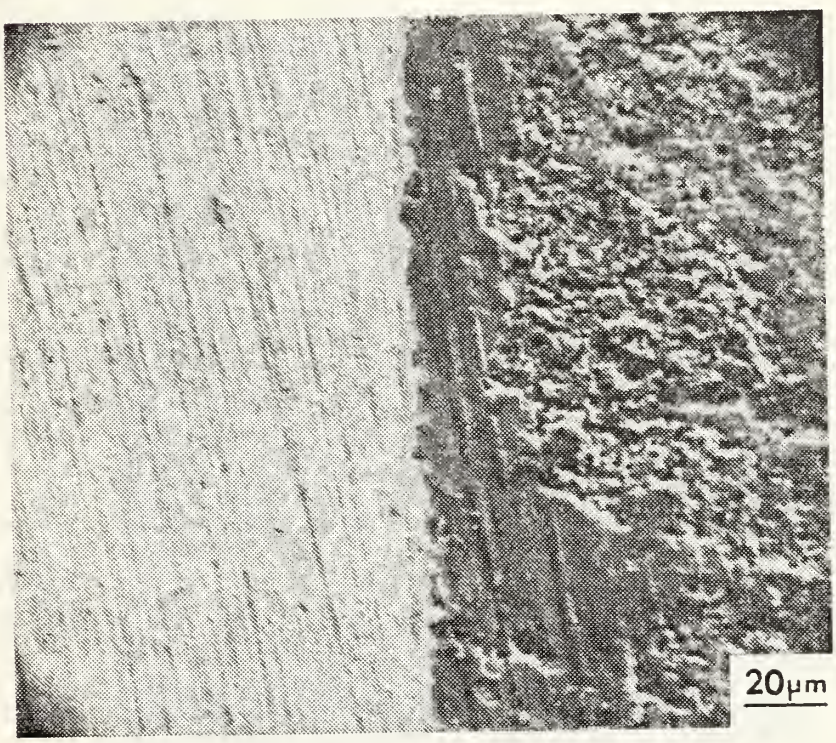

Figure 50. TI/H32 couple exposed for two days, (a) 100X (SEM), (b) 550X (SEM).

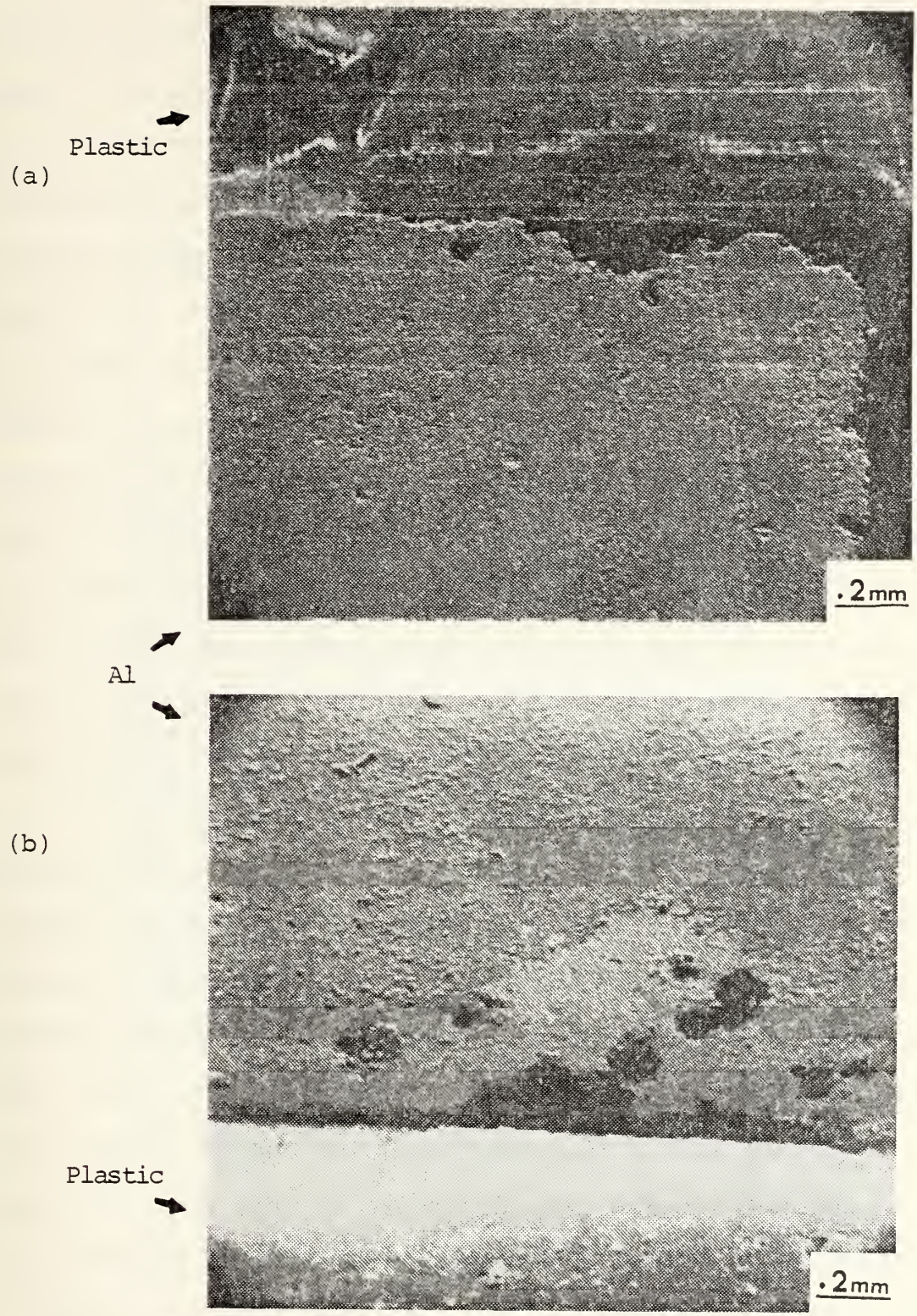

Figure 51. Corrosive attack on (a) H32 in Steel/H32 couple exposed for three weeks, 55X (SEM), (b) H32 in Brass/H32 couple exposed for eight weeks, 55X (SEM).

mounting of the test coupons in such a way that the cathode/anode joint was crevice free. To confirm the suspicion that a crevice or step was present at the Al/plastic interface prior to corrosion exposure, a test sample was prepared using the same procedure that was followed to prepare the other samples, and was mounted on a SEM stub for examination. The results of observations of the Al/plastic interface are shown in Figure 52. Those observations confirm that the interface between the metal and the plastic contained a definite step. This obviously occurs because the softer plastic is sanded away more readily than the metal during the surface preparation procedure, leaving the edge of the metal raised and exposing an extended corner to the electrolyte, producing a high current density line.

As previously shown (Figure 50(a)) localized dissolution occurred at the anode/cathode joint, and correlations between the position of dissolution cavities and corrosion product accumulations on the joint were readily apparent. Observations showed that even though a flat tight metal to metal joint was present prior to immersion, attack at the joint rapidly opened up a crevice-like cavity along the interface. Examples of attack at the joint after two days exposure are shown in Figure 53 and 54. The variation in extent of this interfacial cavity explains the observed variation in corrosion product coverage along the joint mentioned earlier. Figure 55 shows examples of interfacial dissolution distribution after somewhat longer exposures.

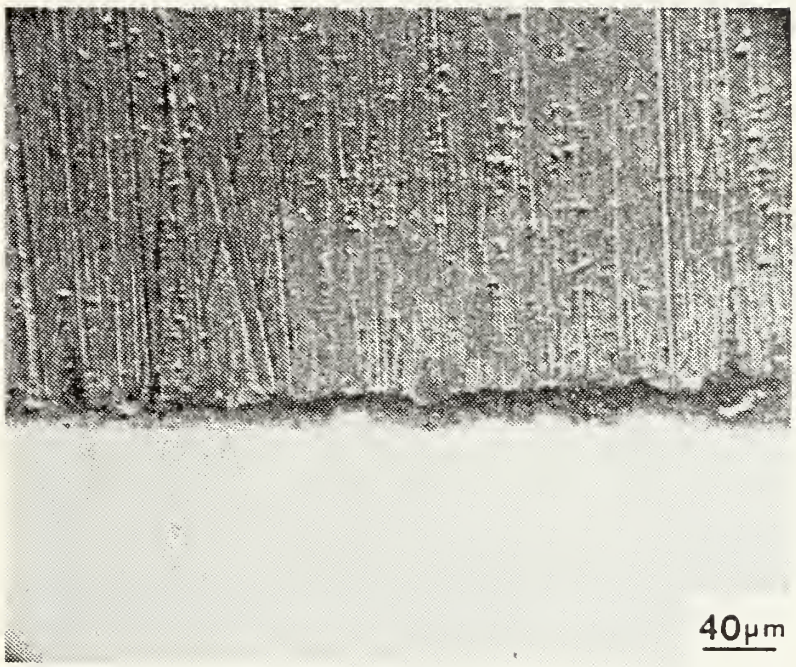

Figure 52. 240X SEM photograph of plastic and metal (dark) interface on coupled specimen.

(a)

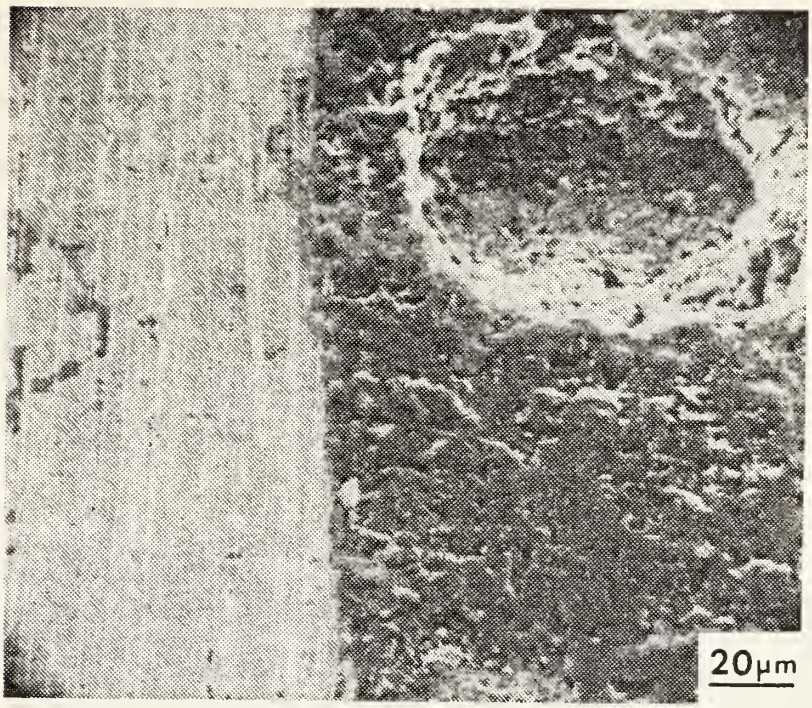

(b)

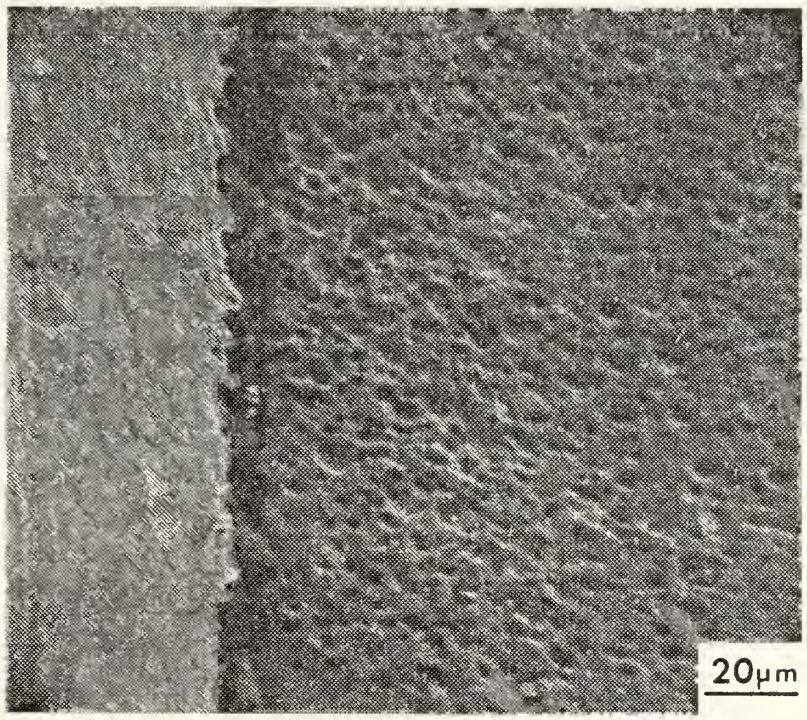

Figure 53. (a) Brass/H32 couple exposed for two days, 550X (SEM),
(b) TI/H116 couple exposed for two days, 600X (SEM).

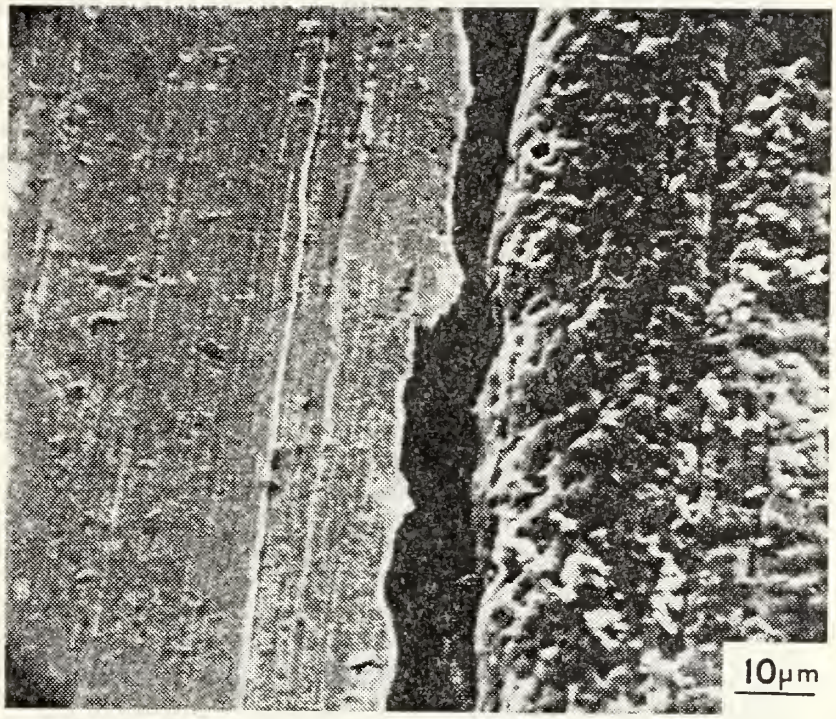

Figure 54. Steel/H32 couple exposed for two days, 1050X (SEM).

(a)

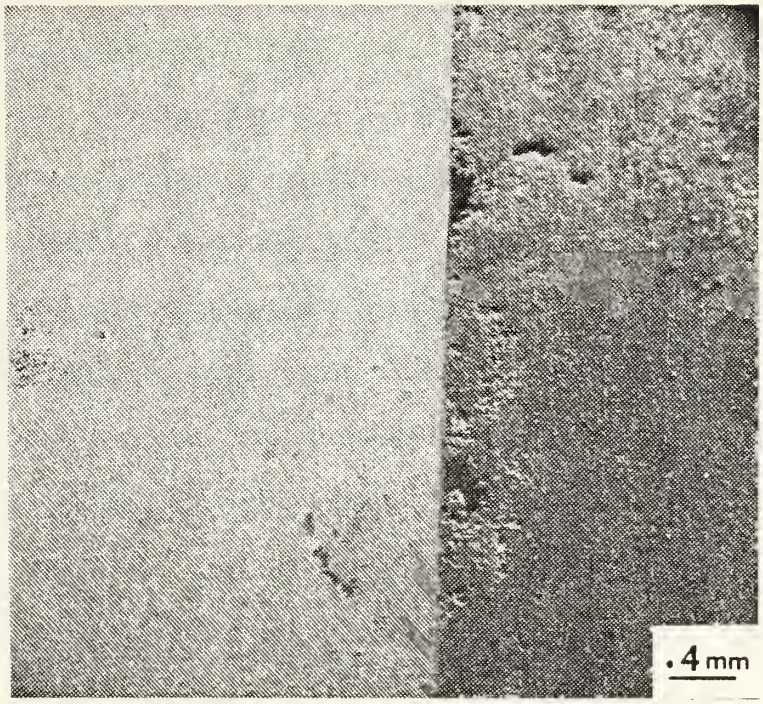

(b)

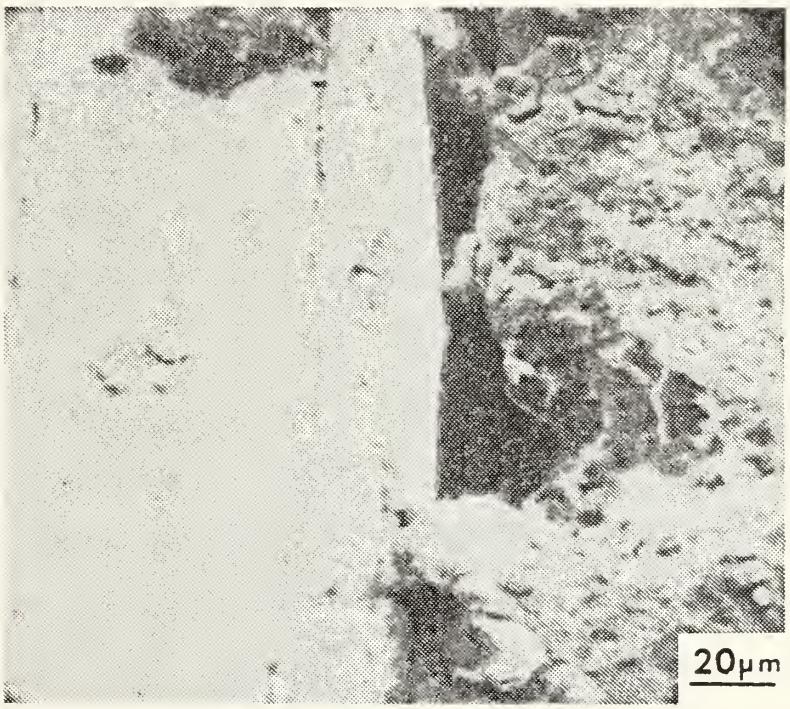

Figure 55. (a) TI/H32 couple exposed for two weeks, 22X (SEM)
(b) Brass/H32 couple exposed for eight weeks, 550X (SEM)

From these observations, some ideas can be developed which describe the sequence of processes involved in the attack of the galvanically coupled anodic Al. Upon immersion, the raised edges of the Al and the anode/cathode interface act as current concentrating sites, due to the non-uniform geometry and the galvanic potential respectively. This action, together with the likely presence, or development of, slight crevices at the interfaces provide sites at which localized corrosion can take place. Since the potentials of the coupled cathodic metals were more noble than the critical pitting potential of the Al, dissolution will tend to start at these areas (and also possibly at other areas where imperfections exist in the oxide). As the other areas of the Al become more passive (covered with a protective oxide film) the unfavorable area ratio accelerates corrosion in areas that have started to dissolve. As the cathode and anode of the bimettallic couples become covered with deposits, and the total galvanic current decreases, areas which are being attacked most aggressively develop an anode/cathode relationship with immediately adjoining areas thus producing the low-corrosion "corridors" observed near the locations of highest attack. In a sense, these "corridor" regions are being cathodically-protected by the localized anodic action. As time goes by the localized attack dominates the corrosion process and large dissolution caviities are developed on the Al.

IV. CONCLUSIONS

The following conclusions have been reached as a result of this work.

1. Galvanically induced corrosion of 5086 Al alloy is independent of temper condition for the time period studied (less than three weeks).

2. For exposures of less than twenty-four hours, the rate of corrosive attack of the anodic member of couples, based on current density measurements, can be ordered from highest to lowest at Ti/Al, brass/Al, steel/Al.

3. The physical features of the samples studied (the presence of raised edges and crevices) act to concentrate the corrosive attack at the edges of the Al.

4. Formation of insulating films and structures on the cathodic and anodic metals acts to reduce the effect of dissimilar metal coupling. The source of these films is dissolution of the anodic Al, upon which the Al corrosion product accumulates, or from which it can migrate to the cathodic member and accumulate. These coverage effects cause a decrease in galvanic current density with increasing exposure time.

5. Growth of an oxide layer on the Al leads to concentration of corrosive attack at localized areas. This causes severe pitting to take place during which a cathode/anode relationship is developed with immediately adjacent areas.

6. Heavy accumulations of corrosion product on the Al anode are associated with underlying dissolution cavities.

LIST OF REFERENCES

1. Masubuchi, I., "Materials to Fight Marine Environments," Materials Engineering, v. 78, p. 27-38, January 1971.

2. Pourbaix, M., Atlas of Electrochemical Equilibria in Aqueous Solutions, 2nd ed., p. 168-175, National Association of Corrosion Engineers, 1974.

3. Hart, R.K., "The Formation of Films on Aluminum Immersed in Water," Transactions of the Faraday Society, v. 53, p. 1020-1027, 1957.

4. Uhlig, H. H., Corrosion and Corrosion Control, 2nd ed., p. 334-347, Wiley, 1971.

5. Butler, G., and Ison, H.C.K., Corrosion and Its Prevention in Waters, p. 82, Reinhold Publishing Co., 1966.

6. Sprowls, D. O., High Strength Aluminum Alloys with Improved Resistance to Corrosion and Stress-Corrosion Cracking, paper presented at the Tri-Service Corrosion Conference, Philadelphia, Pennsylvania, 26-28 October 1976.

7. Keelean, M. R., Microscopic Investigation of Interface Corrosion of Steel - Aluminum Explosively Bonded Material Exposed to Periodic Sea Water Spray, M.S.M.E. Thesis, Naval Postgraduate School, Monterey, California, 1976.

8. Strasburg, W., "Survey of Corrosion Problems of Destroyer Type Ships," NAVSEC travel report ser 78-6101C, 25 January 1971.

9. Summerson, T. J., Aluminum Association Task Group Exfoliation and Stress Corrosion Testing of Aluminum Alloys for Boat Stock, paper presented at Tri-Service Corrosion of Military Equipment Conference, Dayton, Ohio, 29-31 October 1974.

10. Doig, P. and Edington, J. W., "The Influence of Solute Depleted Zones on the Stress - Corrosion Susceptibility of Aged Al - 7.2 Mass % Mg and Al - 4.4 Mass % CU Alloys," Proceedings of the Royal Society of London, v. 339, p. 37-47, 1974.

11. Czyryca, E. J. and Hack, H. P., Corrosion of Aluminum Alloys in Exfoliation - Resistant Tempers Exposed to Marine Environments For Two Years, paper presented at Tri-Service Corrosion of Military Equipment Conference, Dayton, Ohio, 29-31 October 1974.

12. Brooks, C.L., "Aluminum - Magnesium Alloys 5086 and 5456 - H116," Naval Engineers Journal, v. 82, p. 29-32, August 1970.

13. Haynes, G. S. and Baboian, R., "Reducing Galvanic Corrosion with Transition Metals," Materials Performance, v. 16, p. 36-39, February 1977.

14. LaQue, F. L., Corrosion Handbook, p. 416, Wiley, 1948.

15. Mansfeld, F. and Kenkel, J. V., "Laboratory Studies of Aluminum Alloys," Galvanic and Pitting Corrosion - Field and Laboratory Studies, ASTM STP 576, p. 20-47, American Society for Testing and Materials, 1976.

16. Baboian, R., "Investigation of Galvanically Induced Localized Corrosion," Localized Corrosion - Cause of Metal Failure, ASTM STP 516, p. 145-163, American Society for Testing and Materials, 1972.

17. Baboian, R., "Electrochemical Techniques for Predicting Galvanic Corrosion," Galvanic and Pitting Corrosion - Field and Laboratory Studies, ASTM STP 576, p. 5-19, 1976.

18. Cummings, J. R., Masters Thesis, to be completed December 1977, Naval Postgraduate School, Monterey, CA.

19. Aluminum Standards and Data 1976, 5th ed., p. 15, 92, The Aluminum Association Incorporated, 1976.

20. Woldman, N. E. and Gibbons, R. C., Engineering Alloys, 5th ed. p. 739, 1163, 1409, Van Nostrand Reinhold Company, 1973.

21. National Association of Corrosion Engineers, NACE Standard TM-01-69, Test Method: Laboratory Corrosion Testing of Metals for the Process Industries, 1969.

22. Kester, D. R., Duedall, I. W., Conners, D. N., and Pytokowicz, R. M., "Preparation of Artificial Seawater," Limnology and Oceanography, v. 12, p. 176-178, December 1967.

23. Mansfeld, F. and Kenkel, J. V., Electrochemical Testing of Galvanic Corrosion, paper presented at Tri-Service Corrosion of Military Equipment Conference, Dayton, Ohio, 29-31 October 1974.

24. Mansfeld, F. and Kenkel, J. V., "Laboratory Studies of Galvanic Corrosion, I. Two-Metal Couples, Corrosion, v. 31, p. 298-302, August 1975.

25. LaQue, F. L., Marine Corrosion, p. 194, 195, Wiley, 1975.

26. Pettibone, J. S., and Kane, R. L., "Titanium," Corrosion Resistance of Metals and Alloys, 2nd ed., edited by LaQue, F. L. and Copson, H. R., p. 647, 648, Reinhold, 1963.

27. Fontana, M. and Green, W., Corrosion Engineering, p. 33, 177, 178, McGraw-Hill, 1967.

28. National Association of Corrosion Engineers, NACE Basic Corrosion Course, p. 7-12, 1975.

29. Godard, H. P., "Examining Causes of Aluminum Corrosion," Materials Protection, v. 8, p. 25, 1969.

30. Wright, P. W., A Scanning Electron Microscope Study of the Corrosion of Sacrificial Hull Anodes under Simulated Ship Service Conditions, M.S.M.E. thesis, Naval Postgraduate School, Monterey, California, 1976.

INITIAL DISTRIBUTION LIST

		No. Copies
1.	Defense Documentation Center Cameron Station Alexandria, Virginia 22314	2
2.	Library, Code 0142 Naval Postgraduate School Monterey, California 93940	2
3.	Department Chairman, Code 69 Department of Mechanical Engineering Naval Postgraduate School Monterey, California 93940	1
4.	Professor A. J. Perkins, Code 69Ps Department of Mechanical Engineering Naval Postgraduate School Monterey, California 93940	6
5.	LT John S. Locke Naval Reactors Representative Office Energy Research and Development Adm. P.O. Box 2053 Mare Island, California 94592	2

Thesis 172632
L784 Locke
c.1 Investigation into the effect of dissimilar metal coupling, potential, and processing on the mode and distribution of galvanic corrosion attack on 5086 aluminum alloy in synthetic seawater.